THE UNIVERSITY OF MANITOBA

WALL SHEAR STRESS IN DEVELOPING TURBULENT PIPE FLOW

by

J. K. REICHERT

A THESIS

SUBMITTED TO THE FACULTY OF GRADUATE STUDIES
IN PARTIAL FULFILLMENT OF THE REQUIREMENTS
FOR THE DEGREE OF MASTER OF SCIENCE

DEPARTMENT OF MECHANICAL ENGINEERING

WINNIPEG, MANITOBA
DECEMBER, 1973

ABSTRACT

The problem of measuring mean wall shear stresses in developing turbulent pipe flow has been studied. Experiments on air flow in the first 73 diameters of a four-inch pipe were undertaken for Reynolds numbers between 31,000 and 134,000 (based on radius). Similarity techniques classically applicable to fully developed flow have been extended to the developing flow region. Measurements of the axial and Reynolds number dependences of the wall shear stress were made using a calibrated, flush mounted, hot film probe. The hot film measurements were compared with similar measurements obtained by the Preston tube and cross plot techniques. The shear stress measurements and extensive mean velocity profile measurements indicated that between 20 and 40 diameters, the velocity profiles "overshoot" the developed profile shape while the wall shear stress achieves a minimum value. A physical model relating the velocity profiles, wall shear stresses and static pressures has been proposed to account for the non-monotonic flow development. A turbulent sublayer structure and indications of a sublayer burst phenomenon were found.

ACKNOWLEDGEM ,TS

The a nor would like to thank Dr. R. S. Azad for the guidance and direc on which he has provided during the course of this work, and Mr. H. Hummel for helpful discussion and technical advice. The fi iical assistance of the National Research Council of Canada is gr efully acknowledged.

TABLE OF CONTENTS

LIST OF TABLES AND FIGURES

LIST OF SYMBOLS

d, D	pipe diameter
r, R	pipe radius
u, U	longitudinal component of flow velocity (time average)
v, V	radial component of flow velocity (time average)
x, X	longitudinal position coordinate
y, Y	radial position coordinate
U*	friction velocity
U+	dimensionless velocity = $\frac{U}{U*}$
Y+	dimensionless position = $\frac{YU*}{\nu}$
q_w	the heat transfer from a heated wall plate
A, B	slope and intercept parameters in the analytic hot film calibration equation
Cf	skin friction coefficient
Cp	specific heat at constant pressure
Pcone	contraction cone static pressure drop
Pfilm	total power dissipation from the heated film sensor
Pr	Prandtl number
Rcold	unheated film probe resistance
Re(m,d)	Reynolds number based on mean velocity and pipe diameter
Re(m,r)	Reynolds number based on mean velocity and pipe radius
Rprobe	total resistance of the film probe including both the film and leads
Rsensor	resistance of the heated film during constant temperature operation
Vbulk, VB	bulk velocity
Vfilm	voltage drop across the heated film probe
Vo	free stream velocity for the flow over a flat plate
ΔPp	Preston tube differential pressure measurement
ΔT	temperature elevation of the hot film above the tunnel air temperature

α	temperature coefficient of resistivity for the hot film
λ	friction factor = 4 x Cf
ϕ	thickness of the thermal boundary layer over a heated film probe
ν	air kinematic viscosity
ρ	air density
λeff	effective thermal conductivity accounting for increased conductivity due to turbulent exchange
τ_w	wall shear stress
$\vec{w}$	vector of flow velocity with longitudinal and radial component magnitudes u and v
μ	air dynamic viscosity

1. INTRODUCTION

1.1 The Nature and Importance of Wall Shear Stress

In a turbulent flow, momentum can be transferred by two basically different processes. On the macroscopic or continuum scale, momentum is transferred by both the mean and fluctuating components of the velocity vector. The mean component serves to transport mass and thus momentum along the mean flow direction. The turbulent or fluctuating component, while it can not cause a net mass flow across the mean flow direction, can result in a net transverse momentum flux due to turbulent cross stream mixing of fluid of different speeds. This turbulent component of the momentum flux is termed the Reynolds stress. On the microscopic scale, momentum can be transferred in all directions by kinetic molecular motion. When a mean velocity shear exists in the flow the net momentum transport due to molecular motion is in the direction of increasing velocity gradient. This gradient dependent, molecular scale, momentum transport is called the viscous shear stress. The standard turbulent boundary layer models have considered the region of steepest velocity gradient nearest to the flow boundary to be a laminar like region and have adopted the jargon "laminar sublayer". In this wall region the turbulent momentum transport is overshadowed by the molecular phenomenon of viscous shear stress. Indeed, at the wall, where the classic "no slip" condition requires that velocities must be zero, the total shear stress can only be due to the viscous component of shear. The viscous shear stress evaluated at the boundary of

the flow is called the wall shear stress (τ_w).

A net transverse transport of momentum from a region implies that the total momentum in that region is changing with time. By Newton's second law a net force with magnitude equal to the rate of momentum change must be acting on the region. Thus when there is viscous momentum transport in the wall region a force appears to retard the fluid flow and an equal and opposite force appears to act on the wall. The wall shear stress is a direct measurement of this drag or skin friction force per unit area of wall surface. For some simple geometries, such as flow over a flat plate or flow in straight pipes and ducts, where there is no normal component to the mean velocity, this wall shear stress comprises the total drag force between the fluid and wall. The wall shear stress and its dimensionless counterpart, the skin friction coefficient, are of fundamental technological importance in mechanical design for fluids. The design engineer must predict the forces and energy losses which affect mechanical equipment when designing to operate efficiently with fluids.

Much theoretical and experimental work has been done in the heat transfer field to relate convective heat transfer quantities to the more easily measured fluid flow quantities. When the molecular diffusivities of heat and momentum are equal, that is when the Prandtl number equals 1, the processes of convective heat transfer and momentum transfer are mathematically and physically analogous. The basic equation relating the turbulent shear stress to the turbulent heat flux is called the Reynolds' analogy in recognition of its originator.

In practise, convective heat transfer coefficients for the wall region can often be estimated with a knowledge of the skin friction coefficient combined with an empirical or theoretical expression for the dimensionless heat transfer variables. In fact, it is this analogy between heat transfer and momentum quantities which justifies on a theoretical level the attempt to measure wall shear stress by a heated film technique.

Aside from these practical considerations, the wall shear stress is an important quantity in pure research on turbulent boundary layer behavior. Its use as a dimensionless scaling parameter for boundary layer velocities and distances in the transverse direction is virtually universal. A quantitative comparison of any experimental work in turbulence with the experimental and theoretical findings of others using different test equipment is possible only after τ_w is determined. Most often equations are written using U*, the friction velocity as the scaling parameter where U* is defined in terms of τ_w.

1.2 Wall Shear Stress Measurement Techniques

Briefly, the current experimental wall shear stress measurement methods fall into two separate groups. As divided by Brown and Joubert in their detailed review of the measurement techniques (5), there are momentum methods and wall similarity methods.

Momentum methods consist of either momentum balances or attempts to evaluate the momentum boundary layer equations and then to solve them for the wall shear stress variable. The momentum methods are

best applied in a fully developed, symmetrical flow. The static pressure gradient technique used for calibration in this study is a momentum balance method.

Wall similarity methods are developed from the concept that the mean flow structure near the flow boundary, in different turbulent flow regions, and particularly for the zero pressure gradient case, have a fundamental physical similarity. That is, the flow can be described by equations of the same basic form. Members of this category include the mean velocity profile method, based on the lagarithmic velocity profile law, the heat transfer methods, based on the similarity of the sublayer region closest to the wall, and methods based on the similarity of flow around obstacles like the Preston tube.

Flow similarity methods are only useful for measurements in flows where similarity is known to exist. These similarity methods have been used successfully in mild adverse pressure gradients by Ludweig and Tillman (14), but the application of similarity techniques to developing turbulent flow raises a question concerned with at which point the flow can be considered as having developed a similar structure. Since it is the region nearest the wall where the boundary layer development starts, it is reasonable to expect that the methods depending upon similarity only in the flow closest to the wall may be useful in regions where the outer flow structure does not yet follow the log law. Thus we might expect the hot film or Preston tube methods to be applicable in regions of early turbulent boundary layer development where mean profile methods may fail.

Schraub and Kline (23) have recently studied the flow in the fully developed turbulent boundary layer with and without arbitrary pressure gradient. They have concluded that the basic turbulent flow structure is not significantly changed from the zero pressure gradient case for moderate pressure gradients. While the existence of a linear mean velocity profile in the sublayer was clearly shown, non-universal behavior was observed in the usually logarithmic region for pressure gradient flows. This further suggests the possible continued utility of the sublayer similarity dependent methods where log law methods may fail.

In this study, we have applied two wall similarity methods, the hot film technique and the conventional Preston tube method, to the problem of shear stress measurement in developing pipe flow. The apparatus for both approaches has been calibrated in the fully developed region using the classic static pressure gradient procedure.

2. WIND TUNNEL EQUIPMENT AND BEHAVIOR

2.1 Basic Wind Tunnel Equipment

The basic tunnel equipment which was used in this study has been described by Azad and Hummel (2). Briefly, the tunnel is of low speed, open circuit design with a rough surfaced tripping element installed to initiate the turbulent boundary layer growth. The flow develops along a test section consisting of several pieces of 101.6 mm. i.d. steel pipe with an overall length of 7.85 meters before discharging through a diffuser into the laboratory. As equipped the mean operating speeds of the tunnel can range from 10 to 50 m/sec in the test pipe. In summarized form, the principal tunnel specifications are as follows:

Tunnel drive:

400V, 52.5 amp rated 25 h.p. D.C. motor (mfgr. Compton and Parkinson) with a "Varimag" controlled power supply for speed adjustment (mfgr. Lancashire Dynamo Ltd.).

Blower equipment:

Spring mounted centrifugal type fan with fixed blade angle. Fan diameter: 2 ft., Blade width: 1 ft. Inlet: flared, 2 ft. diameter with variable pitch guide vanes (mfgr. Chicago Blower Co.).

Flow conditioner section:

3 ft diameter duct partitioned by 6 medium mesh screens in two groups and provided with a canvas coupling section to reduce the transmission of fan vibration. Overall length: 22 ft.

Contraction cone:

Plaster of Paris and fiberglass construction, equipped with 2 static pressure rings to measure pressure drop across the cone. Contraction ratio: 89 to 1.

Roughness section:

A 4-inch length of test section pipe lined inside, towards the downstream end, with a 3.5 inch wide strip of Silicon carbide floor surfacing paper. Grit type 4-F (mfgr. 3M Company).

Test section pipe:

Several sections of steel pipe (¼ inch wall) with a machined and polished, hydraulically smooth inner surface and fittings for flush, butt connections of the sections. Inside diameter: 101.6 mm. Available section lengths: 25, 45, 105, 205, 355, 405 cms.

Diffuser section:

Machined, cast aluminum diffuser with an 8 degree divergence angle and 45 cm. straight inlet section.

2.2 Peripheral Wind Tunnel Equipment

The following is a list of peripheral tunnel equipment used routinely to determine the tunnel operating point, the ambient air density and viscosity and also for the measurement of pressure.

- Betz projection manometer (slow response, .1 mm. H_2O scale graduations)

- Trimount inclined manometer (nominal fluid specific gravity = .827)
- Hero methanol manometer with adjustable inclination angle
- Magnetic pickup device with pulse shaping amplifier for monitoring fan rotation rate
- Wall mounted, mechanically aspirated psychrometer
- Standard mercurial Fortin-type barometer

2.3 Wind Tunnel Calibration

On the basis of Bernoulli's equation for ideal incompressible flow, we expect that the mean velocity in the pipe is related to the static pressure drop across the contraction cone according to

$$VB \propto \sqrt{\frac{Pcone}{\rho}}$$

where the air density ρ is a function of the barometric pressure, tunnel air temperature, and the moisture content of the air. The proportionality factor in the above relation was determined from measurements of the mean velocity, the contraction cone static pressure drop and the air density for several tunnel operating points. The data were plotted in figure 1. The constant of proportionality obtained from the data on this graph is 4.31 where the units for the variables are as indicated on the figure.

The mean velocities for the figure were computed by numerical smoothing and integration of the velocity profiles measured for the different tunnel operating points. The velocity profile data were

obtained by traversing the pipe with a total pressure tube and using the adjacent static pressure ring measurement to calculate the dynamic pressures. The invariance of static pressure across the pipe (less than 3%) had been verified previously with separate static pressure tube traverses. Although by continuity, the mean velocity is necessarily independent of longitudinal position, the data used for the mean velocity calibration was taken at a position 72.3 diameters downstream of the beginning of the roughness element. At that point the flow was assumed to be fully developed and a rough check on the mean velocity was permitted by comparison with the three-quarter radius velocity. Where the flow is developing, the centerline velocity is a function of the longitudinal traverse position. This is illustrated on the calibration curve for measurements of centerline velocity taken at 36.84 and 72.27 diameters. These calibration curves are in reasonable agreement with previously existing curves for our tunnel which were taken with a slightly different overall pipe length and a less accurate procedure for air density determination.

The mean velocity calibration curve is a function of the pipe geometry and length and also the roughness element, but it is independent of the equipment upstream of the contraction cone. For this reason the tunnel calibration is not subject to drift. A calibration based on the fan r.p.m., the power input, or some similar parameter rather than the cone pressure will vary since the fan efficiency depends upon warm up time, temperature, motor speed stability and tunnel leaks in the flow straightener section. These considerations suggest

that a separate calibration against the cone pressure should be performed each time the fan speed is to be used as an indicator of the tunnel air speed. For the case in which the tunnel speed is varied rather quickly, the flow temperature changes are small and given constant conditions in the straightener section, these repeated checks are probably unnecessary. The variation of motor speed with contraction cone pressure is plotted in figure 2. The motor speed was determined by electronic counting of voltage pulses caused by a toothed wheel on the motor shaft near a magnetic pickup.

Because of its response, the Betz manometer is particularly suited for monitoring the cone pressure drop. The Betz was replaced by the Trimount inclined manometer so that the high accuracy, wide range scale, and easy reading features of the Betz could be used for the total pressure tube traverse measurements. Adjustment of the tunnel speed to particular operating values was made easier by permanently mounting the Trimount near the motor speed controller. The Trimount was calibrated against the Betz cone pressure readings and a linear function was fitted to the data to facilitate conversion of the Trimount readings to mm. of water. While average readings of the cone pressure were potentially more difficult to make because of the faster response of the Trimount, this was compensated by using fairly long leads to the contraction cone pressure taps.

2.4 Tunnel Warm Up and Stability

After the tunnel is turned on, the flow structure establishes itself quite quickly, however, the tunnel does not attain stable equilibrium with the laboratory open return loop for some time due to heating of the air which occurs at the blower. The principal heat sources appear to be the fan bearings, which can conduct heat to the fan housing, and also the drive motor which can conduct heat to the fan itself through the drive shaft. A certain amount of heating may also be due to friction at the fan blades. The result is that after motor speed adjustment the tunnel air temperature will rise and at a slower rate the ambient air temperature of the laboratory will also rise. The corresponding decrease in air density can be expected to affect both the mass flow rate down the pipe and the fan speed. Changes in bearing friction with temperature can also cause the fan speed to vary. The net effect is that observed cone pressures tend to increase for lower motor speed settings and decrease at the higher settings. These observations imply that considerable warm-up time is required before experimentation can proceed. For the higher tunnel speeds approximate equilibrium is approached after from one-half to one hour of warm-up while for low speeds, shorter warm-up is sufficient. Even after considerable warm-up random variations in the motor speed occur as indicated by the cone pressure fluctuations observed with slow response Betz manometer. Van Der Spiegel (25) has estimated this motor speed variation to be ±.43%. Even after thermal equilibrium was established, it was observed that occasional rapid

increase or decreases in the tunnel air temperature of the order of two or three degrees F. corresponded to the automatic start-up or shut-down of the laboratory ventilation system. The tunnel air temperature elevation above the ambient lab temperature is graphed as a function of Reynolds number for several experimental runs to illustrate the magnitude of the problem (figure 3). This flow temperature variation can affect the power loss from any heated sensing element in the flow and in particular, proved to be a difficulty in making hot film measurements of the wall shear stress at higher Reynolds numbers.

2.5 Wind Tunnel Vibration, Leaks and Resonance

The tunnel is remarkably free from vibration due to several specific design features. The fan itself is mounted on a spring frame and the fan section is isolated from the contraction cone by a canvas coupling. The flow straightener section is supported by canvas straps. The test section pipes are quite heavy and a heavy guage track and trolly system supports the pipes at several points on foam cushions.

One problem had been leakage from the tunnel in the flow straightener sections where the screens were installed. These joints had widened since the tunnel was constructed, and previous attempts to seal them with putty, masking tape and other materials had failed due to both the temperature and pressure of the escaping air. A fabric backed heating and ventilating tape known by the trade name "Duro Dyne" eventually proved to be a satisfactory solution. While upstream leaks

would not affect the mean velocity vs. cone pressure calibration, they could produce asymmetries in the flow.

The effect of removal of the roughness section on the overall tunnel behavior at the lowest speeds was of particular interest. The tunnel cone pressure drop and hence mean velocity was observed to oscillate regularly with a period of approximately 3 seconds and an amplitude of 2 mm. of water. This occurred consistently for mean cone pressures up to 18 mm. of water. This resonance phenomenon was not detectable when the roughness section was installed.

3. THE HOT FILM TECHNIQUE

3.1 Historical Introduction and Theory

Virtually all of the early theoretical work on the hot film technique as applied to the measurement of wall shear stress is premised on the existence of a laminar-like sublayer. The more recent experimental work on the flow in the wall region (Shraub and Kline (23) or Reiss and Hanratty (19)) has shown that the sublayer region of a turbulent boundary layer is physically quite dissimilar to laminar flow. In fact, turbulent exchange due to "burst" phenomenon is quite significant. The simple observance of fluctuations in the hot film output is alone sufficient to illustrate the inadequacy of a laminar sublayer model for the film. A theoretical analysis of the heat transfer from a heated wall film giving consideration to this new physical picture has not yet been carried out due to the qualitative nature of these new ideas. Despite the shortcomings of their models, it has been the classical analysis of Fage, Falkner (8), Ludweig (13) and others which has led to the development of the hot film technique and although modifications to account for the newly observed phenomenon will certainly appear in the future, the classical analysis still provides simple physical insight into the hot film method.

3.1.1 Fage and Falkner

A mathematical theory for the steady state heat transfer from a surface to a laminar, two dimensional boundary layer was developed as early as 1931 by Fage and Falkner (8). Their derivation is based upon a consideration of the heat balance for conduction and convection at a point in the linear wall region of the boundary layer. A solution for the temperature distribution in the layer was deduced and used to obtain an expression for the normal gradient of temperature at the wall. The intensity of heat transfer from a flat boundary surface could then be expressed in terms of the boundary layer variables by employing the Fourier rate equation. The theoretical result at which they arrived was that for the steady state case of a heated plate, maintained at constant temperature elevation, and of fixed dimensions, the total heat transfer from the plate is proportioned to the square root of the free stream velocity. Assuming the Blasius solution for the laminar boundary layer wall shear stress ($\tau \propto Vo^{3/2}$), Fage and Falkner had theoretically predicted that the heat transfer from the plate is proportional to the cube root of the wall shear stress. The prediction was verified experimentally by themselves for relatively large foil plates of various rectangular dimensions. The total heat transfer from the foil was determined by a measurement of the joule heat loss. Speculating upon the usefulness of their findings when the boundary layer is turbulent, they performed four experiments in different turbulent boundary layers and concluded that the heat transfer from the foil was not affected by the turbulence.

Further, they found that their theoretical predictions were rather insensitive to the assumption of a linear wall region.

3.1.2 Ludweig and Tillman

H. Ludweig, in 1950 (13), considered the specific case of steady state heat transfer from a heated wall to a turbulent boundary layer when, in general, the thermal boundary layer extends beyond the linear region of the flow. The basic differential equation for the heat transfer was written as

$$\rho C_p (\vec{w} \text{ grad } T) - \text{div } (\lambda_{eff} \text{ grad } T) = 0$$

which is in the same form as that used by Fage and Falkner, except that an effective thermal conductivity (λ_{eff}) has been used to account for the apparent increase in thermal conductivity due to turbulent exchange. The effective thermal conductivity was shown to be a function of Y+ and Pr. Without actually solving the differential equation, Ludweig deduced an expression for the temperature distribution which involves an unknown function of U+, Y+ and the fluid constants. Application of the derived temperature distribution to the evaluation of the Fourier rate equation at the wall demonstrated the existence of a unique functional relationship between the heat transfer and U+ combined with physical constants of the fluid and wall. The diminsionless velocity U+ is defined in terms of τ_w ($U^* \equiv \sqrt{\frac{\tau_w}{\rho}}$), so that aside from the non-dynamic constants of the fluid and wall, and of course the difference in temperature between the film and the fluid, the heat loss from a heated wall element to the turbulent boundary

layer was shown to be uniquely related to the wall shear stress by a function which could be determined by calibration. Specializing the situation to the simpler case for which the thermal boundary layer above the heated wall plate lies entirely within the linear region of the turbulent boundary layer, Ludweig showed that the heat loss is actually dependent upon the cube root of the wall shear stress. Guided by these theoretical considerations, Ludweig designed and calibrated a heated plate shear stress measuring instrument.

Ludweig and Tillman (14) used Ludweig's instrument for measurement of the wall shear stress in the turbulent boundary layers occurring in channel flow under varying pressure gradient conditions. The device was calibrated in a plate flow situation using shear stresses evaluated from the Shultz-Grunow formula, but only sparse detail is given concerning the actual hot plate operation. The experimenters point out that the hot plate instrument is not affected by secondary flows, presumably because secondary flows do not penetrate into the laminar-like sublayer assumed for their model. Considering the newer sublayer models, their claim can be justifiably questioned.

3.1.3 Liepmann and Skinner

In 1954 Liepmann and Skinner (12) considered the operation of a heated element in laminar flow from a dimensional point of view. They too derived a 1/3 power relationship between the heat transfer from a short heated strip and the wall shear stress. Their approach was to develop an expression for the thickness (ϕ) of the thermal

boundary layer which arises from the conduction of heat into the fluid and the downstream transport. Exploiting the analogy between heat and momentum transfer they were able to write ϕ as a function of the fluid constants and the wall shear stress. The quantity $\Delta T/\phi$, where ΔT is the difference bewteen the heated film and free stream temperatures, was taken as a representative temperature gradient for the thermal boundary layer. The Fourier rate equation was then used to relate the heat transfer at the wall (q_w) to the wall shear stress. By this procedure they demonstrated that

$$q_w \propto \Delta T \cdot \tau_w^{1/3}$$

for a fixed probe position. Liepmann and Skinner assumed the existence of a laminar-like sublayer to generalize their derivation to the turbulent boundary layer case.

A discussion of the effects of compressibility and changing ΔT for high Mach number flow is of particular interest in their paper. While our tunnel speeds are low enough to assume incompressible flow, we do experience fairly large flow temperature changes due to mechanical heating at the fan. Their point is that as long as the ΔT changes are small enough to not significantly affect the physical constants of the fluid and particularly the dynamic viscosity, then the calibration constants for the sensor will not change. More recently Bellhouse and Shultz (4) have quantified this result by stating that for changes in ΔT of up to $4^{o}C.$, the calibration coefficients A and B in the equation

$$\tau_w^{1/3} = A \frac{q_w}{\Delta T} + B$$

may be treated as constants, provided of course ΔT is changed. Using either the simple power law for viscosity suggested by Liepmann and Skinner,

$$\frac{\mu_1}{\mu_2} = \left(\frac{T_1}{T_2}\right)^{.76}$$

T_1 and T_2 are absolute termperatures

or by interpolation of tabulated viscosity measurements, it can be found that a change in the flow temperature of $5^{o}F$ can cause a near 1.3% change in the dynamic viscosity at typical film operating temperatures.

Liepmann and Skinner developed and tested a heated wire sensing element which was cemented flush into a groove in the wall. The behavior of the wire was found to be similar to that for Ludweig's heated plate and again provided experimental confirmation of the 1/3 power calibration equation.

3.2 Hot Film Equipment

The Disa subminiature probe model number 55A93* was used for the hot film measurements in this study. The sensor element is a rectangular nickel film .75 mm. by .15 mm. which is sputtered onto the flat end of a cylindrical quartz rod. The film is overlayed with a protective quartz coating. The particular probe model used in our

*Available from Disa Electronik A/S, DK-2730, Herlev, Denmark

experiments was equipped with a 3 μ quartz layer which is thicker than on a similar model designed specifically for non conducting fluids. While the increased thermal inertia caused by the thicker quartz layer decreased the high frequency response of the film at maximum velocity from 175 KHZ to 30 KHZ (manufacturer's figures) this was not considered to be a problem for mean shear stress measurements. Also any decrease in the heat transfer from the film to the flow due to this thicker quartz layer is accounted for in the calibration of the probe.

A mounting block was designed to hold the probe and allow for adjustment of its position in the pipe (figure 4). The block provides a snug sliding fit for the cylindrical probe body. A set screw secures the probe once its depth into the pipe wall has been adjusted. A piece of wind tunnel pipe 105 cm. in length was chosen as a test section. Ten holes spaced in a line at 4 in. intervals were provided along this section to receive the probe and its mounting block. The latter could be secured to the outside of the pipe with two screws. Holes not in use were fitted with plugs. A pair of diametrically opposed static pressure holes were drilled and fitted with taps on the pipe circumferences for each mounting hole. Once the probe was fitted into the mounting block, it could be calibrated in the fully developed turbulent flow region against the shear stress values inferred from the static pressure gradient along the test section. Movement of the test section as a whole to different positions in the tunnel was not expected to change probe calibration and would facilitate

measurements at roughly 10 diameter intervals. Further, it was hoped that transferring the mounting block and probe to other mounting holes in the test section would not change the heat transfer from the film to the pipe and hence would not require recalibration. As detailed in Appendix V, this was not found to be the case.

The film was operated in the standard constant temperature anemometer configuration using the Disa model 55M01 main anemometer unit and standard bridge 55M10 (5 m. cable mode). Mean bridge voltages were measured using the Disa model 55D31 digital voltmeter equipped with a variable time constant.

3.3 Probe Mounting Procedure

When considering the mounting of the flat film probe into the curved pipe wall, it is necessary to decide upon some criteria and corresponding tolerances for the term "flush". Certainly for adequate operation we require that the film and the bottom of the thermal boundary layer above the film be within the laminar sublayer region. Also, any protrusion of the probe into the flow must not appreciably disturb the flow over the probe. To satisfy these criteria with a comfortable margin of error, Geremia (9) has suggested that the maximum permissible protrusion of the probe should be an order of magnitude less than the sublayer thickness. Considering the sublayer region to extend from the wall to a Y+ of 5.0 and using the definition of Y+, this maximum permissible protrusion is given by $.5\sqrt{U^*}$. This quantity was evaluated using U* values determined by the pressure

gradient technique for fully developed turbulent flow. The maximum permissible protrusion ranges from .094 to .035 mm. as the tunnel Reynolds number, based on diameter and centerline velocity at 37 diameters, varies from 47,000 to 169,000. Using a 4 in. pipe and a similar Disa probe with the same flat end diameter of 2.1 mm., Geremia has calculated that the center of the probe protrudes .012 mm. into the flow when the face of the probe forms a chord for the pipe cross section.

The required accuracy for mounting was achieved by observing the inside wall of the test section pipe at a glancing angle with a 400 power binocular microscope. The probe was slid into the mounting block which had been positioned in the first mounting hole. The probe was rotated to align the longest side of the film with the pipe axis and was inserted to a depth which made the edges on a chord perpendicular to the pipe axis appear flush under the microscope. Subsequent removal and insertion of the probe into either the first or last holes on the test section did not appear to change this probe mounting. Other mounting holes could not be checked with the microscope.

In addition to the requirement that the film lie within the sublayer, we also require that the probe be operated within limits such that the thermal boundary layer above the probe lies within the sublayer region. Criteria for this condition and analysis for our probe are presented in Appendix III.

3.4 Probe Orientation

If we consider the physically naive laminar-like sublayer model, our primary consideration for film orientation is that the thermal boundary layer, at least over the extent of the film, be thin and certainly not much greater than the sublayer thickness. This is achieved by minimizing the length of the heated sensor in the main stream direction. No particular consideration is required for the transverse film dimension. However, as previously mentioned, it is obvious from current sublayer work that the sublayer has a turbulent structure and the wall shear stress has a corresponding fluctuating component. Morrison and Kronauer (16) have presented spectrum results for turbulent pipe flow which indicate that near the wall (Y+ = 3.80) fluid velocity fluctuations occur with a wave length approximately three times longer in the axial direction than in the circumferential direction. This indicates that for comparable spatial averaging of the fluctuating shear stress, it would be reasonable to have the axial dimension of the sensor approximately 3 times that of the circumferential dimension. This is nearly accomplished by the dimensions and orientation of our film.

3.5 Hot Film Operation

3.5.1 Measurement technique

The hot film probe was operated in the usual constant temperature mode at a constant resistance (Rprobe) of 12.50 ohms as set on the Disa anemometer. This corresponds to an overheat ratio for the probe

of approximately .6. The nominal sensor resistance at 20°C, as specified by the manufacture was 7.08 ohms with lead resistances equal to 1.00 ohms. Characteristic anemometer output voltages for this operating point were in the range of 7.5 to 8.5 volts, depending upon both the tunnel air temperature, the ambient laboratory temperature and of course the flow conditions.

Because of the relatively large fractional change in the sensor resistance per degree change in temperature, the nickel film could be used as a highly sensitive resistance thermometer. A measurement of the film cold resistance (Rcold) was taken with the anemometer bridge before and after each shear stress measurement. Using this resistance, measured to within .002 ohm, and the temperature coefficient of resistance for the film, the actual cold film temperature was deduced. When the film was then heated to the operating resistance in preparation for a shear stress measurement, a good estimate of the true temperature elevation of the film above the tunnel ambient was obtained. This procedure was particularly important for the higher Reynolds number flows where the tunnel ambient temperature could rise as much as 20°F above the lab ambient.

The probe temperature elevation and the mean joule heat loss from the probe are sufficient data to determine the shear stress from the probe calibration. The mean joule heat loss was calculated from the mean anemometer output voltage which is the mean voltage applied to the series combination of the bridge top resistance (50 ohms) the lead resistance (1 ohm), and the sensor resistance (Rsensor = 11.50 ohms). Since, in operation, the only effective variable resistance is the sensor, the voltage

drop across the hot film (Vfilm) is found by multiplying the anemometer output by the ratio

$$\frac{\text{Rsensor}}{\text{Rsensor} + 51.0}$$

The film power loss is then given by

$$\frac{(\text{Vfilm})^2}{\text{Rsensor}}.$$

Thermal stability for the electronic equipment was maintained by allowing the units to remain powered during the entire course of the experimental work. Drift was not considered to be a problem and in general the anemometer behaved dependably.

3.5.2 Thermal characteristics

Many measurements of the unheated film resistance at different flow temperatures were taken during the course of the experiment (figure 5). These were used to determine the temperature coefficient of resistivity (α) for the film. After thermal equilibration, when the tunnel had been running for a long time, the temperature of the air flowing in the diffuser was considered to be nearly the same temperature as the unheated flush mounted sensor. The diffuser air temperature was measured to within .2 degrees F. using a mercury in glass thermometer suspended in the diffuser flow. The least squares linear regression equation for the temperature and sensor resistance data was found to be

$$\text{Rcold} = 14.17 \times 10^{-2}\ T\ ^{0}\text{F} + 6.076$$

with a standard error in the regression coefficient of $.06 \times 10^{-2}$. The

α value at 20°C deduced from this result was found to be .338 $^{+\ .061}_{-\ .020}$ %/°C where the errors were calculated from extreme error limit lines for the graph. This value compares favorably with the manufacturer's specification of .35%/°C.

The extreme sensitivity of the film resistance to temperature change is illustrated by the observation that putting a hand on the tunnel pipe in the vicinity of the probe mounting could warm the probe sufficiently after a minute to cause readily noticeable changes in the balance of the anemometer bridge used to measure the cold resistance.

While the cold sensor resistance at 20°C was estimated to be 7.029 ohms by the least squares method, based on all the data points, probably a more accurate estimate is 7.037 ohms based on a visual linear fit of the data, excluding the most scattered points. The nominal Disa value for the sensor resistance at 20°C is 7.08 ohms.

3.6 Probe Calibration

3.6.1 Principle

The operating point of the hot film probe is defined by its elevation temperature ΔTo (the difference between the probe temperature and the ambient tunnel air temperature) and by the film power dissipation. Briefly, the theoretical analysis of the probe operation has led to the 1/3 power law relating the probe operating point to the wall shear stress. The equation is written in the form

$$\tau_w{}^{1/3} = A \frac{q_w}{\Delta To} + B$$

where A and B are generally functions of the probe operating point but may be treated as constants for small elevation temperature ranges. The object of the hot film calibration procedure is to obtain experimentally the relationship between the three variables, wall shear stress, probe elevation temperature and power dissipation and to compare the actual probe behavior with this theoretical 1/3 power equation. Having assessed the validity of the theoretical equation, an analytic fit of the calibration data can be attempted.

The probe is mounted in the fully developed flow region so that an independent pressure gradient technique can be used to measure the wall shear stress variable. Having calibrated the probe, a measurement of the probe operating point determines the wall shear stress. The same calibration can be applied to other probe locations along the wall where the sublayer mean velocity profile is similar. For developing pipe flow, the wall region is assumed to react quickly to the presence of the wall and is expected to have achieved universality where the outer boundary layer and core regions are still developing. This implies that the probe calibration can be used to infer wall shear stresses at downstream positions where the core region has not yet achieved the fully developed structure. For calibration purposes, the wall shear stress is varied by adjustment of the tunnel speed. The film operating point can be changed by adjusting the anemometer overheat ratio to operate the film at different resistances and therefore different temperature elevations. The mean anemometer output voltage could be used directly to calculate the total anemometer bridge power

dissipation. Alternately, the actual film power loss can be obtained as described in the film operation section.

3.6.2 Calibration technique

Briefly, the calibration procedure consisted of an adjustment of the tunnel speed, a systematic variation of the probe operating resistance with corresponding mean anemometer output voltage measurements, and a measurement of the differential wall static pressures along the test section. The test section was located well downstream of the contraction cone where the flow was considered to be fully developed.

After some preliminary calibration work, twelve contraction cone pressures were adopted for the primary calibration. The selection covered a range of wall shear stresses up to .387 mm. of water. The measurement range was limited by the extreme nonlinearity of the probe output voltage which rendered high values of shear stress unresolvable (theoretically $\tau_w \propto V^6_{film}$) The highest contraction cone pressures utilized were near 112 mm. of water while the tunnel is easily capable of 190 mm. of water.

The probe elevation temperature range included in the calibration was adequate to cover the changes in elevation temperature introduced by the variation of the tunnel air temperature with fan speed. The probe elevation temperature was changed by systematically decreasing the film operating resistance from 12.50 ohms to 11.80 ohms in steps of .02 ohms as indicated on the anemometer equipment. The anemometer output voltage was offset by a fixed voltage of 7.30 volts on the Disa signal

conditioner and was then measurable on the millivolt scale of the Disa digital voltmeter. The voltmeter was adjusted for a long time constant input filter to give a good average value. While millivolt sensitivity was obtained in this manner, the overall error in the probe output voltage could have been as large as .01 volt. This error was due to slow random drifting of the offset voltage which could be observed with a differential voltmeter. Increased accuracy and resolution of higher shear stresses could have been obtained had a wide range integrating millivoltmeter been available.

Static pressure gradients were determined from pressure measurements taken at the test section piezometric rings using the Hero variable inclination methanol manometer. The differential static pressures were measured at each of the nine tap positions relative to tap No. 1, covering a pipe length of 36 in. Fairly long tubing was used to the pressure rings in an effort to increase the manometer time constant and smooth out pressure fluctuations.

The probe was calibrated 3 times in all. The primary calibration provided the data used to infer shear stresses from the probe operating point when the probe was subsequently located in the developing pipe flow region. After these developing flow measurements were completed a second calibration was performed to check on drift. For this checking purpose the calibration did not need to be as extensive as the primary calibration and only 3 shear stress values were used. The final calibration was performed with the probe mounted in test position No. 10 rather than No. 1. This was done so that the calibrated probe could be

used for stress measurements in the region immediately behind the roughness section. These three calibrations are referred to by numbers 1 to 3 respectively. The calibration shear stresses are tabulated in tables I to III

3.6.3 Calibration data

The differential static pressure measurements used to determine the calibration wall shear stresses are plotted on figure 6 for the primary calibration. A best fit line for each set of data was fitted by eye. It can be seen that taps No. 6 and No. 9 consistently gave pressure differential readings which appear to be low. Considering these apparently systematic errors, it was decided that the best results could be obtained by a subjective fit rather than by a purely analytic least squares fit. The required static pressure gradients were determined from the slopes of these fitted lines. The corresponding wall shear stress values were calculated by using the equation

$$\tau_w = - \frac{dP}{dX} \frac{R}{2}$$

which is developed in Appendix I.

The shear stresses determined by this pressure gradient technique are plotted parametrically with the probe operating point calibration data for the primary calibration in figures 7(a) and 7(b). Figure (a) displays the total anemometer bridge power loss on the abscissa while figure (b) shows the actual film power loss. The actual film power loss for calibration 2 and 3 are plotted in figures

7(c) and 7(d) respectively. Any of the 3 variables could have been chosen as the parametric variable, but our calibration procedure made this representation the most direct. The parametric curves define the calibrated operating "surface" in the three variable space of wall shear stress, film power loss, and film temperature elevation. To a first approximation these parametric curves are parallel and linear. These calibration plots could have been used directly to interpolate the shear stresses graphically from the probe operating points. Interpolation is difficult and inaccurate because of the non-linearity of the shear stress parameter for the curves. For operational use, it was found necessary to reduce the calibration data into an analytic form.

3.6.4 Analytic fit

The linearity and parallelism of the parametric calibration curves over the calibration range of the probe indicates a constant ratio between the power dissipation and the film elevation temperature for a fixed shear stress and suggests the utility of this ratio in reducing the calibration data. Following the theoretical form of the calibration equation, the calibration data was replotted using the ratio of the film power loss (Pfilm) to temperature elevation (ΔT) as the ordinate and the cube root of the wall shear stress as abscissa, with the temperature elevation as a parameter (figure 8). The temperature elevation parameter was restricted to a range of $295 \pm 10^{o}F$ which covers the ranges experienced due to tunnel temperature

variations. 295°F was chosen as a typical film elevation temperature.

The parametric curves are nearly parallel and are assumed to be so for the purposes of a simple analytic fit. Using the least squares method a linear equation was first fitted to the 295°F parametric curve for the primary calibration. The slope coefficient A and the intercept coefficient B in the fitted equation

$$\frac{Pfilm}{\Delta T} = A \tau_w^{1/3} + B$$

were found to have the values .0290 and .1104 respectively. The slope of the corresponding linear fit calibration lines for other ΔT's has approximately the same value. The intercept B is dependent on the ΔT parameter. The nature of this dependence was determined by plotting the ratio variable (Pfilm/ΔT) against ΔT for a fixed shear stress value. (any shear stress value could be chosen since the slopes of the parametric ΔT curves were all the same). The resultant graph (figure 9) shows that the variation of the intercept with the temperature elevation variable is linear. A subsequent linear fit of this plot led to the result that the appropriate correction to the ΔT = 295°F intercept to obtain the intercept for some other ΔT is given by

$$- 8.0 \times 10^{-5} (\Delta T - 295).$$

When combined with the equation for the 295°F line, the complete calibration is described by the single analytic expression

$$\frac{Pfilm}{\Delta T} = .0290 \tau_w^{1/3} + (.1104 - 8.0 \times 10^{-5} (\Delta T - 295)).$$

This expression could be rearranged and solved to give the calibrated wall shear stress for any combination of probe temperature elevation and power loss.

A similar procedure was followed to obtain an analytic expression for the final calibration (calibration 3). The analytic result in this case was found to be

$$\frac{Pfilm}{\Delta T} = .0290\,\tau_w^{1/3} + (.1115 - 9.0 \times 10^{-5}\,(\Delta T - 295)).$$

These analytic fits to the calibration data have been used extensively for the calculation of the shear stresses from the probe measurements taken at other pipe locations.

3.6.5 Discussion

The coefficients A and B determined for the analytical description of the probe calibration are purely empirical and can not be expected to apply to other probes or even to our probe when operating in a different range of shear stresses or elevation temperatures. Not only can the calibration equation coefficients vary, but for larger wall shears or elevation temperatures the 1/3 power law itself may break down.

No attempt was made to determine the temperature dependence of the coefficient A because of the parallel character of the calibration lines over the temperature elevation range. The temperature dependence of the B coefficient is small, changing B only by approximately 1% for changes in the elevation temperature of $10^{o}F$.

This confirms the statement of Bellhouse and Shultz (4) claiming that the calibration coefficient may be treated as constants for temperature changes of up to $4^{o}C$. Note however, that while any corrections to A or B are themselves minor, it is necessary to change ΔT in the Pfilm /ΔT ratio. This requirement is illustrated clearly by the seemingly anomalous probe behavior observed during preliminary calibration work on a graph of probe power loss versus wall shear stress (figure 10). As higher wall shear stresses and fan speeds were achieved, the tunnel air temperature rose and in this way the probe elevation temperature decreased despite the constant film temperature operation mode. The relationship between the direct, uncorrected probe output voltage and the tunnel speed and temperature is discussed in more detail and with reference to some preliminary experimentation in Appendix IV.

As seen from the respective values of A for the two different probe mountings (calibrations 1 and 3), change in mounting did not affect the slope of the calibration data curves. Only the intercepts for different ΔT values have been altered such that the ΔT values for the final calibration have been generally shifted from the primary calibration $295^{o}F$ line and have been spread apart; that is, the intercepts have been both shifted and scaled by changing the probe mounting. The intercept coefficient B for a given ΔT is directly related to the power dissipation from the probe when there is a no flow and hence a zero shear stress condition. Considering that a large percentage of the heat loss from the film occurs by conduction through the probe substrate and eventually through the mounting block,

it is understandable that mounting changes can alter this B term. Despite the fact that numerically, the B coefficient has been changed by only about 1%, the overall change in the calibration is considerable as observed by direct comparison of figure 7(d) with figure 7(b) for the primary calibration. This is again because the 1% change in the total power loss from the film is quite significant relative to the small percentage of the total film power loss due to convection over the probe. This indicates that a good mounting block design to maintain a constant calibration despite mounting changes must ensure that the thermal conductivity from the probe body to the mounting is a constant value. This was a basic fault in our mounting block design.

The slope coefficient A is related to the heat loss from the probe due to the convective shear flow over the probe. It is encouraging that the coefficient has the same value for both mounting calibrations, indicating that the flow dynamics over the probe and hence probe mounting geometry are similar.

We note finally that some attempts were made to interpolate wall shear stress values directly on the original calibration graphs using a computer technique. This proved to suffer from the same inaccuracy to which visual interpolation was subject; namely, the extreme non-linear dependence of the probe operating point on the shear stress variable. No improvement was attainable using the calibration data directly rather than using the analytic equations. In the same way it is felt that no significant improvements in accuracy were possible by using higher order analytic computer fits

of the calibration data although such analysis could become necessary if much larger ranges of elevation temperature were experienced.

4. HOT FILM MEASUREMENTS

4.1 Summary of Data

Hot film skin friction measurements were taken at 8 axial positions in all. The test section was moved several times throughout the course of the experiment. The various pipe arrangements used to obtain the range of axial positions are illustrated in figure 11. The axial positions have been measured relative to the beginning of the roughness element. At each pipe move care was taken to ensure that the probe itself was not disturbed and that the overall tunnel geometry was not changed. The primary calibration was used to interpret the wall shear stress values from the probe output for all of the positions except the position nearest to the contraction cone (X/D = 1.5). At this position, because the probe had been transferred to the opposite end of the test section pipe and recalibrated, the newer calibration (calibration 3) was used. At least eleven Reynolds numbers were studied at each axial position. In this way it was hoped that a fairly complete picture of shear stresses in developing flows would emerge. The measured experimental data and the derived quantities are tabulated in tables IV - XI. Each table contains the data for a particular axial position for the probe (see pp. 99 - 108).

4.2 Measured Quantities and Calculations

The data record for each trial consisted of four groups of measurements.

1. Ambient laboratory conditions of room temperature, aspirated wet bulb temperature and atmospheric pressure were measured before and after each trail. The average values were used to calculate the physical properties of the air.

2. The tunnel operation parameters consisting of the tunnel ambient air temperature at the diffuser outlet and the contraction cone pressure drop were recorded before and after each trial. The tunnel temperature along with the air moisture content determined from the ambient lab conditions were used to calculate the air density and viscosity in the tunnel. The density, viscosity and cone pressure drop were sufficient information to calculate the mean flow velocity from the calibration equation and hence the flow Reynolds' number was obtained. These basic calculations are detailed in Appendix II.

3. The unheated probe resistance at tunnel conditions was measured and then, when the probe was subsequently heated to its operating resistance, the anemometer output voltage from the probe was recorded. The film overheat temperature ΔT was calculated using the cold probe resistance and the temperature coefficient of resistivity for the probe. As detailed in the film operation section the anemometer output voltage was used to calculate the actual voltage across the film resistance and then the power

loss from the probe.

4. The differential static pressures along the test section and relative to tap number one were recorded for each trial.

4.3 Derived Friction Quantities

The film power loss and the elevation temperature values for each trial were substituted into the appropriate fitted analytic calibration equation presented in the calibration section to determine the shear stress value. The shear stress and the tunnel air density were combined to calculate the friction velocity (U*) according to the definition

$$U^* \equiv \sqrt{\frac{\tau_w}{\rho}} .$$

The skin friction coefficients (Cf) were calculated using these U* values and the mean flow velocity according to the definition

$$Cf \equiv 2 \left(\frac{U^*}{Umean}\right)^2 .$$

4.4 Probability Density Measurements

Aside from the mean friction quantities described above, the fast response of the hot film probe to turbulent fluctuations in the flow permitted an exploratory study into the dynamic behavior of the shear stress. To obtain a basic statistical description of this behavior the probability density function for the shear stress variable

was measured for some different Reynolds' numbers and axial positions. The measurements, technique and results are discussed together at a later point (sec. 8.6).

5. THE CLASSIC PRESTON TUBE TECHNIQUE

5.1 Principle

The Preston tube technique for the measurement of wall shear stress in a turbulent boundary layer is closely related to the hot film technique in that both methods depend upon similarity in the wall region of the flow. In principle, if the mean flow near the wall in different regions of a turbulent boundary layer can be described by equations of the same form, differing only in the local values of the flow variables such as ρ, ν, τ_w, etc., then it might be expected that the mean flow over an obstacle placed in similarity regions will be analogous and will produce related effects on the obstacle. In particular, Preston (18) has shown that the difference between the total pressure at the open end of a total pressure tube lying on the wall surface and facing into the flow, and the static pressure recorded at the wall, is only a function of the tube geometry, the physical constants of the fluid, and the wall shear stress. It is feasible to calibrate such a tube and static pressure tap arrangement in fully developed flow using the momentum balance static pressure gradient technique, so that a simple measurement of this pressure difference can be related to the wall shear stress. Preston demonstrated conclusively that his experimental findings were a consequence of wall region flow similarity. Since the success of the technique depends only on flow similarity in the immediate region of the probe we can utilize the Preston arrangement in regions where the

over-all flow may not be fully developed but where wall region mean flow similarity exists.

5.2 Preston Equipment

A Preston tube was constructed from a piece of brass tubing 44 mm. long (1.5 mm. o.d., .75 mm. i.d.). The tube end was bevelled and smoothed and the tube was mounted flush along the inside wall of a 25 cm. length of pipe. Four static pressure holes distributed around the pipe circumference 2 mm, behind the tube mouth were connected to the low pressure side of the Betz manometer, while the high pressure side was connected to the Preston total pressure tube. The pipe section as a unit was moved to obtain different axial positions along the tunnel. In this way the tube geometry could not vary from the initial calibration arrangement. The tubing to the manometer was kept long to minimize pressure fluctuations. Accurate differential pressure measurements could be made to within less than .1 mm. of water at the lower Reynolds numbers. Due to tunnel speed variations only an estimate to the nearest .1 mm was possible at higher speeds.

5.3 Calibration

The Preston tube was calibrated at an axial position of 76.6 pipe diameters. Calibration shear stress values were interpolated from the initial calibrated values which were derived from static pressure gradient measurements and were also used for the hot film calibration.

Following the technique suggested by Preston and followed by Patel (17) the non dimensional variables

$$x^* = \log_{10} \left(\frac{\Delta Pp\ d^2}{4\rho\ \nu^2}\right) \quad \text{and} \quad y^* = \log_{10} \left(\frac{\tau_w\ d^2}{4\rho\ \nu}\right)$$

were computed. ΔPp denotes the Preston tube measured differential pressure and d is the outside diameter of the tube. The calibration data has been plotted in this form in figure 12. The results obtained by Preston, Patel and the National Physical Lab are plotted on the same graph for comparison. Our data agrees well with the N.P.L. results and is fitted to within 1% by the simple linear expression

$$y^* = -1.561 + .9132\ x^* \ .$$

To relate the difference between our result and Preston's result, we have indicated the actual percentage variation in wall shear stress value corresponding to the separation between the data lines in these non-dimensional coordinates. Patel has commented that Preston's original calibration appears to contain an error which may account for the rather large disagreement between the N.P.L. results and Preston's results. Further, Patel suggests that Pitot displacement corrections to account for the velocity gradient across the Pitot tube may attribute to the discrepencies among various experimenters. No attempt has been made to correct our Preston tube results for these displacement effects. The linear calibration equation given above was used to compute the Preston tube wall shear stress values from all of the subsequent Preston tube differential pressure measurements.

5.4 Measurements

The axial positions for the Preston tube measurements were selected at approximately 5 diameter intervals. This rather high concentration of axial positions was considered to be necessary to verify conclusively the longitudinal behavior of the shear stress which had been indicated by preliminary analysis of the hot film data. It was felt that 5 diameters was about the minimum axial separation over which significant changes in the Preston tube readings could be resolved. Seven Reynolds' numbers in the range of 25,000 to 165,000 (mean and radius) were chosen. The air density and viscosity were calculated for each trial from measurements of the ambient lab and tunnel conditions just as for the hot film measurements. The quantity $\log_{10} \left(\frac{\Delta Pp\ d^2}{4\rho\ \nu^2}\right)$ was determined for each trial and τ_w was calculated using the formula

$$\tau_w = \text{ALOG}_{10}\ (-1.561 + \log_{10}\ (\Delta Pp) + (-.086758\ \log_{10}\ (\frac{\Delta Pp\ d^2}{4\rho\ \nu^2}\ ))$$

which is derived directly from the Preston tube calibration equation. The final shear stress results are tabulated in Table XII.

6. VELOCITY PROFILE MEASUREMENTS

In conjunction with the shear stress measurements, an extensive program of velocity profile measurements has been undertaken for our tunnel. It was clear that to obtain some physical insight into the shear stress measurements, it would be necessary to have a clear picture of how the overall flow character and the wall shear stress variable are related. Further, we wished to check upon the utility of the cross plotting technique introduced by Runstadler, Kline and Reynolds (21) for the determination of wall shear stresses from profile measurements. It was realized that the required assumption of a flow similarity law could severely limit the applicability of the method for our developing flow profiles.

In order to obtain as complete a picture as practicable, profile data was taken at 12 axial positions at approximately 5 diameter intervals along the tunnel pipe and for 7 Re(m,r) numbers ranging from 50,000 to 152,000 (except for the position X/D = 72.3, where fully developed flow was considered to exist and a more detailed study with 13 Reynolds numbers was carried out).

The dynamic pressures, and hence velocity profiles, were obtained from differential pressure measurements (Betz manometer) between a traversing total pressure tube and a piezometric ring. The pressure ring had 4 static pressure taps distributed around the pipe circumference. The total pressure tube was constructed from thin walled 1 mm. o.d. stainless steel tubing. The assumption of a constant static pressure across the tunnel had been verified to

within 2 - 3% by traverses with a static pressure tube for a wide range of Reynolds numbers at an axial position near 36 diameters.

The traversing mechanism employed a long, finely threaded screw for positioning and as a result was subject to some backlash error in setting. This became particularly apparent for positions near the wall where slight errors in position could cause considerable changes in the dynamic pressure measurement. Although a continuous traverse across the pipe was utilized to minimize the backlash error, it is possible that the overall uncertainty in the positions relative to the pipe wall could amount to 1 mm. A total of 60 differential pressure measurements were recorded to each traverse of the pipe diameter. For the region within 1 cm. of the wall on either end of the traverse, data was taken at 1 mm. intervals, while in the central flow this interval was increased to 2 mm. The raw and reduced data has been extensively tabulated and put in a form suitable for computer analysis.

Much work remains to be done before the full potential for this large mass of experimental data is achieved. At this point, aside from the cross plot profile analysis, only a few preliminary studies, which have been immediately useful for construction of a physical model to account for our shear stress measurements, have been undertaken. Although a fair amount of numerical work dealing with developing turbulent pipe flow has been published, the actual amount of experimental data has been surprisingly sparse such that our data may at present be among the most complete available.

7. CROSS PLOTTING TECHNIQUE FOR FRICTION VELOCITY

7.1 Principle

The cross plotting technique introduced by Runstadler, Kline and Reynolds (21) to obtain the wall shear stress from velocity profile measurements assumes the existence of a universal velocity profile. Specifically, for fully developed flow, the widely accepted log law profile

$$\frac{U}{U^*} = A \log_{10} \left(Y \frac{U^*}{\nu} \right) + B \qquad \left(U^* = \sqrt{\frac{\tau_w}{\rho}} \right)$$

is taken as a constraint equation for (U, Y) pairs over some range of Y values. The values of ρ and ν are assumed to be constant and known for the flow. The empirical universal constants A and B have been determined by many experimentalists and for our purposes were assigned the values 5.6 and 5.0 after Coles (6). Theoretically, if it is known that this law describes the flow velocity profile over some radial range and if the values of the local variables ρ, ν and U* are known, then the profile in this range is completely specified. Conversely, if a (U, Y) pair is known along with ρ and ν then there is a unique U* value which exists such that the constraint equation is satisfied. Each experimentally determined (U, Y) pair which lies in the logarithmic region will yield such an estimate for the local friction velocity. An average of these estimates for the universal profile region is expected to be a good approximation for the actual friction velocity.

7.2 Application to Developing Flow

While the existence of the logarithmic universal law has been well established for fully developed flow and the usefulness of this cross plotting technique for developed flow has been illustrated by Shraub and Kline's work (23), a problem arises in developing flow where the identification of a logarithmic profile region becomes increasingly difficult as we consider positions closer to the pipe entrance. Compared to fully developed flow, the region over which the relatively flat profiles for developing flow can be described by the universal log law becomes greatly restricted. However, because of the smooth, monotonic nature of the profile, there is always some region (perhaps very small) over which the log law does accurately fit the profile—even for very flat profiles. Of course every (U, Y) pair can be used to generate a U* estimate, but only for the radial region where the flow actually follows the universal log law will these U* estimates be clustered around and indicative of a single U* value.

To avoid this difficulty in identification of the region described by the universal law, the plotting method suggested by Shraub and Kline has been employed. U* estimates were calculated for every point in the profile regardless of its radial position with respect to the logarithmic region and these U* estimates were plotted against the radial position. For radial positions in the universal logarithmic region, the U* estimates should be scattered around a constant U* line, while for other positions, the data is expected to progressively deviate from this line. Our interest lies therefore

in the region of the plot for which the U* estimate is constant for a range of radial positions, or equivalently, where

$$\frac{\partial U^*_{\text{estimate}}}{\partial Y} = 0$$

For developing flow the radial range for which the U* estimates are constant may be very narrow because the universal log region is itself very small, but the criterion that is given above can always be applied. In practise it was found that as we proceeded through a typical profile computing U* estimates, the estimates were at first low near the wall, rose to a maximum and nearly constant value in the universal log region and then dropped again as we approached the pipe center. For less developed flow it was found that this plateau of constant U* estimates became a progressively sharper peak as the region fitted by the universal log law decreased.

The data generated by the cross plot of log technique is valid only so far as the developing flow profiles exhibit the same universal behavior as fully developed flow. While for near developed flow there is reason to expect that the profiles are nearly described by the universal log law, there is little justification for an assumption of any universal law for the developing flow. The values of friction velocity returned from the application of the cross plot technique are strictly valid only for fully developed flow and their numerical correctness for the developing flow is entirely a matter of speculation. Because of its dependence on the profiles, the greatest utility of the data in developing flow is as an indicator of changes in the trend of the profiles as they become fully developed.

7.3 Analysis Procedure

Newton-Ralphson iteration was applied to obtain the U* estimate which satifies the universal log law profile equation for a particular (U, Y) pair and known ρ and ν. Briefly, given some function $f(Z) = 0$ satisfying certain conditions, the root can be obtained by numerical iteration from an initial guess where the n^{th} estimate for the root is given by

$$Z_n = Z_{n-1} - \frac{f(X_{n-1})}{f'(X_{n-1})} .$$

To facilitate the use of this method, the universal law using Coles' parameters was programmed in the form

$$f(U^*) = \frac{\exp(L/U^*)}{U^*} - K = 0$$

where $L = \frac{U}{2.44}$ and $K = \frac{Y}{\nu \exp(-5.0/2.44)}$.

8. RESULTS AND ANALYSIS

8.1 Calibration Results

The static pressure gradient results have already been discussed in detail in connection with the hot film probe calibration (see part 3.6). At that point the pressure gradient results were presented for the three hot film calibrations and their method of analysis was discussed. These same measurements have been used for both the Preston tube calibration and for the non-dimensionalization of velocity profiles measured in the calibration region. For these purposes the required calibration shear stresses were interpolated graphically from a large scale plot of the pressure gradient shear stresses. This plot is reproduced in figure 13. We note that the relative scatter between the different calibrations is small which is indicative of the small experimental error in the pressure gradient calibration method.

8.2 Check on Fully Developed Flow

8.2.1 Universal friction law

The basis of the calibrations for both the Preston tube and the hot film techniques are wall shear stresses determined by the standard momentum balance method using longitudinal static pressure gradient measurements in the fully developed turbulent flow. It should be verified that our flow can indeed be accepted as fully developed. A check can be made by comparing the shear stresses determined by the pressure gradient method with the extensive experimental and theoretical results of other investigators.

Prandtl's universal law of friction for smooth pipes and fully developed turbulent flow is given in non dimensional form (refer to Schlichting (22)) by,

$$\frac{1}{\sqrt{\lambda}} = 2.0 \log_{10} (R(m,d) \sqrt{\lambda}) - .8$$

where λ is 4Cf. This result has been verified by Nikuradse and several others to be in excellent agreement with experimental data measured in fully developed flow and provides a convenient check of our calibration position flow. Our primary calibration shear stresses are plotted along with Prandtl's law in figure 14. Agreement between the theoretical result and our measurements is to within 2% which is within the accepted scatter of the experimental data cited to verify Prandtl's result.

The relative scatter among our data points on figure 14 is small. It is apparent from the graph that consistently smaller values of shear stress have been measured than those predicted by Prandtl's law and that the deviation of these values from Prandtl's law increases with Reynolds number. This small but consistent deviation may be indicative of an asymptotic approach of our flow to the fully developed case, however, the flow at 72.3 diameters may be called fully developed within accepted experimental standards. Data obtained from the completely independent cross plot of logarithms method, which is based upon velocity profiles measured in the calibration position, falls along a line which is nearly parallel to that for static pressure calibration data. This indicates that the small deviation

from Prandtl's law is a genuine characteristic of the pipe flow and adds further credibility to our calibration measurements.

Also included on this graph is the curve derived by Blasius for turbulent pipe flow.

$$\lambda = .3164\ (Re(m,d))^{-.25}\ .$$

This law has also been found to be useful for low Reynolds number turbulent flow. As observed by Schlichting, the Blasius equation agrees well with the Prandtl universal law up to Re $\simeq$ 100,000, but deviates progressively more beyond this point.

8.2.2 Velocity profile similarity

Prandtl's universal friction law and Blasius' friction equation are derived from analytic expressions for the universal mean velocity profile in the flow. In particular, the case for a universal logarithmic profile region for fully developed turbulent pipe flow has been well established experimentally (see the review by Coles (6)). Velocity profiles measured over a range of Reynolds numbers at our calibration position and expressed in terms of the dimensionless velocity $U+ = \frac{U}{U*}$ and the dimensionless radial position $Y+ = Y\frac{U*}{\nu}$, using friction velocities derived from shear stress values interpolated from the calibration measurements, are presented in figure 15. The logarithmic "laws" established experimentally by Nikuradse (curve B), Patel (curve C) and Coles (curve D) are presented for comparison.

Our profile data is logarithmic over an extensive radial region although, as exhibited by our data, this logarithmic profile must break down both near the pipe center, and in the immediate vicinity of the wall. Near the wall both the failure to correct for displacement effects caused by large velocity gradients across the end of the total pressure tube and the small errors in the radial positioning of the traversing mechanism can account for the increased data scatter and the deviation from the log law.

The accentuated slope of the logarithmic region of our profile data relative to the results of other investigators and the slight dependence of this logarithmic region on Reynolds number does not necessarily indicate that the flow is not fully developed. The various experimentally determined log law coefficients which appear in the literature are somewhat dependent on the particular experimental facility. The possibility of a Reynolds number dependence for the log law and hence no strict universality is still an unsettled question. Hinze (10) has illustrated this point using data from several sources. More recently the Reynolds number dependence of the universal log law has been discussed by Afzal and Yajnik (1), although their work deals with lower Reynolds number flows (Re(m,d) up to 10000).

The theoretically derived Blasius seventh power law velocity profile has also been plotted on figure 15 using the dimensionless co-ordinates (curve A). The Blasius profile is in fair agreement with our data over a considerable range and provides a better fit to the

data near the pipe center than the log law profiles.

8.3 Hot Film and Preston Tube Friction Results

8.3.1 Friction velocity data

The axial dependence of the wall shear stress as measured with the hot film probe is illustrated in figure 16, where friction velocity has been plotted against axial position with Reynolds number as a parameter. The axial position has been non-dimensionalized using the tunnel pipe diameter. Since the measurements for different axial positions for a particular Reynolds number were taken at different times and it was not always possible to readjust the tunnel operating point to precisely the same Reynolds number, the average has been taken as the nominal value. Variation of the actual Reynolds numbers around the nominal number was typically less than 2%.

The data for axial positions greater than 35 diameters from the inlet is quite regular and conforms well with the calibration values at 73.0 diameters. The relatively small data scatter in this region characterizes the experimental error associated with the hot film technique. The variation of the measurements at 57.4 diameters relative to the calibration values yields an error estimate of about 3%.

In the axial range between 10 and 35 diameters the data displays a minimum in friction velocity values. While most conspicuous for the higher Reynolds numbers, this phenomenon occurs

with near the same fractional change in U* values for the lowest Reynolds numbers. The trend for increased friction velocities as we consider axial positions closer to the pipe entrance than this minimum is curtailed for positions in the immediate vicinity of the entrance. This abatement of friction velocities at the entrance exhibits a marked dependence on Reynolds number such that for the highest group of Reynolds numbers the entrance region values are much lower than for the fully developed flow region, while for the lowest Reynolds numbers the friction velocities are actually higher than at any other position.

The Preston tube results (figure 17), with their increased density of axial positions, confirm the trends suggested by the hot film data. Although these features are less accentuated, the excellent agreement between adjacent axial measurements and the overall smoothness of the data attest to their significance. It is evident from a comparison of a few similar Reynolds numbers (figure 18) that the Preston tube is less responsive to the wall shear stress than the hot film device.

8.3.2 Preston tube insensitivity

To account for the relative insensitivity of the Preston tube we must re-examine the theoretical background for the technique. Ludweig and Tillman were the first to present experimental evidence (14) for the now widely accepted fact that if the variables U and Y describing the mean axial velocity at a distance Y above the wall are scaled by combinations of the local flow quantities ν, ρ and τ_w (in

the form $Y+ = \frac{U\tau}{\nu} Y$; $U+ = (\frac{1}{U\tau}) U$) then, in a limited region near the surface, the boundary layer velocity profiles can all be described by the same function

$$F\ (U+,\ Y+) = 0\ .$$

This is what is meant by the expression "wall region similarity". In particular, this implies that a measurement of U and Y quantities for the profile and a knowledge of the constraint function F are sufficient to determine the scaling factors. Every pair of U and Y measurements for a particular profile in this limited wall region must satisfy F and will lead to the same fixed scaling factors. Alternately, the measurement of some quantity X which is a function of the velocity profile and whose measurement specifies some (U, Y) point on the profile, and hence a (U, Y) pair that satisfies F, is sufficient information, along with the constraint F, to fix the scaling factors. (In the particular case of the Preston tube technique X is a measurement of the dynamic pressure a fixed distance from the wall). That is, there exists a functional relationship G between X and the local variables $\nu,\ \rho, \tau_w$ which can be expressed in the form

$$X = G\ (\nu,\ \rho, \tau_w)\ .$$

In particular, there then exists a function H and a non-dimensional combination of the local variables ℓ, such that

$$H\ (X',\ \ell) = 0,$$

where X' is the measurement of X non-dimensionalized by the local

variables. This H is again a universal function which will be valid wherever the constraint F holds. H can be determined by calibration. This is in essence the justification for the technique as given by Preston (18).

We see that the Preston measurement is related to the shear stress only so far as the Preston measurement characterizes the velocity profile, which is related through the wall region profile similarity to the wall shear stress.

Changes in the wall shear stress, while directly reflected by the profile velocity gradient in the sublayer, do not necessarily cause large changes in the profile farther out in the similarity region, where the Preston tube center is located. This is especially true for the logarithmic part of the similarity region where the scaled U and Y variables are related by the log function which is relatively insensitive to changes in its argument—as compared to say the linear region which exists in the sublayer. As we move farther out from the wall into the similarity region through first the linear sublayer region and then the log region, we find that the profile is progressively less sensitive to perturbation in the wall shear stress. For the Preston tube this is potentially a critical factor where the similarity region may be extremely thin—such as near the beginning of the boundary layer. In contrast to this indirect measurement of shear stress through the similarity law, the convective heat transfer from the hot film probe is directly associated with the flow, and in particular, the velocity gradient in the immediate vicinity of the wall. Thus it is

not unexpected that the Preston tube results are not as responsive to the wall shear stress as are those for the hot film.

In addition we might mention at this point that the Preston tube is subject to the usual integrating and displacement effects experienced by any total pressure tube. The Preston tube measurement is effectively a spatially averaged value over the open end of the Preston tube. This averaging contributes to a deceptive stability in the total pressure measurements. Further, in high velocity gradient regions this spatially averaged measurement will not generally coincide with the actual value at the geometric center of the tube, but rather with the value at some displaced position. In the boundary layer this effective tube position will be further from the wall than the geometric tube position and hence higher than actual shear stresses will be estimated as the gradient increases from that for the calibration. This is again reason to expect that the minimum in shear stress which occurs in the developing boundary layer will be underestimated by the Preston tube technique.

8.3.3 Entrance effects

The depression of friction velocity values near the pipe entrance for both the Preston tube and the film are likely the result of flow disturbances introduced by the boundary layer tripping element at the pipe entrance. As described in the section on tunnel equipment, the boundary layer tripping element is a 3.5 inch wide liner of silicon carbide floor surfacing paper. The grains are randomly

distributed with a density of 10 to 15 grains per cm^2 onto a smooth backing .7 mm. thick. The grains can project as much as 2 mm. into the flow while the Preston tube has an outside diameter of only 1.5 mm. Klebanoff and Diehl (see p. 98 of Rotta (20)) have made measurements of the turbulent flow over a flat plate in the presence of assorted disturbing elements which indicate that an element of height h can affect the mean velocity profile a distance as great as 100 h downstream. Hence, we can expect that the measurements taken with both the Preston tube and the hot film in the first few diameters have been modified by the presence of the roughness element.

The Klebanoff and Diehl results, as presented by Rotta (20), indicate that in the shadow region of the disturbing element the mean velocity gradients can be very much reduced and the mean velocity profile is in effect displaced upwards from the wall. In the case of the Preston tube, the pressure measurements behind the roughness would be low, corresponding to the pressure which would be measured at a point much closer to the wall for the undisturbed profile. This effective displacement of the Preston tube towards the wall would cause lower shear stress values to be interpreted from the calibration. Of course these measurments would no longer have any significance with regards to the actual shear stress occurring at the wall because the shadow region profile and the calibration region profile would not generally be similar.

In the shadow region of the roughness element the hot film device can also be expected to indicate lower shear stresses because of the reduced velocity gradient above the probe and hence decreased heat transfer

from the probe. In this case however, the hot film measurements are related to the actual changes in the wall shear stress although quite probably the character of the turbulent behavior immediately behind the roughness is dissimilar to that of the unperturbed boundary layer and we might expect that the probe calibration is not exactly correct for the disturbed flow region.

It appears therefore, that in this entrance region extending a few pipe diameters downstream of the roughness element, a complicated combination of effects due to extremely thin boundary layers, the breakdown of similarity flow, and the roughness element flow blockage and perturbation, produces results which are not illustrative of the overall tendency to increased friction velocities for decreased axial positions.

8.3.4 Skin friction coefficient data

Friction results are usually presented in non-dimensional form using the skin friction coefficient

$$Cf = 2\left(\frac{U^*}{Umean}\right)^2 = \frac{2\tau_w}{\rho(Umean)^2}$$

where Umean, the mean velocity, is used as the non-dimensionalizing parameter. The friction measurements for both the hot film and Preston tube techniques are presented as skin friction coefficients in figures 19 and 20. For these graphs the dimensionless axial position X/D relative to the beginning of the roughness has been chosen as abscissa and the data is plotted with Re(m,r) as the parameter.

The skin friction coefficient is defined in terms of the first power of the wall shear stress, whereas the friction velocity is defined in terms of the square root of the wall shear stress. The relatively large scatter apparent in these friction coefficient graphs is due to both this inherent sensitivity of the friction coefficient and the error which can be attributed to the mean flow values used for non-dimensionalization.

Both graphs adequately illustrate the friction minimum and the general trends observed for the friction velocity curves. However, the skin friction coefficient data exhibits a slower axial recovery from the friction minimum than might be interpreted from the friction velocity plots.

As illustrated by the Preston tube results, the skin friction coefficients at a fixed axial position generally decrease with increasing Reynolds number. Further, as the Reynolds number is increased, the separation between the parametric skin friction curves tends to decrease. The behavior of the hot film skin friction coefficient results are obscured by the data scatter. The Reynolds number dependences of the hot film measurements for developing and near developed flow are more clearly revealed by figures 21 and 22 respectively, where Reynolds number has been plotted as the abscissa and axial position is the parameter.

8.4 Velocity Profile Results

A suitable method of illustrating the general axial behavior of the velocity profiles is to plot the ratio of measured velocity to bulk velocity for a specific radial position against the axial position. This plot has been produced for the centerline of the profile and a radial position 5.1 mm. from the wall (figure 23) for a bulk velocity of 40 m/sec. Because of the uncertainty in the profile position relative to the wall the 5.1 mm. position velocity was calculated as the average of 4 values, 2 from each end of the profile.

To obtain data for the same bulk velocity for all axial positions, it was necessary to interpolate the data measured for different tunnel speeds at each axial position. To facilitate this procedure, the values of the centerline velocity for the set of different Reynolds number profiles measured at a particular axial position, were plotted against the bulk velocities for those profiles. This was repeated to produce a graph of centerline velocities versus bulk velocities for each axial position. A similar procedure was followed for the velocities assigned to the 5.1 mm. radial position. The data on these graphs was surprisingly linear and there was no difficulty in obtaining a good interpolation of the velocity for a 40 m/sec bulk velocity.

The striking feature of figure 23 is that it reveals clearly that the profiles in developing flow do not simply adjust asymptotically from the flat entrance region profile to the fully developed profile. As the core region flow accelerates, upon entering

the pipe, its velocity actually overshoots the value finally attained in the fully developed flow. As would be expected from continuity, the flow near the wall, typified by the 5.1 mm. radial position, undershoots the fully developed value.

As we consider regions close to the entrance where the profiles are flat over a fairly large radial region, the ratio of U/Ubulk is intuitively expected to approach 1 for all radial positions. This trend is depicted by our results except for the data nearest the entrance. In this region the effects of the roughness tripping element are evident. In the shadow region of the roughness, near the wall, low velocities are measured which, due to continuity, must give rise to elevated centerline velocities as observed.

From figure 23 we have evidence that the flow near the wall, although well beyond the sublayer, attains its fully developed speed in a shorter longitudinal distance than does the centerline velocity. This lends support to the hypothesis of a rapidly developing profile similarity in the region immediately adjacent to the wall. Further, because the minimum velocity for the wall region flow occurs closer to the entrance than the maximum of the centerline we have the suggestion of a causal relationship between the two.

8.5 Cross Plotting Technique Friction Results

The friction velocity values determined by the cross plot of logs technique for velocity profiles at the 72.3 diameter axial position have been used to calculate the data which appears on

figure 14. Comparison of the data with that of the static pressure-momentum balance technique and the theoretical fully developed flow skin friction law due to Prandtl shows that the cross plot method overestimates the true U* value. The degree of overestimation depends directly on the values of the coefficients A and B chosen for the universal profile equation. A recalculation using the coefficients determined by Nikuradse, (A = 5.75, B = 6.5) rather than those of Coles, show a marked shift in the data towards the values determined directly by the momentum balance method. Aside from this offset, the cross plot values follow the trend of the momentum balance data quite well, confirming the utility of the cross plot method for fully developed flow.

The cross plot of log friction velocities are plotted against axial distance in figure 24 for a range of Reynolds numbers comparable to that for the hot film results. As cautioned in the description of the cross plot technique, the numerical values calculated using the method (aside from the fixed offset due to the choice of coefficients A and B) need not be the same as the actual U* value in the developing regions where the logarithmic universality of the fully developed velocity profile may not apply. As we move from the developed flow towards the pipe entrance, the generated U* values tend to increase smoothly until X/D $\sim$ 25 to 30 where a distinct change in character occurs and the generated values decrease to a minimum between 10 and 15 diameters. This behavior is remarkably analogous to the behavior observed for the friction velocities measured by both the hot film and

Preston methods, but all that can be said with certainty is that the cross plot results are indicative of some deviation in the smooth development of the velocity profiles. However, it appears that the cross plot technique can predict, with some success, the shear stresses in the developing flow--which suggests that the developing flow may exhibit a universality not unlike the fully developed flow.

8.6 Hot Film Probability Densities

As previously mentioned, the observed fluctuations in the shear stress probe output are themselves sufficient basis for discarding the simple laminar sublayer model. It was apparent from observation of the oscilloscope image of the hot film probe output, that there were occasionally large positive voltage pulses occurring. To quantify this observation, a gated single channel analyser (S.C.A.) and a timed pulse counter were used to obtain the unnormalized probability density function for the probe output signal. We have attempted to interpret the distributions by considering the more recent bursting models to the sublayer (see for example Runstadler, Kline and Reynolds (21)).

The output signal directly from the probe and anemometer system (unlinearized) was amplified by a factor of 20 using a Disa signal conditioner (model 55D26) set for a wide band pass. The 3 db. down points for the low and high pass filters on the conditioner were set at 6.3×10^5 HZ. and 10 HZ, respectively. The S,C,A, channel width was adjusted to ,10 volts and the instrument was centered to give the distribution peak at 1.50 volts. Data for four

distributions, each at a different Re(m,r) was taken first at an axial position of 73.0 diameters in the fully developed region and then in the developing flow at 10,5 diameters.

Counting intervals of 10 seconds were sufficient to accumulate between 10^4 and 10^5 counts when the analyzer channel was positioned near the peak of the distribution. At the outer tails of the distribution it was necessary to sample for up to 500 seconds to accumulate sufficient counts. The number of events for each point in the distributions was normalized to a ten second counting interval. These density functions are plotted in figures 25(a) and 25(b). A logarithmic vertical scale has been used to plot the data because of the large range in the number of counts, which covers about 5 orders of magnitude. This method of plotting has the property that it emphasizes the low probability events in the tails of the distributions.

In all cases the extended right tail of the distribution towards higher voltages confirms the observation of relatively rare high voltage pulse events in the probe output. The distributions show a tendency to flatten and spread to achieve a more pronounced high voltage tail as the Reynolds number is increased. The distributions for the 73.0 and 10.5 diameter axial positions are virtually identical for comparable Reynolds numbers. This indicates that the turbulent behavior of the sublayer at these two positions has a similar character and supports the hypothesis that the sublayer development occurs over a much shorter inlet length than does the development of the overall flow structure. Further, since the hot film shear stress measurements are based on averaged values of the fluctuating non-

linear probe output voltage, it is important that the character of these fluctuations not change appreciably in order that the averaging process yield comparable results and that the probe calibration remain valid.

Since, for the constant temperature film operation mode, the probe output voltage is proportional to the square root of the power dissipation from the hot film, the extended high voltage tail for the hot film output voltage distributions is indicative of a phenomenon which causes rather infrequent but effective increases in the power dissipation from the film. Generally an increase in the output voltage of the anemometer occurs in response to increased heat transfer from the probe. The anemometer functions by increasing the voltage applied to the probe so that the joule heating of the probe will increase and maintain the film temperature and hence resistance constant in the new heat transfer situation. For the flush mounted wall probe these positive voltage pulses must correspond to a disturbance in the thermal boundary layer over the heated film which causes cooler or faster moving air to flow over the probe. The physical process of random, rapid momentum transfer across the sublayer due to occasional large scale ejection of sublayer fluid into the flow and the ensuing inrush or sweeping of turbulent fluid into the sublayer is the basis of the burst models for the sublayer such as proposed by Runstadler et al (21). Such an ejection of fluid from the heated sublayer adjacent to the probe can account for the sudden

increased heat transfer from the probe and the skewed output voltage distributions which we have observed.

While presently this explanation is strictly qualitative, it would seem that conditional sampling of the probe output to study these large positive pulses could yield valuable information about the bursting phenomenon—such as frequency, intensity and duration of the ejection process. An obvious complication which must be considered is the introduction of the thermal boundary layer into the sublayer above the probe. The importance of the burst phenomenon to the boundary layer growth is suggested by the development of the skewed voltage distributions at such an early point in the boundary layer development. Increased burst activity to transport momentum in support of the increased shears at high Reynolds numbers could be indicated by the observed Reynolds number variation of the distribution skewness.

It should be pointed out explicitly that the term "skewness" is used loosely in the above description of the distributions. If in fact the statistical third moments of the distributions and the corresponding statistical skewness factors were calculated, the values would be very close to those for a gaussian distribution. It is only because of the extreme compression of the vertical scale on our logarithmic plot that it is possible to distinguish the distribution structure. To quantify the tail structures of these distributions by the usual statistical techniques it would be necessary to compute much higher moments for the distribution.

9. CORROBORATION OF RESULTS

9.1 Developing Flow Profile Measurements

While extensive experimental work has been undertaken by several workers for fully developed turbulent flow in pipes, the available data for developing turbulent pipe flow is relatively meager. This is quite surprising considering the practical importance of the entrance flow for tubular heat exchangers. There have been several attempts at numerical solutions of the boundary layer equations. A brief but fairly complete review of these studies has been presented by Tullis and Wang (24). These studies invariably assume a simple asymptotic development of the mean velocity profile to the fully developed flow. Our experiments have indicated that this is not the case for pipe flow.

Until now the only definitive emperical results for the developing pipe flow profiles have been those due to Barbin and Jones (3) (Some rather inconclusive data was presented by Deissler in 1950 (26)). Their measurements are for air flow in an eight-inch diameter pipe 29 feet long. The measurements are not particularily extensive and include only one Reynolds number (3.88×10^5 based on mean velocity and pipe diameter). The data was presented as a general background for their turbulence measurements and no specific discussion was directed towards the profile behavior. Their measurements for the variation of velocity along the pipe for the centerline and wall regions concur with the present findings.

Specifically, both the overshoot of the centerline velocity and the undershoot of the wall region velocity which we have observed from our profile measurements are illustrated on Barbin and Jones' graph. The magnitudes and axial positions for the phenomena are comparable. We note however that the entrance effects which we have observed have not been recorded by Barbin and Jones who used a narrow strip of sparsely distributed sand grains glued directly to the pipe wall to initiate transition at the entrance.

No direct measurements of the wall shear stress were reported in Barbin and Jones' paper, however, measurements of the wall static pressure along the entire pipe combined with the computations of the momentum flux from the velocity profiles were used to determine the wall shear stress along the pipe by the momentum balance principle. Because the momentum flux was taken as constant, the computed shear stress values become directly dependent on the wall static pressure gradient. The static pressure measurements are insensitive to the subtleties of the mean velocity profile development and as a result, Barbin and Jones have fitted the pressure data with a smooth decreasing curve with no inflection points. Accordingly, their wall shear stress computations depict a shear which is monotonically decreasing to the fully developed value, Careful scrutiny of wall static pressure measurements, taken with the Betz manometer in our tunnel a considerable time before the present study was initiated, reveals that the wall static pressures definitely exhibit an inflection point in the neighborhood of 30 diameters. Figure 26 illustrates this point and is typical of the static pressure data which has been measured.

9.2 Skin Friction Measurements

After a fairly thorough literature search, only one other study with experimentally determined values of the shear stresses has come to light. We refer to the work of Mizushina et al (15) for which direct measurements of the wall shear stress for the flow of a potassium hydroxide solution in the entrance region of a 2 inch diameter polyvinylchloride tube were made using an electro-chemical mass transfer technique due to Reiss and Hanratty (19). The justification for this technique is analogous to that for our heat transfer method. Mizushina et al have plotted the longitudinal distribution of the local friction factor at the wall for six Reynolds numbers (based on diameter) ranging from 8,450 to 98,800 which includes the two lowest Reynolds numbers used for our hot film studies. Much of the detail of their data has been lost by plotting on a contracted log-log scale. Ignoring the smooth lines which have been drawn through the data, close examination reveals that all of their measurements between 10 and 20 diameters consistently define a local minimum in the skin friction data, except for their lowest Reynolds number. For this lower Reynolds number, the authors conjecture a persistence of laminar flow despite the existence of a trip wire at the pipe entrance. The consistency of the other data on their plot would seem to indicate that the relative minimum is significant but the authors have chosen to ignore it.

The authors' proposal of a universal law for the developing flow using the wall shear stress as a non-dimensionalizing parameter is of particular interest because of the possible implications for the cross plot technique for determination of the wall shear stress.

10. PHYSICAL FLOW MODEL

A fundamental breakdown in the analogy between the growth of a turbulent boundary layer on a flat surface and the growth of a turbulent boundary layer in developing pipe flow is clearly exhibited by the observation, for pipe flow, of a non-asymptotic adjustment of the wall shear stresses to the fully developed flow values. The tendency of the mean profiles to overshoot the fully developed profile is intimately related to this shear stress behavior and is the key to a physical model.

Near the wall, where the total shear stress is predominently due to viscous shear ($\mu \frac{\partial u}{\partial y}$), we can assume that the radial gradient of the mean velocity will be a reasonable indicator for the wall shear stress. In the entrance region of the pipe, where the velocity profiles are quite flat, a large velocity gradient must exist near the wall. We can thus expect that the wall shear stress is high and that the viscous force acting to retard the flow near the wall must also be large. This is illustrated schematically in figure 27, which is based on our results. Within the turbulent boundary layer, which is initialized at the entry, the production of turbulent fluctuations using kinetic energy extracted from the mean flow near the top of the boundary layer combined with the viscous dissipation to heat, result in a growing, decelerating annular flow region extending from the wall. We have called this the outer region. The deceleration of the outer region fluid causes a slackening of the velocity gradient at the wall—which is indicative of diminishing wall shear stress values

compared to those at the entrance. An elementary consideration of continuity suggests that to maintain a constant bulk flow down the tube, the laminar-like axial region fluid, which is surrounded by the boundary layer, must counter by aquiring an acceleration. The acceleration of the axial region must of course be limited by the increasing viscous shear which will accompany the development of intensified velocity gradients in that region. While we therefore expect that an average velocity taken over the core region in the initial development region will increase with longitudinal distance, farther along, at some intermediate longitudinal position where the growing boundary layer has enveloped, eroded, and slowed more the core fluids,an average velocity taken over the core must begin to decrease. The overall acceleration of the core will reverse. As regions closer to the pipe axis decelerate continuity considerations require that the outer flow must begin to accelerate to maintain constant mass flow. The acceleration of the outer flow region gives rise to steeper velocity gradients near the wall—an indication of increasing wall shear stress. We might surmise that this dynamic balancing process continues with decreasing amplitude until the fully developed equilibrium profile is achieved. This is suggested perhaps by the detailed behavior of the hot film friction velocities measured farther downstream, however, there is no justification for this speculation derivable from our simple model.

The relationship between the observed behavior of the developing velocity profiles and the wall shear stress is understandable on the basis of this qualitative model. The implications for the

turbulent characteristics of the flow are unknown and before this qualitative model can be considered for mathematical formulation, extensive measurements to determine this behavior are required.

11. EVALUATION OF THE HOT FILM TECHNIQUE

The results obtained in this study serve to illustrate the great utility of the hot film technique for wall shear stress measurements in developing flow. The flush mounting feature of the probe and the dependence of the probe's operation on the flow only within a few tenths of a millimeter from the wall allows it to be used successfully where the sublayer flow has achieved universality, but where the flow beyond the sublayer is still in the developing stages. The extremely fast response of this instrument compared to the Preston tube makes it possible to study the turbulent characteristics of the sublayer.

While the quality of the friction measurements which are possible with this instrument is high, this is at the expense of greatly increased complexity of operation compared with the Preston technique. The extreme non-linearity of the probe requires that calibration be extremely accurate and this eventually limits the highest shear stresses which can be successfully resolved. The probe operation depends very much on the operating temperature of the probe relative to the fluid and the need to compensate for temperature changes in the fluid and ambient laboratory conditions is critical. These thermal considerations are augmented by the fact that only a very small percentage of the total power dissipation from the film is actually to the fluid. Most of the dissipation is into the probe substrate and mounting. The result is a serious dependence of the probe on the mounting equipment and the contact between the probe body and wall. This factor required that the probe be recalibrated for each change in mounting and

precluded the extensive use of the multiple mounting position test section originally designed for this study. These thermal and mounting problems are considered in detail in Appendix V.

12. SUMMARY

The longitudinal dependence of the wall shear stress for developing turbulent pipe flow has been determined experimentally. The shear stresses do not decrease monotonically to the fully developed value as has been previously thought. Instead, the shear stress was found to achieve a minimum value in the developing flow region and the overall development of the stress takes place over much longer length than had been thought.

The principal measurement procedure utilized a flush mounted heated film which was calibrated in the extensively studied fully developed region. The success of the hot film method depends upon the existence of similarity for the velocity profiles in the immediate vicinity of the wall. Making the rather natural assumption that the boundary layer flow immediately adjacent to the wall adjusts to the presence of the wall quite soon after entry into the pipe, we have accepted the calibration obtained in fully developed flow as valid for the probe when it is located in the entrance length of the pipe.

The hot film results agreed well with measurements obtained with a standard Preston tube arrangement. The Preston tube technique also depends on wall region similarity and its use can be justified in a manner analogous to that for the hot film. However, because the tube extends well into the flow above the wall compared to the flush mounted hot film, its suitability for developing flow is more limited,

Cross plot analysis of velocity profiles measured in the developing flow has produced results indicative of non-monotonic development—in agreement with the hot film results. The close agreement in both trend and magnitude between the hot film and cross plot friction measurements is perhaps unexpected, because the cross plot technique fits the developing profile data to the known universal profile for fully developed flow.

Direct analysis of the longitudinal variation of the centerline and wall region velocity measurements in the developing flow respectively demonstrated an overshoot and undershoot of the fully developed profile values for these regions. This observation is intimately related to the non-monotonic development of the shear stress and has provided the basis for a simple physical model of the developing flow.

The inability of previous investigators to find this shear stress behavior has been traced to the insensitivity of wall static pressure measurements and the resulting erroneous assumption of a monotonically increasing longitudinal static pressure gradient. Careful examination of pressure measurements taken along the wall for the developing flow has established the existence of an inflection point in the longitudinal dependence of the wall static pressure. This inflection point is associated with a minimum in the wall shear stress.

Investigation of the fluctuating output signal from the hot film probe through the measurement of unnormalized probability density functions has provided direct experimental evidence of the "bursting" phenomenon in the sublayer. The probability density measurements in

the beginning of the developed region and in the fully developed region were found to be similar which is in accordance with the assumed rapid development of the sublayer structure. The intensity of the bursting and hence the turbulent structure of the sublayer were found to depend on the Reynolds number.

The studies summarized above have been undertaken for air flow through a four inch diameter pipe and for a Reynolds number range (based on bulk velocity and pipe radius) of from ~ 30,000 to ~ 135,000.

13. CONCLUSIONS

The following conclusions have been drawn on the basis of our experimental measurements, analysis and observations and are expected to be generally valid for developing turbulent pipe flow.

1) Beyond the first few diameters from the pipe inlet, the wall shear stress is high, but contrary to the assumptions of previous treatments, it decreases to a minimum value which is lower than the final constant value that is obtained when the flow is fully developed. The wall shear stress decreases from its initially high values to its fully developed value within 15 diameters and continues to decrease to its minimum value which occurs between 20 and 30 diameters.

2) The longitudinal behavior of the flow centerline velocity is characterized by an overshoot of the fully developed centerline velocity. The longitudinal behavior of the developing flow velocity near the wall is characterized by an undershoot of the corresponding fully developed velocity.

3) The experimental evidence suggests that the monotonically decreasing wall static pressure in developing pipe flow is characterized by an inflection point which occurs in the range of 20 - 30 diameters.

4) The sublayer flow region achieves mean velocity profile similarity behavior within the first few diameters of the

inlet region. The sublayer has a fundamentally turbulent character and exhibits a bursting phenomenon.

5) For the Reynolds number range of this study, neither the wall shear stress nor the mean velocity profiles are fully developed at a longitudinal position of 52 diameters and even at 73.3 diameters the higher Reynolds number flows may be just beginning to achieve full development.

6) The often drawn analogy between flat plate boundary layers and the growing boundary layer in a pipe is inadequate to describe the non-monotonic development of the turbulent boundary layer in a pipe.

7) Anomalous behavior within the first few diameters of the entrance can be related to the effects of the boundary layer tripping element employed to initiate the turbulent boundary layer growth.

14. REMARKS

It has been resolved that the hot film device can be a useful instrument for friction measurements in developing flow and that there is a potential for obtaining new information about turbulent phenomenon in the sublayer. The classic Preston tube technique and the cross plot technique can also be used with moderate success. The success of these later two methods suggests the existence of similarity for developing velocity profiles. Although this has not been established here, it is anticipated that further analysis of the extensive profile data which is now available can resolve this question. Possibly such analysis combined with experiments to define the turbulent structure can lead to a more refined physical model for the developing turbulent pipe flow.

APPENDIX I: The Static Pressure Gradient Technique

In fully developed pipe flow, the velocity profiles are independent of longitudinal position. Hence, the total momentum flux in the direction of flow is a constant and the forces acting on a length of fluid in the pipe along the flow direction must balance to produce a zero net force. The force tending to accelerate the section of fluid is due to the difference in static pressure at the ends of the section. The force tending to retard the fluid is due to friction between the smooth wall and adjacent fluid. Using the following notation,

- ℓ The length of the fluid section
- P1 Static pressure at the upstream end of the fluid section
- P2 Static pressure at the downstream end of the fluid section
- R The pipe radius
- τ_w The friction force per unit area of the wall (i.e. the wall shear stress), we have that,

$$\pi R^2 (P1 - P2) = - 2\pi R \ell \tau_w$$

or

$$\tau_w = - \frac{R}{2} \left(\frac{P1 - P2}{\ell}\right)$$

where the flow direction is taken as positive. For an infinitesimally short fluid section we have that

$$\tau_w = - \frac{R}{2} \left(\frac{dP}{dX}\right) .$$

Thus a measurement of the local static pressure gradient in the fully developed flow directly yields the local wall shear stress.

APPENDIX II Calculation of Air Density, Viscosity and Reynolds Number

For a typical wind tunnel trial, the following quantities were measured in the units indicated.

Pcone	Static pressure drop across the contraction cone (mm. water)
Tf	Tunnel air temperature as measured in the diffuser
TDf	Ambient laboratory dry bulb temperature (^{o}F)
TWf	Ambient laboratory wet bulb temperature (^{o}F)
Bmm	Atmospheric barometric pressure corrected for air temperature, latitude and scale coefficient of expansion (mm. Hg.)

What follows is the analytic procedure which was used to calculate the air density, viscosity and Reynolds number from the above mentioned measurements. This procedure was incorporated into a computer program for the data analysis.

a) Calculation of the dew point (Reference (11)).

First calculate the saturation vapor pressure (Psat) of the laboratory air as follows:

$$Psat' = \text{antilog}_{10} \left[\frac{B \times TWc}{C + TWc} + D\right]$$

and $Psat = Psat' - A\,(Bmb)\,(TDf - TWf)$

where
- $A = 3.70 \times 10^{-4}$
- $B = 7.5$
- $C = 237.3$
- $D = 0.78571$
- TWc = TWf converted to centigrade degrees
- Bmb = Bmm converted to millibars
- Psat = Saturation vapor pressure in millibars

Now calculate the temperature of saturated air which has the same vapor pressure as the laboratory air (i.e. the dew point temperature). Using the Magnus formula we have

$$Tdew = \frac{(\log (Psat) - D)\, C}{(B + D - \log (Psat))}$$

where Tdew is the dew point in ^{o}C,

b) Calculation of the moist air density

First calculate the vapor pressure of the moisture in the laboratory air (VP) as follows:

$$VP = (W + X\ Tdew + Y Tdew^{2} + Z\ Tdew^{3})$$

where W = 4.57570
X = .339922
Y = $.920863 \times 10^{-2}$
Z = $.31060 \times 10^{-3}$
VP = vapor pressure in mm. water.

Now calculate the moist air density using the equation

$$\rho = 1.2929 \frac{273.13}{Tc + 273.13} \left[\frac{Bmm - (.3783)(VP)}{760.0} \right]$$

where Tc = Tf converted to centigrade degrees
ρ = moist air density in gms/liter

It was assumed that this computed tunnel air density was approximately the same as the air density in the tunnel, although the tunnel air is at slightly different pressures along the pipe. This is consistent with the assumption of incompressible flow.

c) Calculation of the air viscosity

The dynamic viscosity (μ) in units of (gm./sec-cm.) was calculated using the empirical result

$$\mu = \left(165.0 + \frac{Tf}{4.0}\right) \times 10^{-6} \quad .$$

Then the kinematic viscosity ν in units of ($cm.^2/sec.$) is given by

$$\nu = \frac{\mu}{\rho \times 10^{-3}} \quad .$$

where μ is in gm./sec-cm. and ρ is in gm./l.

d) Determination of the flow Reynolds number Re(m,r)

First the mean velocity of the flow was determined using the calibration equation for the tunnel

$$VB = 4.31 \sqrt{\frac{Pcone}{\rho}}$$

where Pcone is in mm. of water and ρ in gm./l while VB is in units of m/sec.

The flow Reynolds number based on pipe radius and mean velocity Re(m,r) using the expression

$$Re(m,r) = \frac{(508.0)\ VB}{\nu}$$

APPENDIX III: Criteria for the Hot Film Thermal Boundary Layer

Bellhouse and Shultz (4) have proposed a criterion which when satisfied implies that the thermal boundary layer above a heated element lies within the linear sublayer region of either a turbulent or laminar boundary layer. This is a condition which should be satisfied during the hot film operation. If Qw is the heat flux from the heated element, L is the length of the element, K the thermal conductivity, ΔTo the difference between the element and stream temperatures, Pr the Prandtl number and Cf the skin friction coeffient then their criterion is written

$$1 << \frac{Qw\ L}{K\ \Delta To} < \frac{Pr}{Cf} \quad .$$

The typical power loss from the heated film when operated at a constant resistance of 12.50 ohms is not more than .2 watts. If we consider that as much as 50% of this power may actually be dissipated into the flow rather than into the film substrate, then for the film dimensions (.075 cm. x .015 cm.) the Qw term is typically 89 watts/cm^2. The condition above has been evaluated for the values of the parameters during the lowest and highest Reynolds number trials for the primary film calibration. For these two trials the ΔTo term ranged from 153.6°C to 144.7°C respectively. Using the Cf values determined from the static pressure gradient, the terms in the inequality were determined to be related as follows;

$$1 << 139.8 < 144.8 \text{ (for } Re(m,r) = 31.3 \times 10^3)$$
$$1 << 148.1 < 198.7 \text{ (for } Re(m,r) = 134.3 \times 10^3)$$

In either case the Bellhouse and Shultz criterion is satisfied.

A crude rule utilized by DeSantis, Rakowsky and Page (7) for the same flow condition is expressed mathematically as

$$\frac{U^* L}{\nu} < 64 \, Pr \quad ,$$

Evaluating ν for the typical mean temperature between the film and stream this criterion implies that U* should be less than 1.7 m./sec. This is the case for all but the highest Reynolds number trial used for the calibration.

APPENDIX IV: The Effect of Flow Temperature Changes on the Hot Film Output

The effects of both the tunnel speed and tunnel temperature changes on the hot film probe output voltage are illustrated in figures 28(a) and 28 (b). These figures show results obtained with an X Y recorder during preliminary experimentation with the film probe. The horizontal deflection of the recorder pen was controlled by the hot film probe output voltage while the vertical deflection was determined by the output voltage from a ratemeter. The ratemeter output voltage was linearly related to the number of pulses per second produced by a toothed wheel on the fan shaft (60 pulses per revolution) and hence was directly related to the tunnel fan speed. The Reynolds number for the flow is nearly a linear function of the fan speed as can be seen from figure 2 and the tunnel calibration equation (fan speed $\alpha \sqrt{Pcone} \alpha$ VB). Hence, these records directly provide a crude indication of the dependence of the probe output on the flow Reynolds number.

To obtain figure 28(a), the tunnel had been initially turned off for several hours so that complete thermal equilibrium existed between the lab and tunnel equipment. The fan was started and over the course of about one minute, the fan speed was continuously increased up to the maximum speed. The X Y recorder traced along curve A in the figure. The tunnel was then allowed to run at this maximum speed for twenty minutes. During this time, the tunnel air temperature rose from 74.2 ^{o}F. to 91.0 ^{o}F. The effect of this increasing tunnel temperature and hence decreasing temperature elevation for the heated film element was a decrease in the film

output voltage of more than .2 volts, This is illustrated by section B on the figure. It can also be seen that the tunnel speed increased slightly over this warm up period. Curve C shows the behavior of the probe as the tunnel fan speed was subsequently decreased over the course of a minute until the fan was still. The hysterisis-like appearance of the plotter record is due to the increased tunnel temperature at high speeds and its effect on the probe output, and illustrate the need to consider the probe elevation temperature in the calibration,

Figure 28(b) was obtained shortly after figure 28(a) and in a similar manner except that the tunnel was not run at the high tunnel speed for a long time. The complete trace was obtained in about 2 minutes and illustrates that there was negligible lag between the fan speed and probe output. The slight shift to higher output voltages for the decreasing fan speed part of the record probably indicates that the tunnel was still cooling down from the previous run,

APPENDIX V: Hot Film Mounting Problems

In attempting to interchange the probe mounting block and probe between different mounting holes in the test section pipe, it was found that the average d.c. output voltage from the probe for constant flow conditions can differ the order of 1%, depending upon how the mounting screws for the probe mounting block are tightened when the probe is put in position. At first it was thought that this variation in the output was caused by a change in the probe overheat ratio. Such a change in overheat would be expected if the cold resistance of the film and uncompensated lead combination were to change due to a strain guaging effect. It was hypothesized that a slight misalignment of the probe and probe mount with the pipe receiving hole could cause the end of the probe and hence the sputtered film to distort and change resistance upon tightening of the mounting screws. Similarily if there were a bending moment applied to the probe body, the uncompensated lead resistance could change. It is conceivable that resistance changes as large as .2% could be generated by these mechanical effects. Given an uncompensated lead and probe resistance of 8.1 ohms, this could mean changes in the cold resistance of up to .016 ohms. Actual measurements of the probe cold resistance under extremes of possible strain due to mounting, achieved by tightening only one mounting screw, led to variations in the cold resistance of .006 ohms. Assuming an operating resistance of 12.50 ohms, this variation in cold resistance implies a variation of about .001 in the overheat ratio. From the probe calibration data it was found that

a change in overheat of this order for an overheat near 1.6 would produce a change in the average d.c. output from the probe of 4 or 5 millivolts or about .06% of the total d.c. output under these operating conditions. While the strain guaging phenomenon could be responsible for the observed variation of the unheated probe resistance with mounting, the effect on the heated probe d.c. output would be small.

Further investigation showed that if only the upstream screw on the mounting were tightened then the cold resistance would increase and the average output voltage for the heated probe would also increase. The converse was true when only the downstream screw was tightened. Even when the mounting block was rotated 180 degrees the same upstream-downstream behavior was found. This indicates that the problem likely lies with the drilled hole in the pipe which receives the end of the probe. In particular, if the output voltage from the probe increases for a different mounting position in constant temperature operation, then this implies that more power is being supplied to the probe to maintain its elevated temperature. This would be the case if the heat conduction from the probe were to increase. Since for the hot film probe a large percentage of the heat is dissipated into the probe substrate and then directly, by conduction, into the pipe and probe mounting block, it is quite possible that a very small change in the amount of contact between the probe body and pipe near the film could produce large output changes. Such a change would occur if, for example, the drilled hole in the pipe were slightly angled.

These considerations indicate that a probe mounting design which allows the probe to be relocated, yet which intends to preserve the same calibration for the probe, must ensure that the heat conduction from the whole probe body remains the same in the different mounting positions. This condition is more likely to be achieved when only the probe mounting makes contact with the probe, and when the probe mounting as a whole can replace part of the flow boundary.

REFERENCES

1. Afzal, N. and Yajnik, K. 1973 J. Fluid Mech. 61, 23.

2. Azad, R.S. and Hummel, R.H. 1971 Can. J. Phys. 49, 23, 2917.

3. Barbin, A. R. and Jones, J.B. 1963 A.S.M.E. Trans. 85, D, 29.

4. Bellhouse, B.J. and Shultz, D.L. 1966 J. Fluid Mech. 24, 397.

5. Brown, K.C. and Joubert, P.N. 1969 J. Fluid Mech. 35, 375.

6. Coles, D. 1968 Proc. 1968 AFOSR-IFP-Stanford Conf. on Computation of Turbulent Boundary-layers, vol. 2, pp. 1 - 45.

7. DeSantis, M.J., Rakowski, E.L. and Page, R.H. 1972 paper presented at 25th annual meeting of the Division of Fluid Dynamics, A. Phys. Soc.

8. Fage, A. and Falkner, V.M. 1931 Aero. Res. Council, Lond. Rep. No. 1408.

9. Geremia, J.O. 1972 Disa Information tech. bulletin 13, 5.

10. Hinze, J.O. 1964 In Mechanics of Turbulence (ed. A. Favre), Gordon and Breach.

11. Institution of Heating and Ventilating Engineers. Hygrometric Data for Air Conditioning Calculations. London, I.H.V.E., 1963.

12. Liepmann, H.W. and Skinner, G.T. 1954 N.A.C.A. T.N. No. 3268.

13. Ludweig, H. 1950 N.A.C.A. T.M. No. 1284,

14. Ludweig, H. and Tillman, W. 1950 N.A.C.A. T.M. No. 1285

15. Mizushina, T., Ito, R., Hiromasa, U., Tsubata, S., and Hayashi, H. 1970 J. Ch. Eng. of Japan, 3(1), 34.

16. Morrison, W.R.B. and Kronauer, R.E. 1969 J. Fluid Mech. 39, 117.

17. Patel, V.C. 1965 J. Fluid Mech. 23, 185.

18. Preston, J.H. 1954 J. Roy. Aero. Soc. 58, 517, 109.

19. Reiss, L.P. and Hanratty, T.J. 1963 A.I.Ch.E. 9, 154.

20. Rotta, J.C. 1962 In Progress in Aeronautical Sciences (ed. A. Ferri, D. Kuchemann and L. Sterne), vol. 2, p. 98 Pergmanon Press.

21. Runstadler, P.W., Kline, S.J. and Reynolds, W.C. 1963 Dept. of Mech. Eng., Stanford University, Report No. Md-8.

22. Schlichting, H. 1968 Boundary Layer Theory, 6th. ed., McGraw-Hill.

23. Schraub, F.A. and Kline, S.J. 1965 Dept. of Mech. Eng., Stanford University, Report No. Md-12.

24. Tullis, J.P. and Wang, J. 1972 Naval Ship Research and Development Center, Bethesda, Maryland, Report No. CER72-73JPT-JSW-2.

25. Van Der Spiegel, P.J.A. 1969 M.Sc. Thesis in Mech. Eng., University of Manitoba.

26. Deissler, R.G. 1950 N.A.C.A. T.N. No. 2138.

TABLE I

Calibration wall shear stresses in fully developed flow by the pressure gradient method. (Calibration 1),

$Re(m,r) \times 10^{-3}$	τ_w (mm. H_2O)	U* (m/sec,)	$Cf \times 10^3$
31.3	.028	.483	4.971
43.0	.049	.640	4.627
54.2	.073	.781	4.308
63.7	.098	.910	4.216
71.0	.118	.985	4.054
76.3	.134	1.058	4.044
84.8	.165	1.175	3.983
94.2	.198	1.290	3.872
103.5	.233	1.399	3.751
115.6	.290	1.563	3.716
134.3	.387	1.809	3.624

TABLE II

Calibration wall shear stresses in fully developed flow by the pressure gradient method. (Calibration 2)

$Re(m,r) \times 10^{-3}$	τ_w (mm. H_2O)	U* (m/sec,)	$Cf \times 10^3$
30.4	.026	.467	4.950
70.6	.117	.989	4.100
132.3	.385	1.814	3.693

TABLE III

Calibration wall shear stresses in fully developed flow by the pressure gradient method. (Calibration 3)

$Re(m,r) \times 10^{-3}$	τ_w (mm. H_2O)	U* (m/sec.)	$Cf \times 10^3$
30.7	.026	.469	4.970
52.8	.071	.770	4.481
81.7	.156	1.146	4.056
94.9	.205	1.318	3.927
114.7	.292	1.577	3.767
134.3	.386	1.818	3.570

HOT FILM DATA TABLES IV - XI

The following list is provided to facilitate interpretation of the tabulated hot film data. The list is numbered according to the column number in the data tables.

1. (Pcone) static pressure drop across the contraction cone in units of mm. of water,
2. (Rcold) measured resistance in ohms of the unheated film probe at the ambient tunnel conditions for the trial.
3. (Vfilm) calculated voltage drop across the operating heated film based on the anemometer bridge voltage in volts.
4. (ΔT) calculated film elevation temperature in degrees Fahrenheit,
5. (Pfilm) computed power loss from the heated film in watts or equivalently joules/sec,
6. (ρ) tunnel air density in grams/cc,
7. (ν) tunnel air kinematic viscosity in cm.^{2}/sec,
8. (Umean) mean tunnel air velocity in m/sec,
9. (Rem,d) flow Reynolds' number based on the mean velocity and tunnel diameter,
10. (τ_w) wall shear stress in mm. of water calculated from the fitted probe calibration equation (except for table XI)

11. (U*) calculated friction velocity in m/sec.

12. (Cf) calculated skin friction coefficient. Data entries are multiplied by 1000.

TABLE IV: TABULATED HOT FILM DATA: X/D = 1.5

Pcone	Rcold	Vfilm	ΔT	Pfilm	ρ	ν	Umean	Re(m,r) x 10^3	τ_w	U*	Cf x 10^3
5.4	7.046	1.462	313.6	.1858	1.142	.1607	9.40	29.7	.030	.509	5.88
11.9	7.045	1.471	313.7	.1883	1.142	.1608	13.91	43.9	.049	.646	4.32
18.3	7.050	1.480	313.1	.1896	1.141	.1609	17.27	54.5	.065	.747	3.74
23.9	7.058	1.482	312.2	.1904	1.141	.1611	19.74	62.2	.079	.825	3.50
28.5	7.063	1.484	311.6	.1909	1.139	.1616	21.58	67.8	.090	.880	3.32
34.8	7.069	1.485	310.9	.1914	1.138	.1618	23.85	74.9	.102	.936	3.08
43.8	7.097	1.490	307.7	.1916	1.136	.1625	26.78	83.7	.133	1.074	3.21
55.0	7.090	1.490	308.5	.1930	1.159	.1592	29.70	94.8	.151	1.129	2.89
68.6	7.118	1.490	305.4	.1932	1.157	.1599	33.20	105.5	.191	1.271	2.93
89.7	7.150	1.490	301.8	.1929	1.152	.1610	38.05	120.0	.235	1.414	2.76
112.5	7.192	1.487	297.1	.1923	1.146	.1625	42.72	133.6	.295	1.588	2.76

TABLE V: TABULATED HOT FILM DATA: X/D = 10.5

Rcone	Rcold	Vfilm	ΔT	Power	ρ	ν	Umean	Re(m,r) x 10^{-3}	τ_w	U*	Cf x 10^3
5.7	7.111	1.441	306.2	.1806	1.160	.1583	9.53	30.6	.031	.514	5.81
11.6	7.097	1.452	307.7	.1833	1.151	.1596	13.66	43.4	.045	.619	4.11
18.0	7.116	1.459	305.6	.1851	1.159	.1585	16.97	54.4	.077	.805	4.50
23.6	7.111	1.464	306.2	.1863	1.149	.1600	19.55	62.1	.088	.864	3.91
29.1	7.121	1.466	305.0	.1867	1.147	.1603	21.71	68.8	.103	.939	3.74
33.9	7.139	1.468	303.0	.1875	1.155	.1595	23.36	74.4	.134	1.065	4.16
42.6	7.135	1.473	303.5	.1887	1.145	.1610	26.30	83.0	.151	1.137	3.73
54.7	7.174	1.475	299.1	.1891	1.150	.1606	29.74	94.1	.218	1.363	4.20
71.6	7.172	1.480	299.3	.1905	1.140	.1623	34.16	106.9	.252	1.472	3.71
82.9	7.221	1.476	293.9	.1894	1.144	.1622	36.71	115.0	.314	1.642	4.00
111.0	7.267	1.475	288.9	.1891	1.138	.1638	42.59	132.1	.418	1.899	3.98
154.1	7.331	1.470	282.1	.1879	1.128	.1662	50.39	154.0	.562	2.210	3.85
171.5	7.383	1.463	276.6	.1861	1.119	.1682	53.38	161.2	.652	2.390	4.01
185.1	7.396	1.461	275.2	.1856	1.117	.1688	55.52	167.1	.676	2.437	3.85

TABLE VI: TABULATED HOT FILM DATA: X/D = 17.4

Pcone	Rcold	Vfilm	ΔT	Pfilm	ρ	ν	Umean	Re(m,r) x 10^{-3}	τ_w	U*	Cf x 10^3
5.5	7.079	1.443	309.8	.1811	1.157	.1587	9.43	30.2	.022	.437	3.90
11.5	7.074	1.456	310.4	.1842	1.157	.1587	13.57	43.4	.041	.529	3.81
18.7	7.073	1.466	310.5	.1870	1.157	.1587	17.34	55.5	.066	.751	3.75
24.2	7.084	1.470	309.2	.1879	1.156	.1590	19.74	63.2	.085	.852	3.72
29.5	7.093	1.472	308.2	.1885	1.155	.1593	21.77	69.6	.103	.933	3.67
34.0	7.094	1.475	308.1	.1893	1.157	.1590	23.35	74.6	.115	.988	3.58
44.3	7.112	1.479	306.0	.1902	1.157	.1592	26.68	85.1	.151	1.133	3.61
54.2	7.128	1.481	304.2	.1908	1.154	.1598	29.53	93.9	.186	1.256	3.62
69.3	7.156	1.482	301.1	.1911	1.152	.1605	33.43	105.8	.237	1.421	3.62
84.0	7.172	1.484	299.3	.1915	1.151	.1610	36.84	116.2	.281	1.546	3.52
112.0	7.215	1.485	294.6	.1918	1.145	.1624	42.65	133.4	.385	1.817	3.63

TABLE VII: TABULATED HOT FILM DATA: X/D = 30.7

Pcone	Rcold	Vfilm	ΔT	Pfilm	ρ	ν	Umean	Re(m,r) x 10^{-3}	τ_w	U*	Cf x 10^3
6.1	7.061	1.449	311.8	.1827	1.172	.1566	9.80	31.7	.025	.459	4.39
11.3	7.063	1.460	311.6	.1853	1.172	.1565	13.39	43.5	.044	.609	4.13
18.1	7.065	1.468	311.4	.1873	1.171	.1567	16.95	55.0	.065	.736	3.77
24.2	7.073	1.472	310.5	.1885	1.170	.1569	19.62	63.5	.084	.841	3.68
29.6	7.064	1.447	311.5	.1897	1.175	.1562	21.63	70.4	.094	.885	3.35
34.9	7.082	1.478	309.4	.1901	1.172	.1568	23.53	76.2	.116	.984	3.50
44.5	7.105	1.481	306.8	.1907	1.169	.1576	26.61	85.8	.153	1.132	3.62
54.4	7.117	1.484	305.5	.1916	1.168	.1578	29.43	94.7	.188	1.256	3.64
68.3	7.138	1.486	303.1	.1920	1.164	.1587	33.02	105.7	.230	1.392	3.56
85.5	7.167	1.488	299.9	.1925	1.160	.1597	37.02	117.7	.300	1.591	3.70
111.5	7.205	1.486	295.7	.1921	1.152	.1614	42.41	133.5	.369	1.773	3.49

TABLE VII: TABULATED HOT FILM DATA: X/D = 37.6

Pcone	Rcold	Vfilm	ΔT	Pfilm	ρ	ν	Umean	Re(m,r) x 10^{-3}	τ_w	U*	Cf x 10^3
5.5	7.088	1.443	308.8	.1810	1.150	.1598	9.39	29.8	.025	.464	4.89
11.4	7.079	1.457	309.8	.1845	1.151	.1595	13.56	43.2	.046	.628	4.29
18.3	7.077	1.466	310.0	.1870	1.150	.1597	17.21	54.7	.070	.771	4.02
24.6	7.089	1.471	308.7	.1881	1.149	.1601	19.96	63.3	.094	.894	4.01
35.1	7.106	1.475	306.7	.1892	1.147	.1605	23.86	75.5	.126	1.039	3.80
44.0	7.128	1.477	304.2	.1897	1.145	.1611	26.73	84.3	.163	1.183	3.92
54.0	7.133	1.482	303.7	.1909	1.144	.1613	29.63	93.3	.195	1.294	3.82
68.4	7.149	1.485	301.9	.1917	1.142	.1619	33.38	104.7	.243	1.445	3.75
85.4	7.179	1.485	298.6	.1918	1.137	.1629	37.36	116.5	.302	1.614	3.74
111.8	7.218	1.485	294.3	.1919	1.132	.1643	42.85	132.5	.397	1.854	3.74

TABLE IX TABULATED HOT FILM DATA: X/D = 50.4

Pcone	Rcold	Vfilm	ΔT	Pfilm	ρ	ν	Umean	Re(m,r) x 10^3	τ_w	U*	Cf x 10^3
5.5	7.099	1.442	307.5	.1808	1.155	.1591	8.12	25.9	.028	.486	7.18
11.4	7.092	1.455	308.3	.1842	1.156	.1589	13.53	43.3	.050	.652	4.65
18.5	7.088	1.465	308.8	.1867	1.155	.1590	17.25	55.1	.075	.796	4.26
24.2	7.091	1.471	308,4	.1880	1,154	.1592	19.75	62.1	.094	.894	4.10
29.2	7.095	1.474	308.0	.1888	1.153	.1595	21.68	69.1	.110	.965	3.96
34.3	7.102	1.475	307.2	.1892	1.153	.1598	23.53	74.8	.122	1.019	3.75
43.9	7.119	1.478	305.3	.1900	1.151	.1603	26.65	84.5	.158	1.159	3.78
54.7	7.142	1.480	302.7	.1906	1.149	.1610	29.79	94.0	.202	1.316	3.90
69.3	7.180	1.478	298.5	.1900	1.140	.1625	33.62	105.1	.252	1.473	3.84
84.7	7.197	1.480	296.6	.1906	1.136	.1633	37.23	115.8	.303	1.616	3.77
112.0	7.250	1.478	290.8	.1900	1.129	.1652	43.96	132.1	.409	1.884	3.85

TABLE X: TABULATED HOT FILM DATA: X/D = 57.3

Pcone	Rcold	Vfilm	ΔT	Pfilm	ρ	ν	Umean	Re(m,r) x 10^{-3}	τ_w	U*	Cf x 10^3
5.7	7.076	1.446	310.1	.1819	1.155	.1588	9.54	30.5	.026	.469	4.83
11.6	7.073	1.457	310.5	.1847	1.155	.1589	13.64	43.6	.044	.614	4.05
18.5	7.078	1.466	309.9	.1870	1.155	.1589	17.26	55.2	.071	.774	4.02
24.3	7.088	1.471	308.8	.1881	1.152	.1594	19.78	63.0	.092	.885	4.00
29.9	7.098	1.473	307.6	.1887	1.151	.1597	21.96	69.8	.110	.972	3.92
33.9	7.107	1.475	306.6	.1891	1.151	.1599	23.39	74.3	.126	1.035	3.92
44.0	7.121	1.478	305.0	.1901	1.149	.1604	26.69	84.5	.161	1.172	3.86
53.6	7.135	1.481	303.5	.1907	1.147	.1608	29.48	93.1	.195	1.291	3.84
69.0	7.167	1.480	299.9	.1905	1.142	.1620	33.51	104.0	.242	1.440	3.69
83.1	7.193	1.481	297.0	.1907	1.139	.1629	36.84	114.9	.297	1.600	3.77
112.0	7.233	1.482	292.6	.1910	1.133	.1642	42.87	132.6	.401	1.862	3.77

TABLE XI: TABULATED HOT FILM DATA: X/D = 73.0

Pcone	Rcold	Vfilm	ΔT	Pfilm	ρ	ν	Umean	Re(m,r) x 10^3	τ_w*	U*	Cf x 10^3
5.9	7.091	1.445	308.4	.1816	1.167	.1573	9.70	31.3	.028	.483	4.97
11.1	7.093	1.454	308.2	.1838	1.167	.1573	13.31	43.0	.049	.640	4.63
17.8	7.094	1.461	308.1	.1856	1.165	.1577	16.83	54.2	.073	.781	4.31
24.6	7.109	1.466	306.4	.1869	1.164	.1581	19.82	63.7	.098	.910	4.22
30.3	7.112	1.470	306.0	.1879	1.175	.1566	21.88	71.0	.118	.985	4.05
35.1	7.125	1.471	304.6	.1882	1.176	.1566	23.54	76.3	.134	1.058	4.04
43.6	7.143	1.474	302.6	.1889	1.170	.1576	26.32	84.8	.165	1.175	3.98
54.0	7.159	1.474	300.8	.1889	1.168	.1581	29.30	94.2	.198	1.289	3.87
65.5	7.170	1.477	299.6	.1890	1.167	.1585	32.30	103.5	.233	1.399	3.75
82.3	7.191	1.478	297.2	.1900	1.163	.1593	36.26	115.6	.290	1.563	3.72
112.5	7.236	1.479	292.3	.1902	1.158	.1607	42.50	134.3	.387	1.809	3.62

*From static pressure calibration

TABLE XII: PRESTON TUBE SHEAR STRESS RESULTS (entries in mm, water)

Re(m,r)* x 10^{-3}	AXIAL POSITION (X/D) 1.8	6.3	12.2	16.6	22.0	26.4	32.4	36.8
28.1	.024	.023	.022	.022	.024	.023	.026	.024
66.6	.096	.101	.095	.098	.098	.102	.104	.098
81.1	.134	.140	.133	.139	.140	.138	.148	.140
99.9	.190	.201	.195	.202	.202	.204	.210	.202
123.2	.272	.300	.279	.283	.292	.297	.306	.292
143.0	.348	.390	.381	.380	.407	.404	.423	.407
164.9	.459	.512	.529	.523	.544	.532	.555	.544

Re(m,r)* x 10^{-3}	AXIAL POSITION (X/D) 41.7	46.1	52.0	56.5	61.9	66.3	72.2	76.6**
28.1	.022	.023	.023	.023	.024	.024	.023	-
66.6	.103	.104	.105	.105	.109	.108	.106	.106
81.1	.146	.146	.149	.150	.150	.150	.150	.150
99.9	.209	.121	.217	.216	.218	.221	.221	.220
123.2	.311	.317	.321	.323	.323	.325	.325	.324
143.0	4.22	.432	.435	.438	.439	.442	.442	.438
164.9	.556	.563	.574	.579	.581	.585	.589	.588

*The Re(m,r) entry is an average of the particular Reynolds numbers at each axial position.

**Calibration position

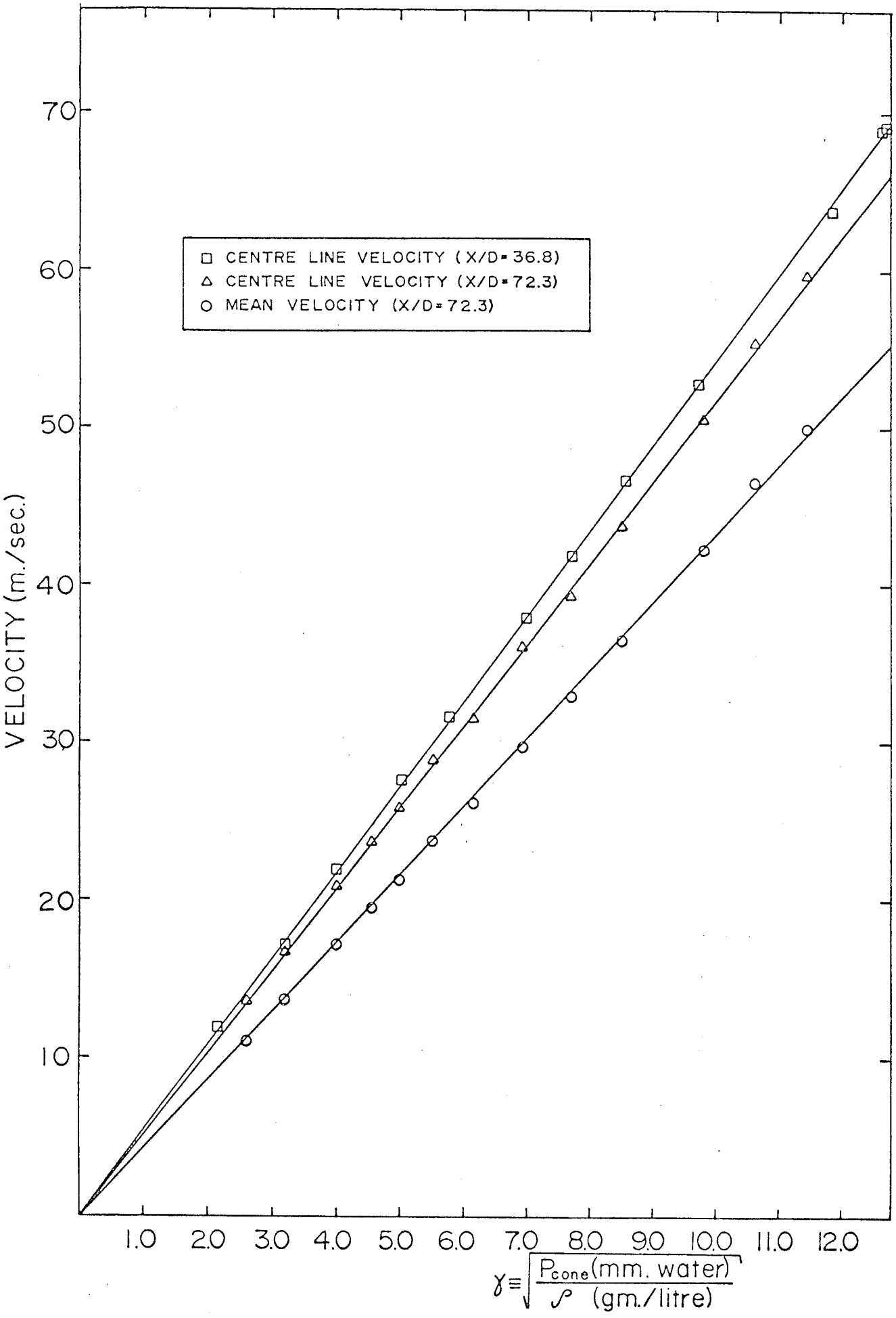

1. Wind tunnel calibration

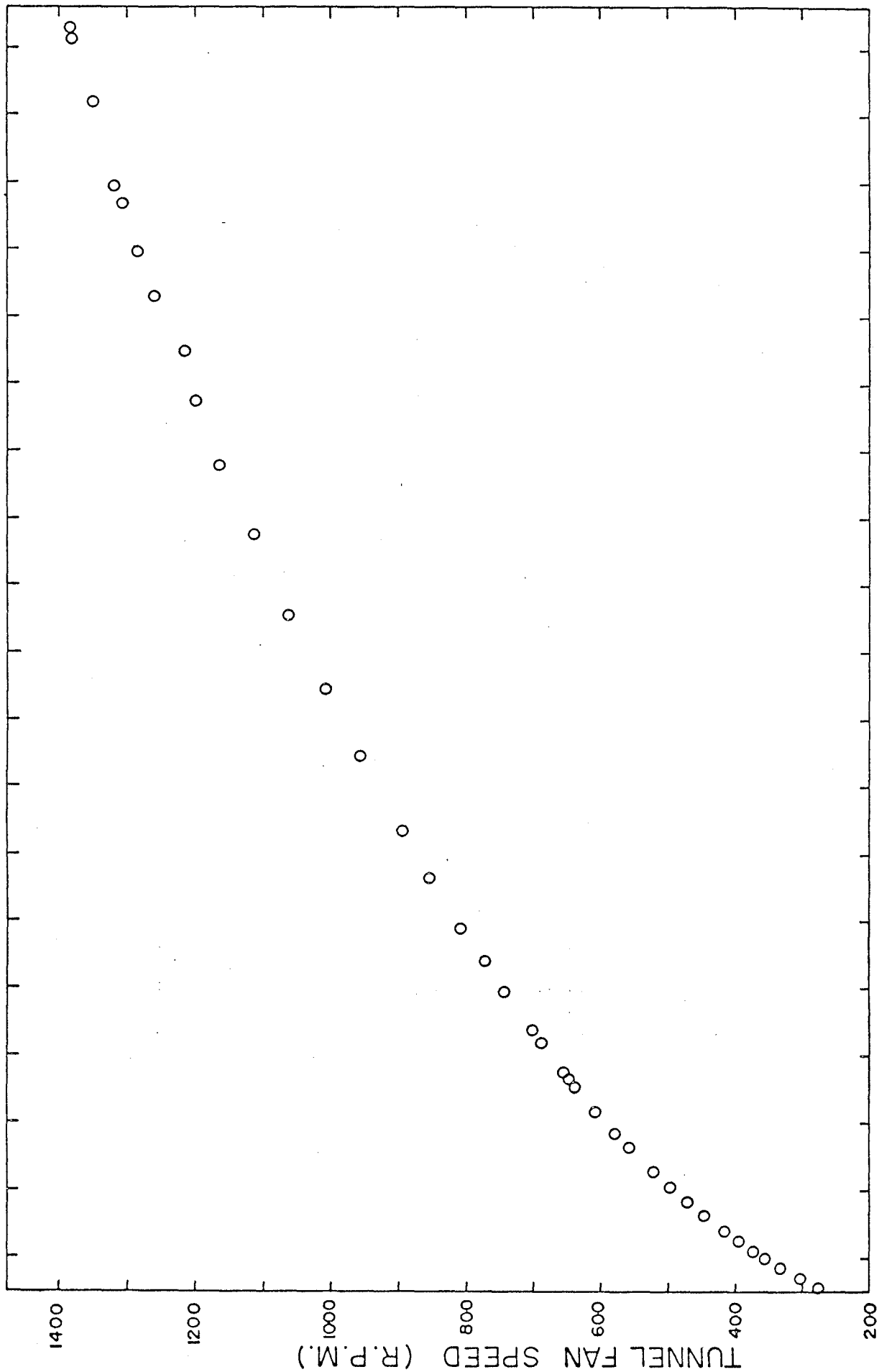

2. Fan speed calibration

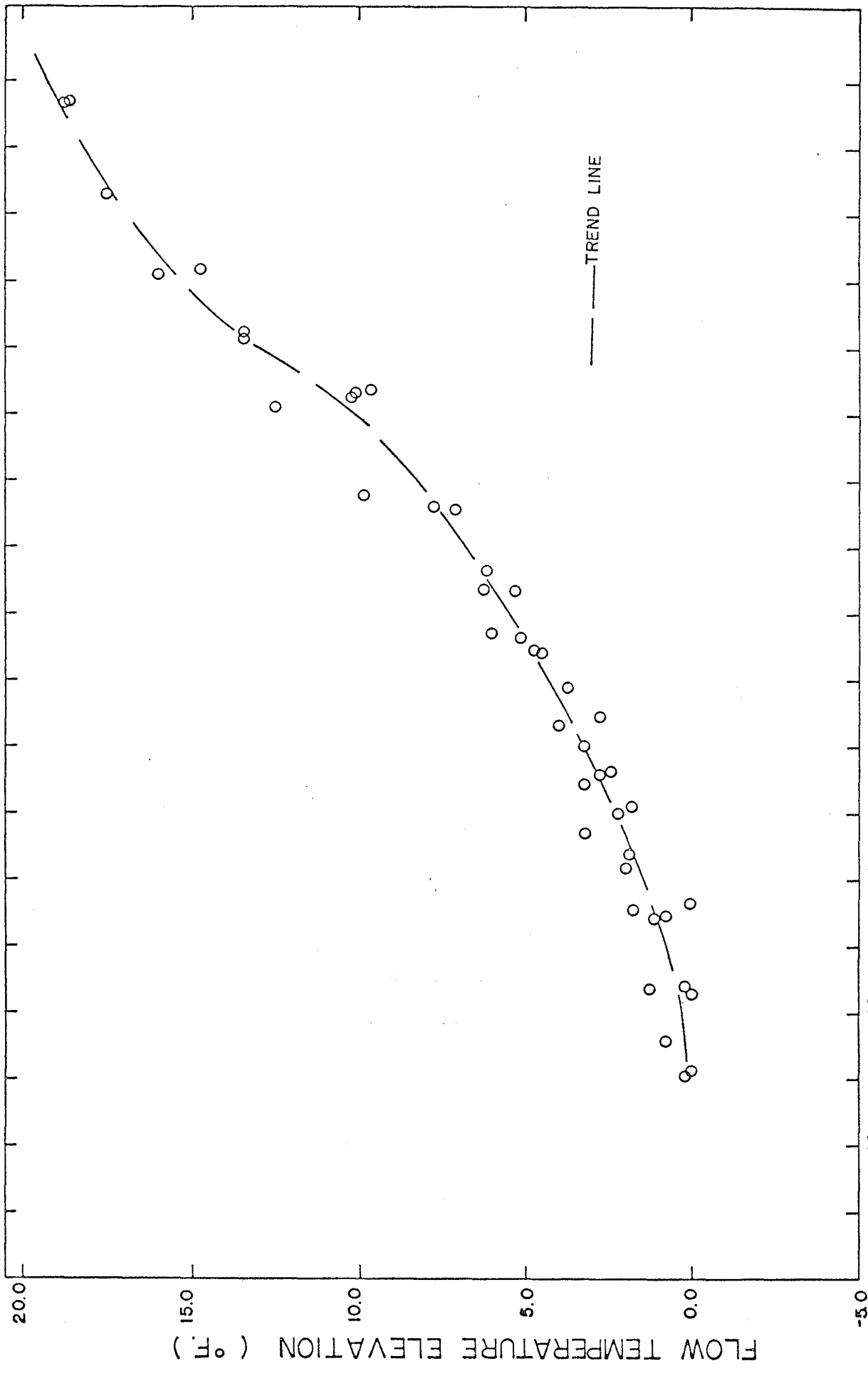

3. Tunnel air temperature behavior

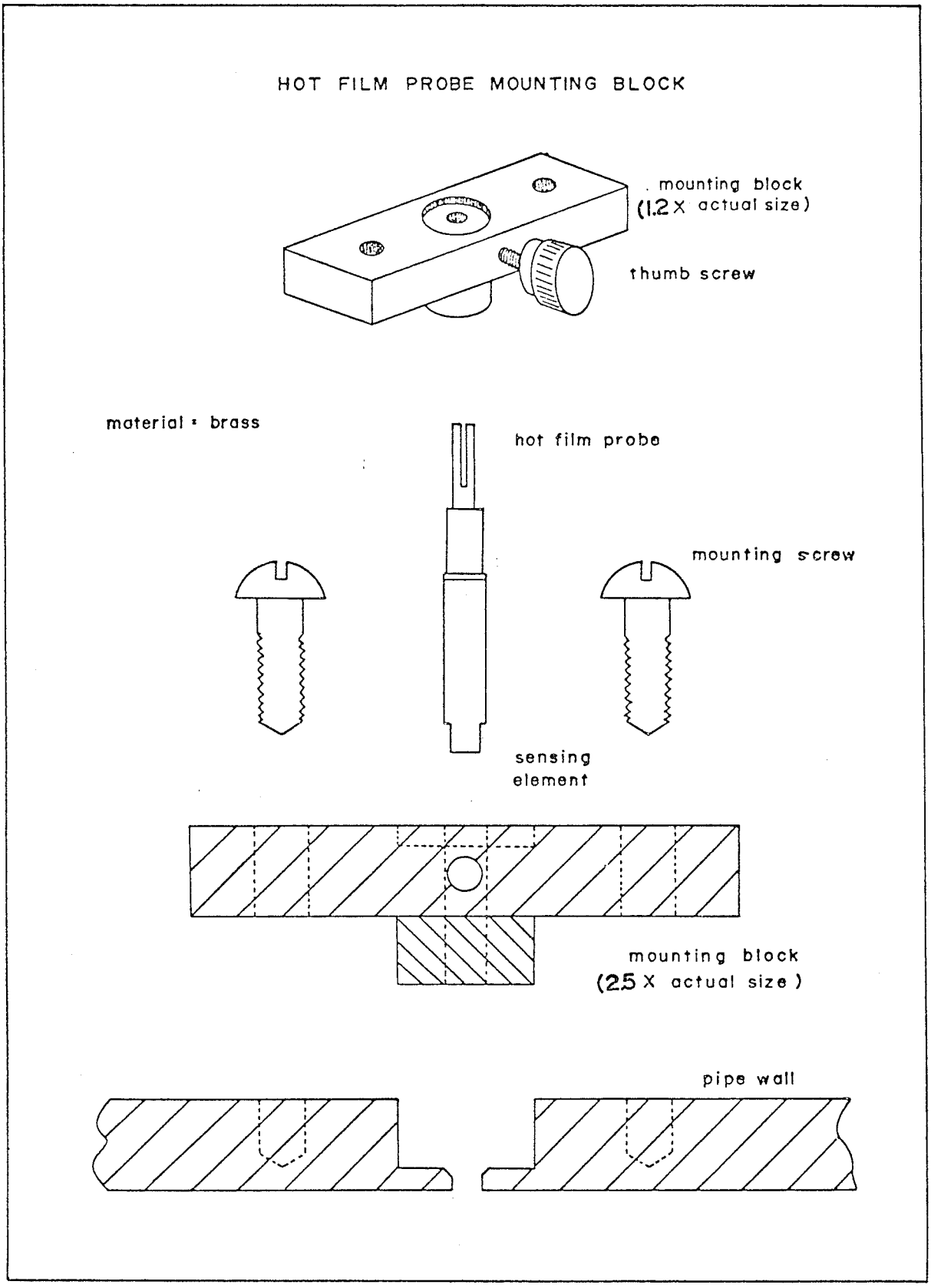

4. Hot film probe mounting block

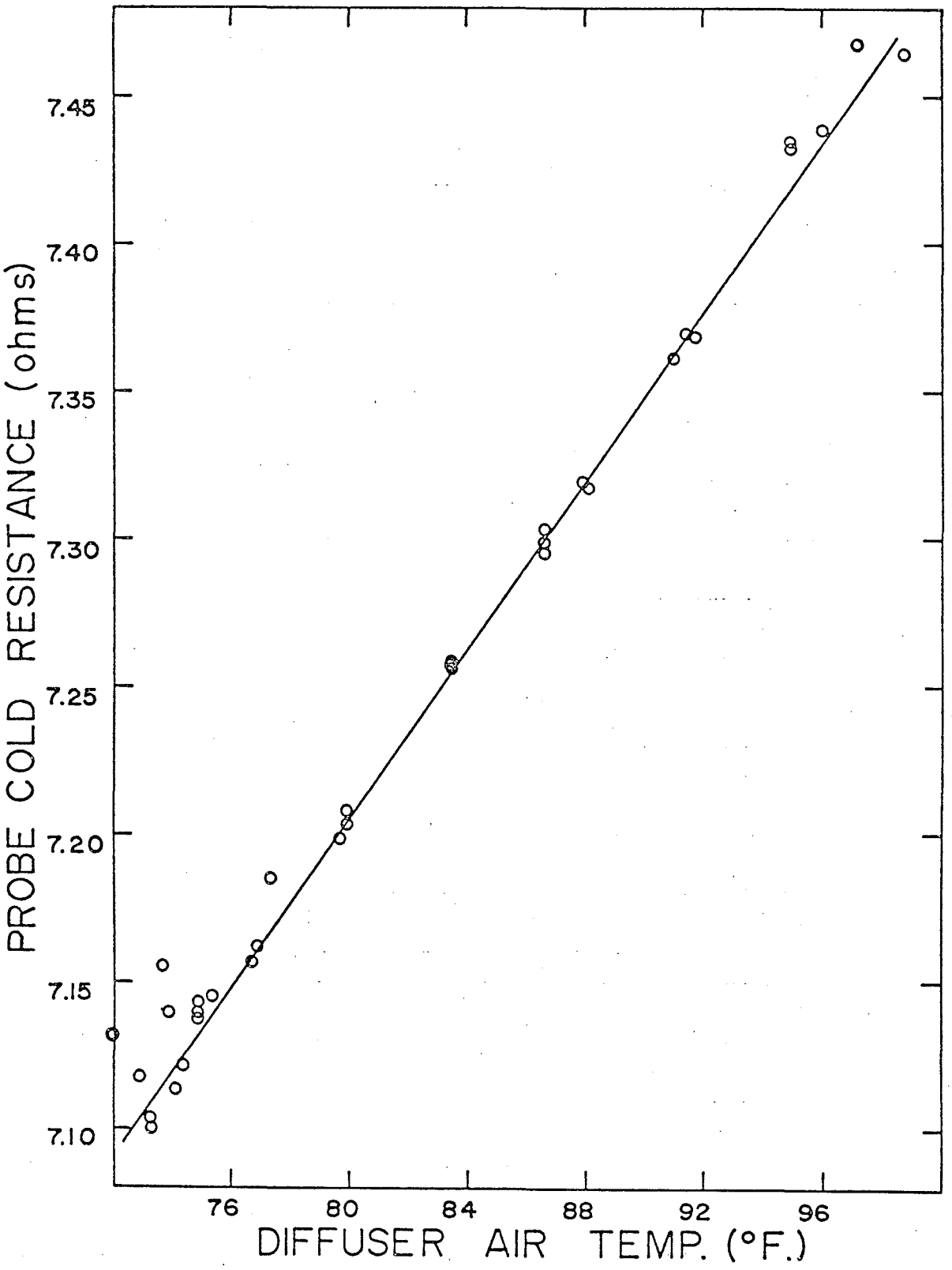

5. Temperature coefficient of resistivity for the hot film

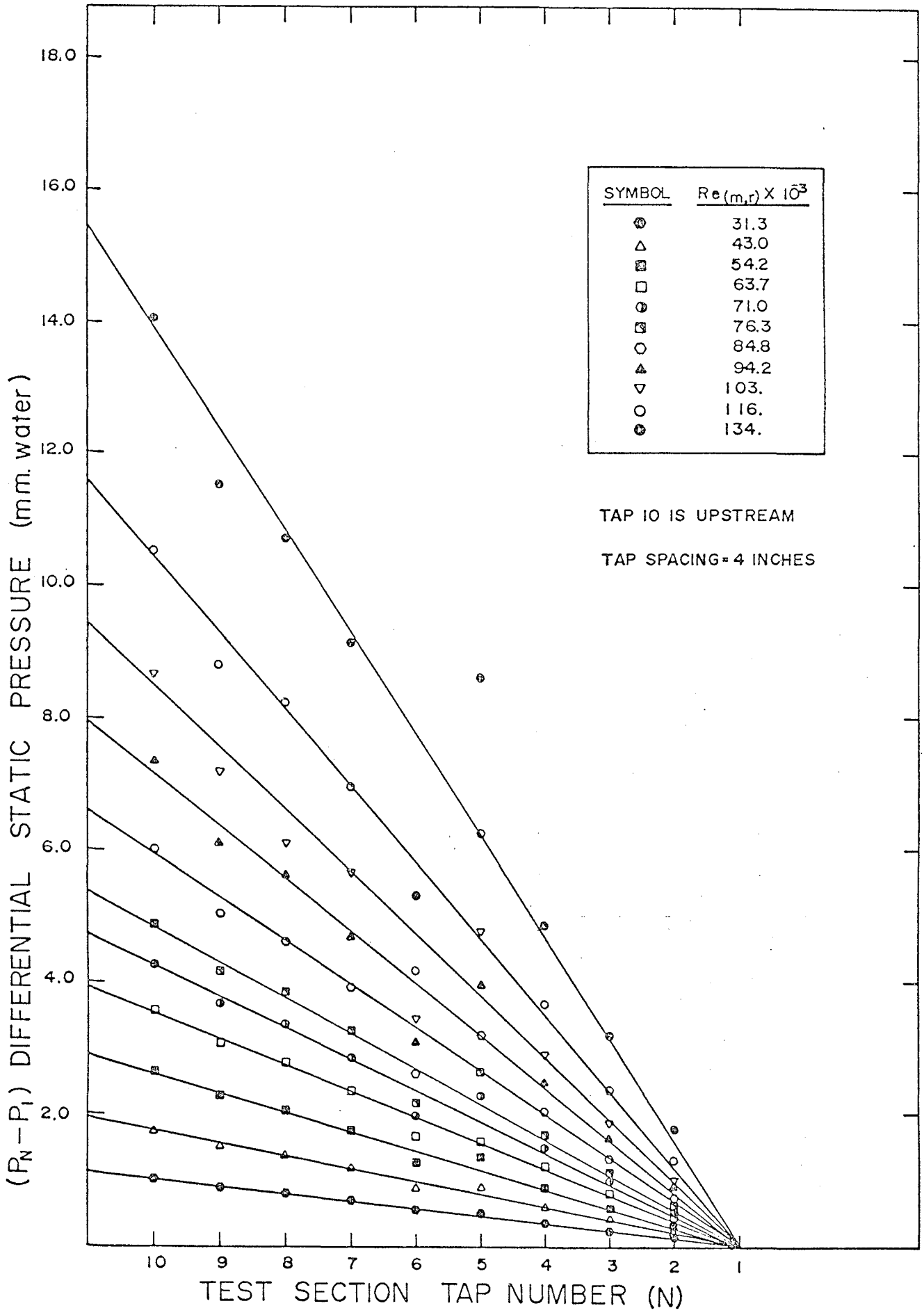

6. Fully developed flow differential static pressure measurements

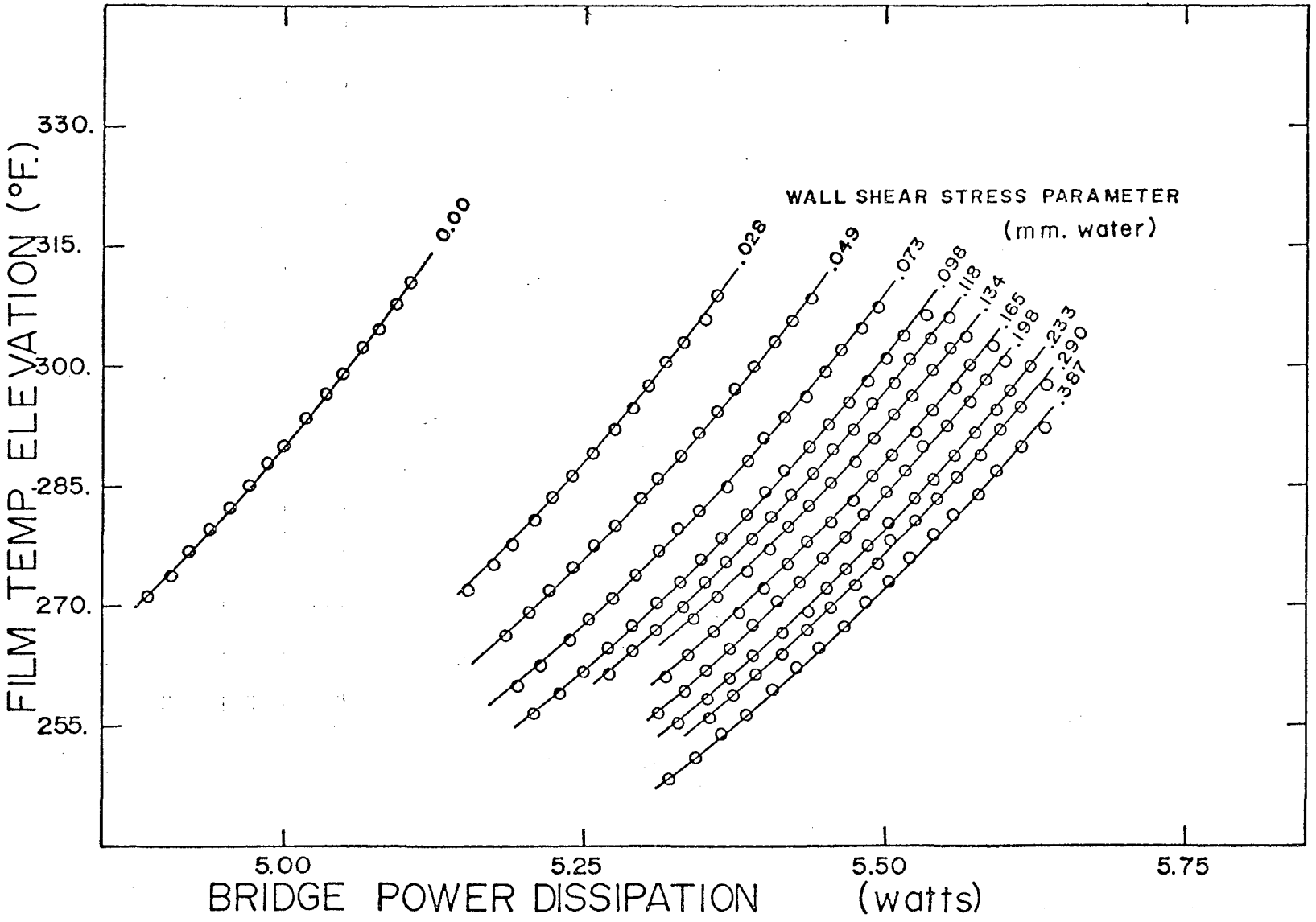

7 a) Bridge power dissipation (Calibration 1)

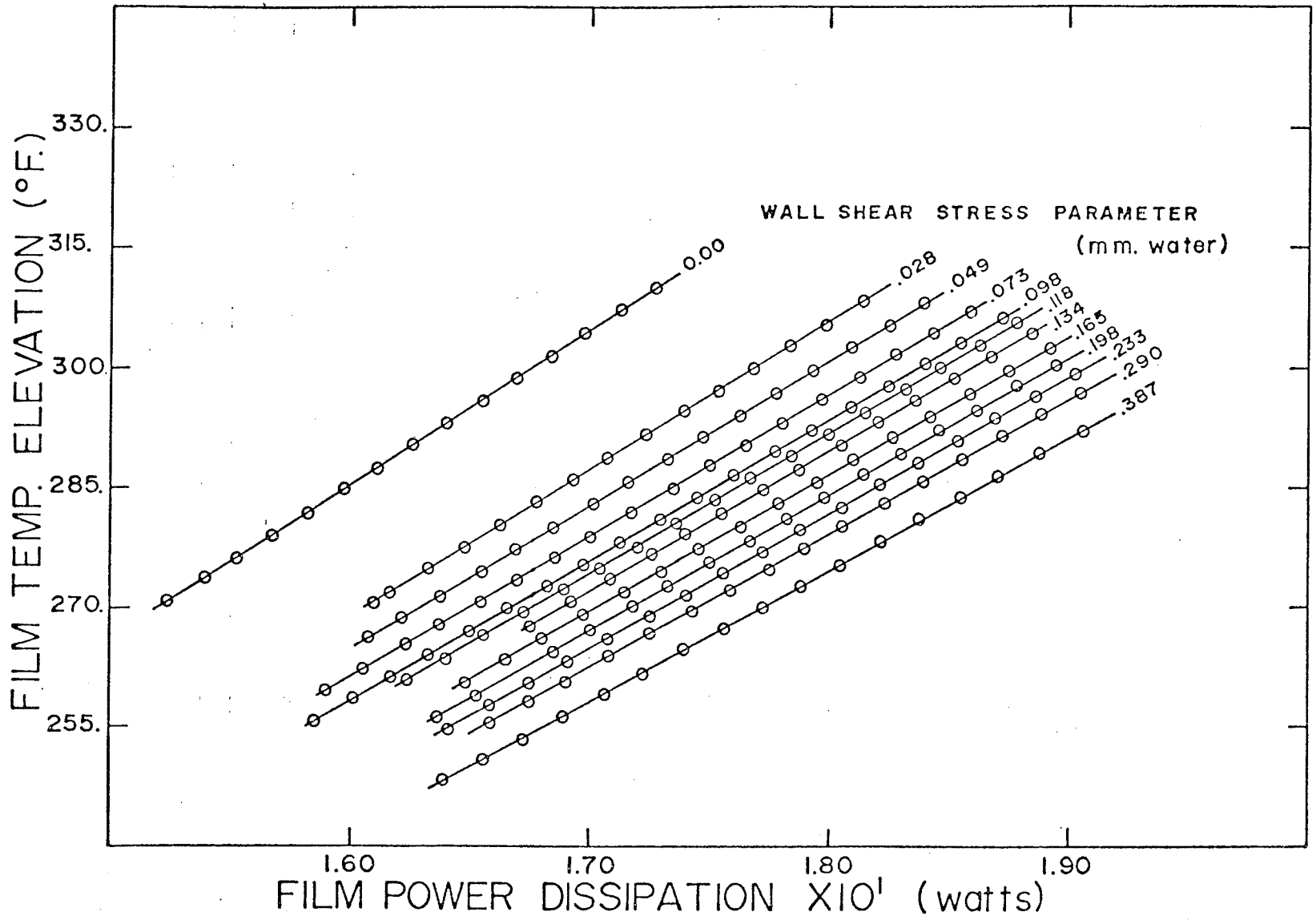

7b) Film power dissipation (Calibration 1)

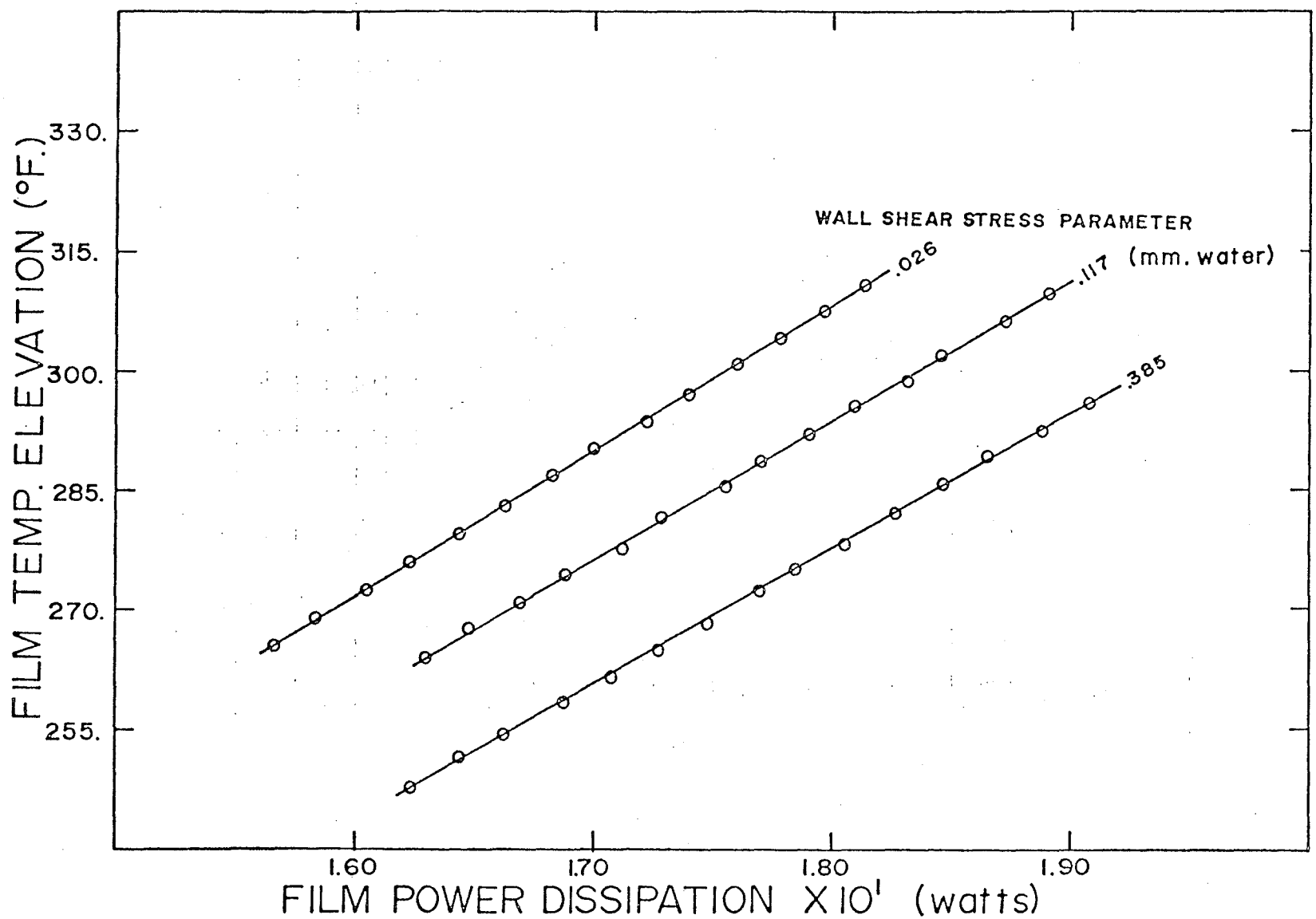

7c) Film power dissipation (Calibration 2)

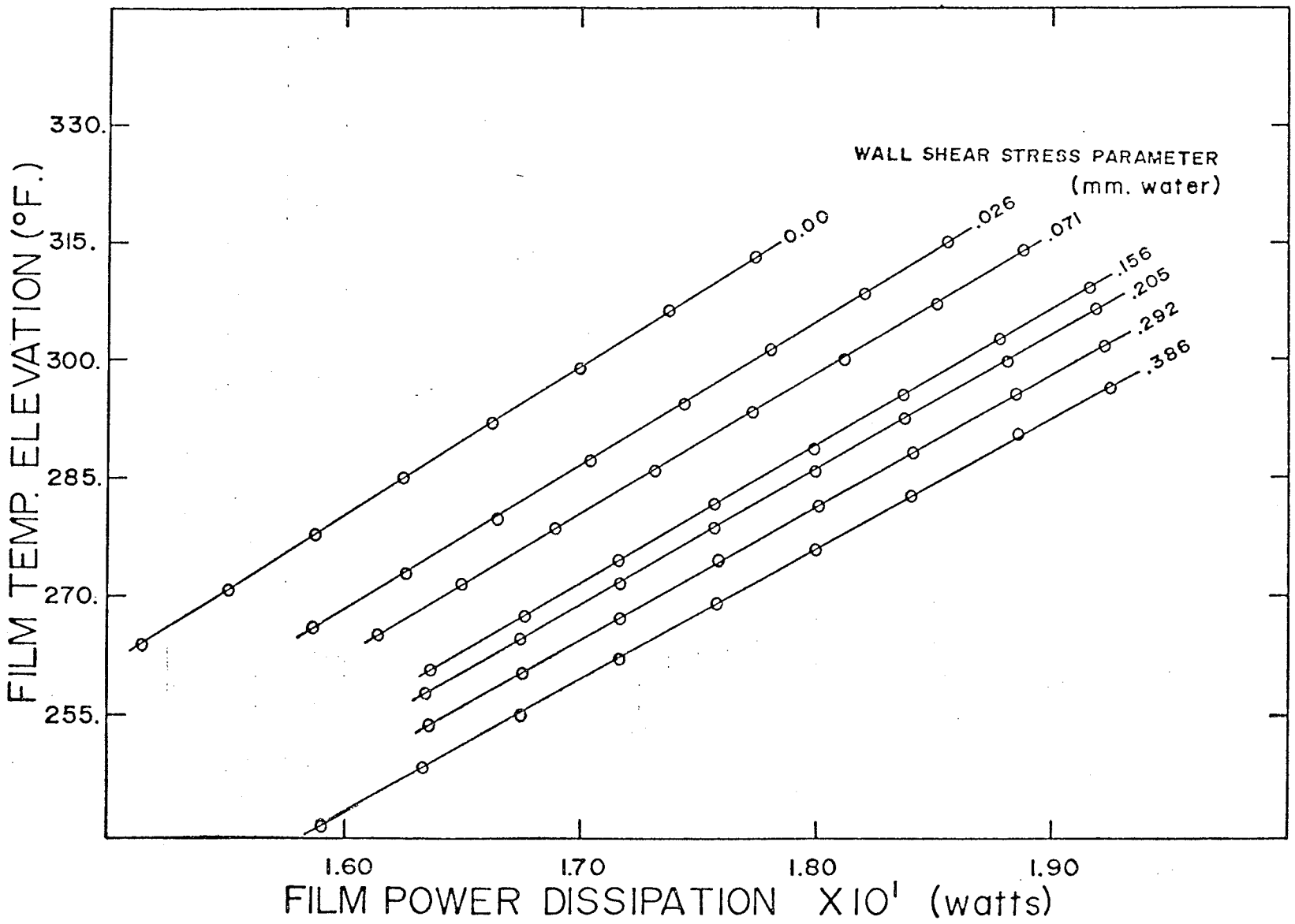

7d) Film power dissipation (Calibration 3)

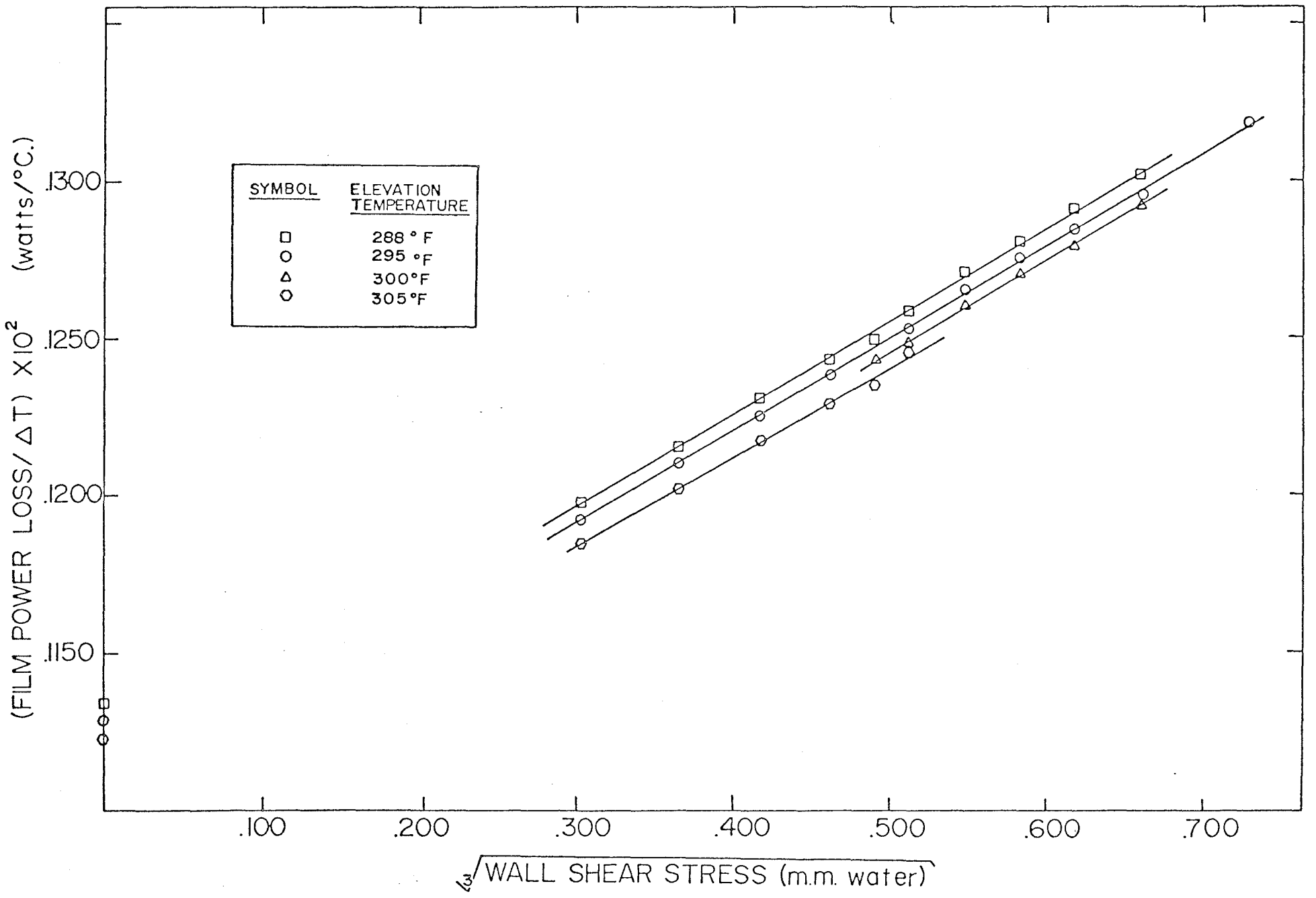

8. Hot film temperature elevation behavior (Calibration 1)

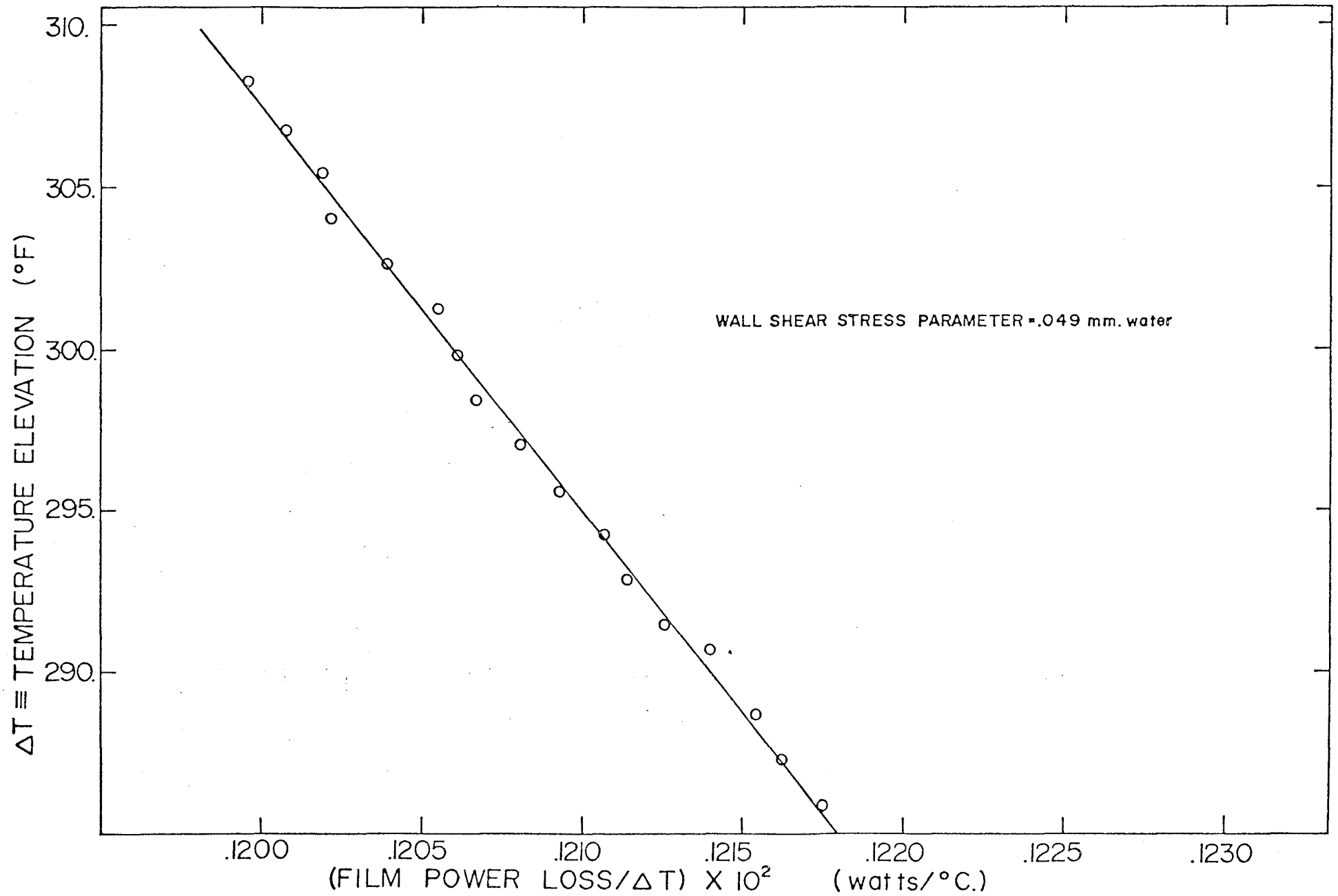

9. Temperature elevation dependence of calibration intercept parameter (Calibration 1)

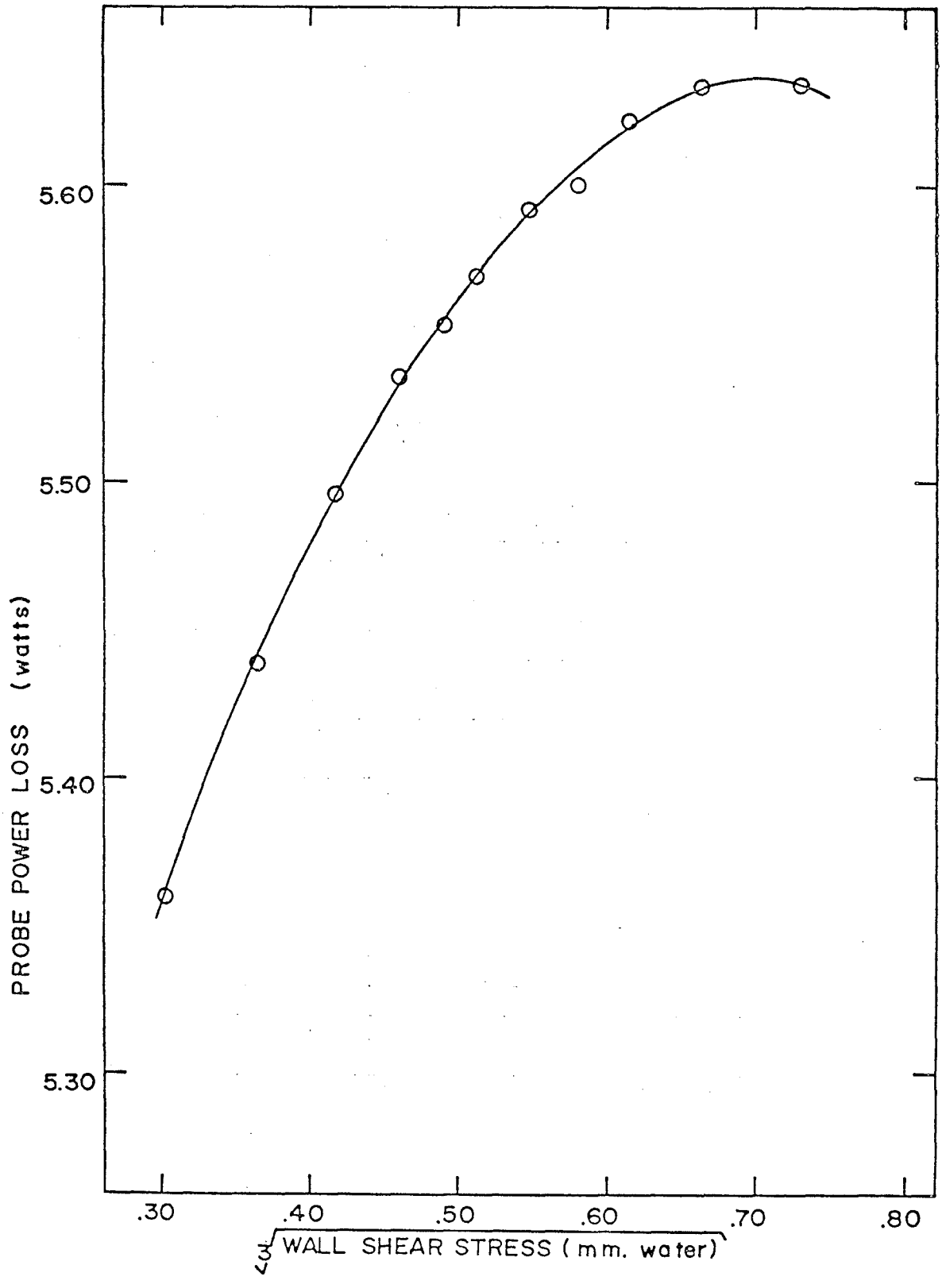

10. Hot film behavior uncorrected for temperature elevation changes

X/D	ARRANGEMENT OF WIND TUNNEL SECTIONS	
1.5*	/R/TEST/405/25/205/45/D	(section lengths in cm.)
10.5	/R/TEST/405/25/205/45/D	
17.4	/R/25/45/TEST/205/405/D	
30.7	/R/205/TEST/405/25/45/D	
37.6	/R/25/45/205/TEST/405/D	
50.4	/R/405/TEST/205/25/45/D	
57.3	/R/25/45/405/TEST/205/D	
73.0	/R/405/25/205/TEST/45/D	

* hot film probe in mounting position 10 rather than 1

R: roughness section

D: diffuser section

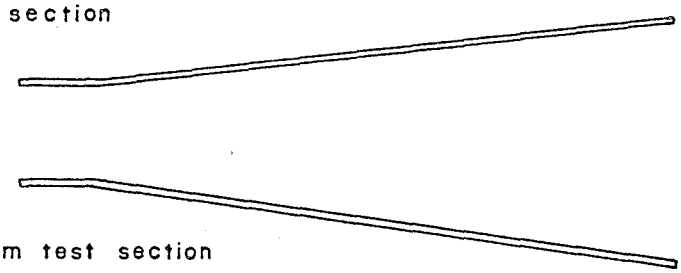

TEST: hot film test section

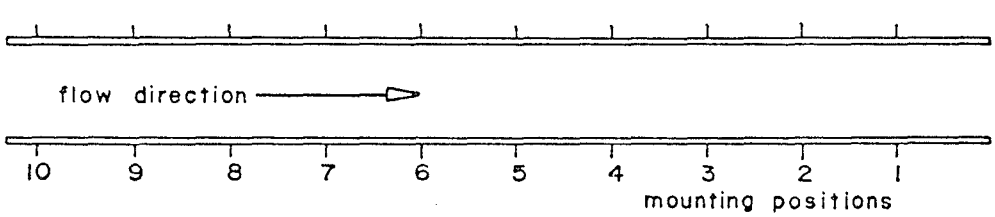

scale: .6 cm. = 2 in.

11. Arrangements of wind tunnel sections

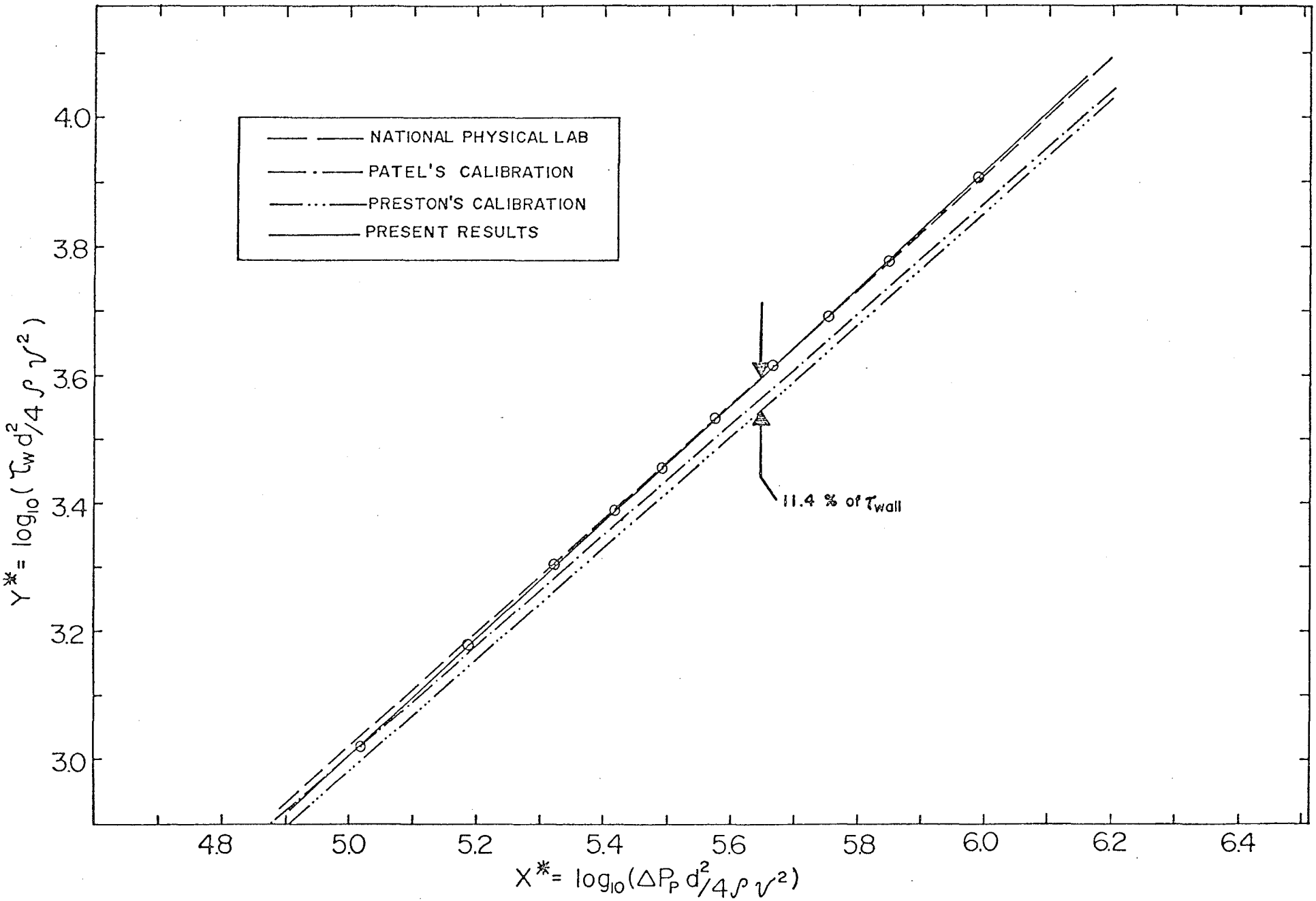

12. Preston tube calibration

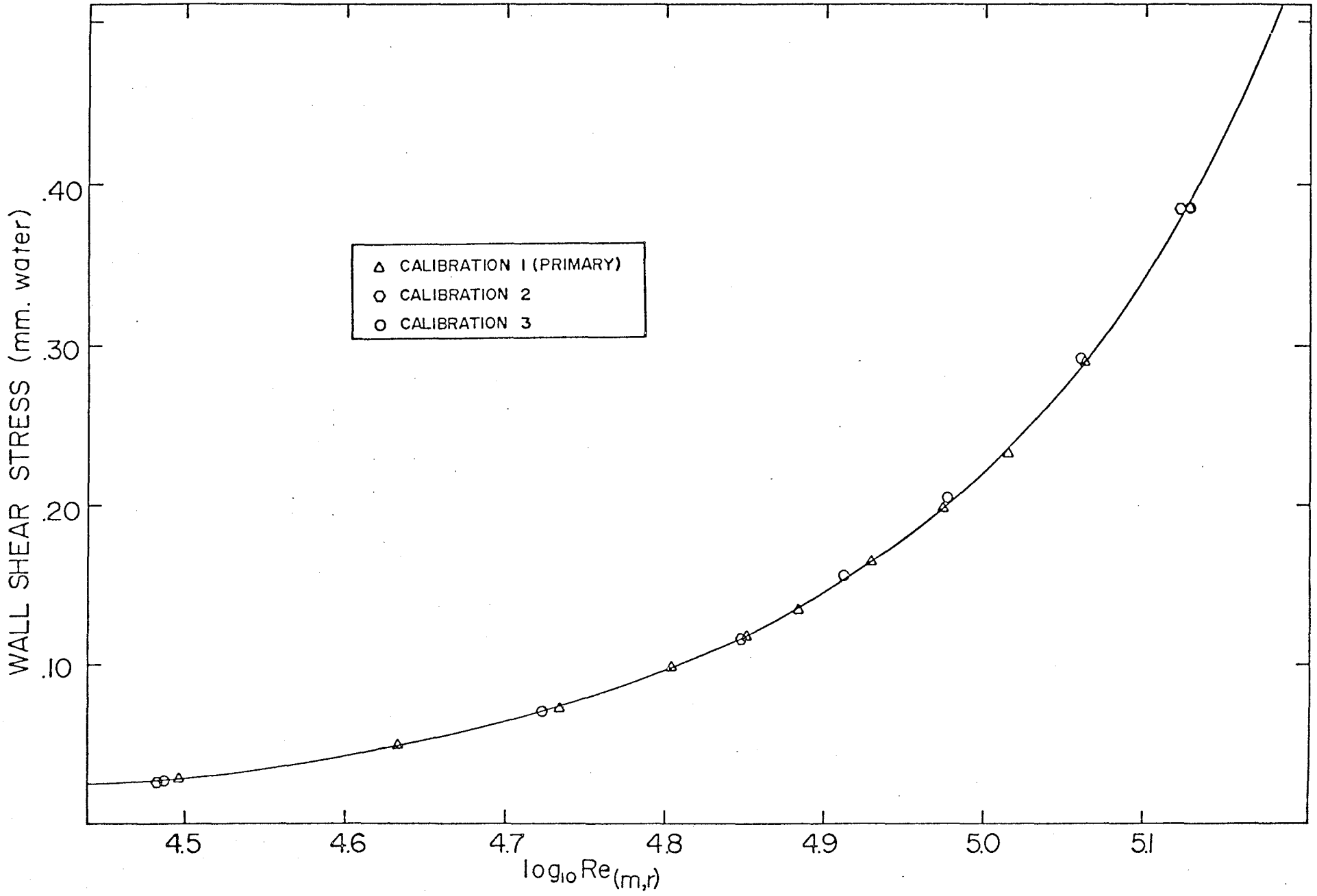

13. Calibration shear stresses for fully developed flow

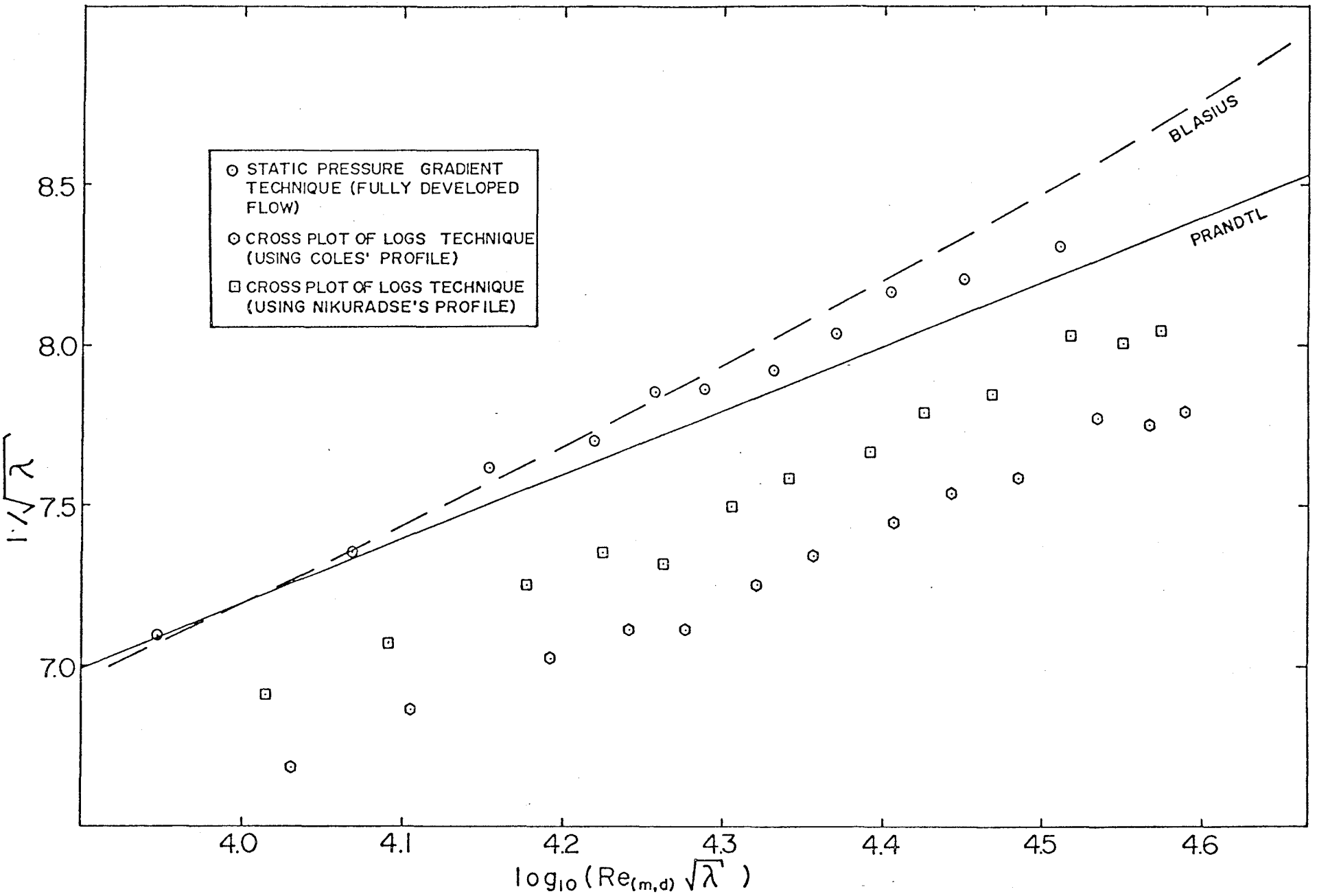

14. Calibration shear stresses compared with the universal friction laws

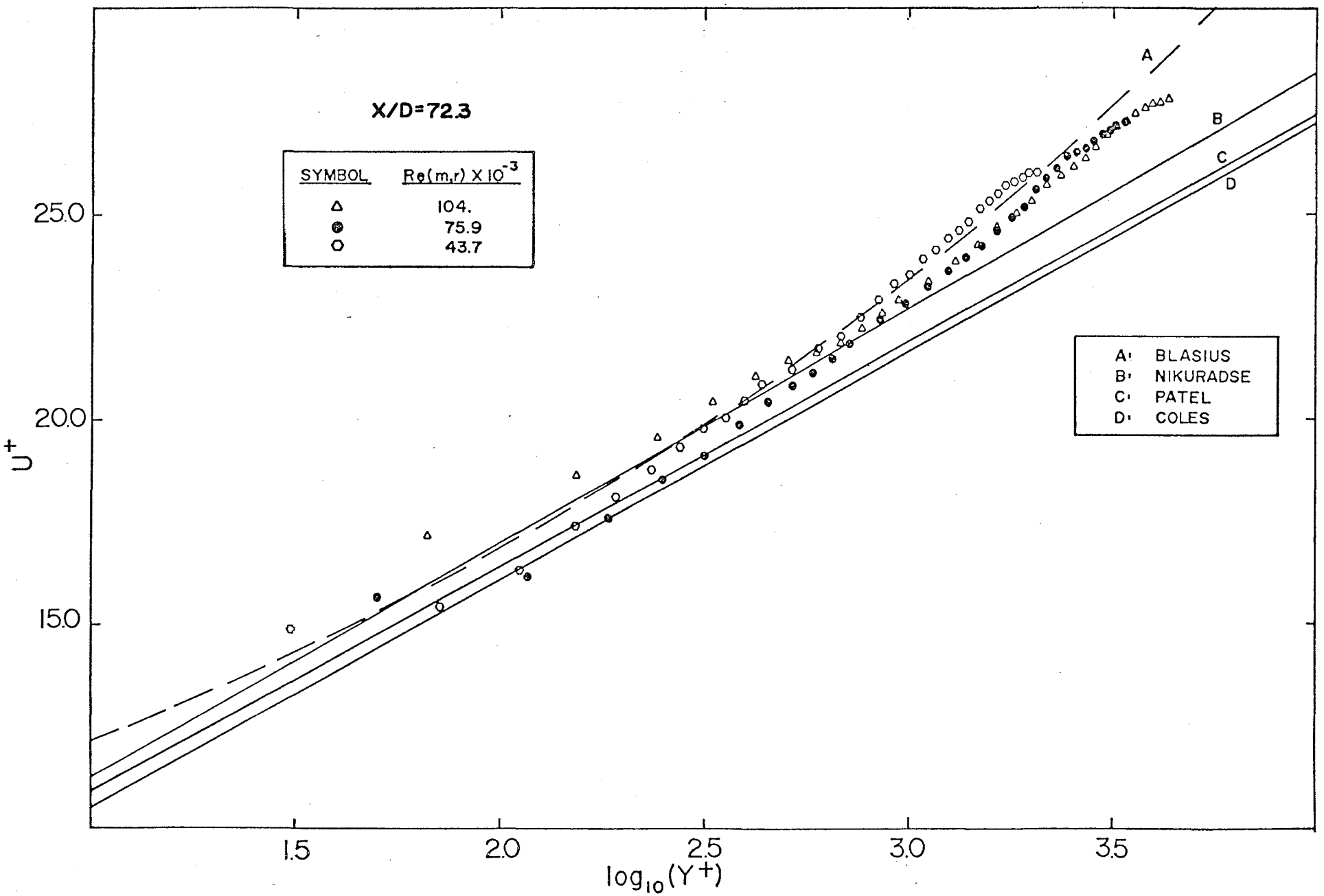

15. Dimensionless velocity profiles in the fully developed region

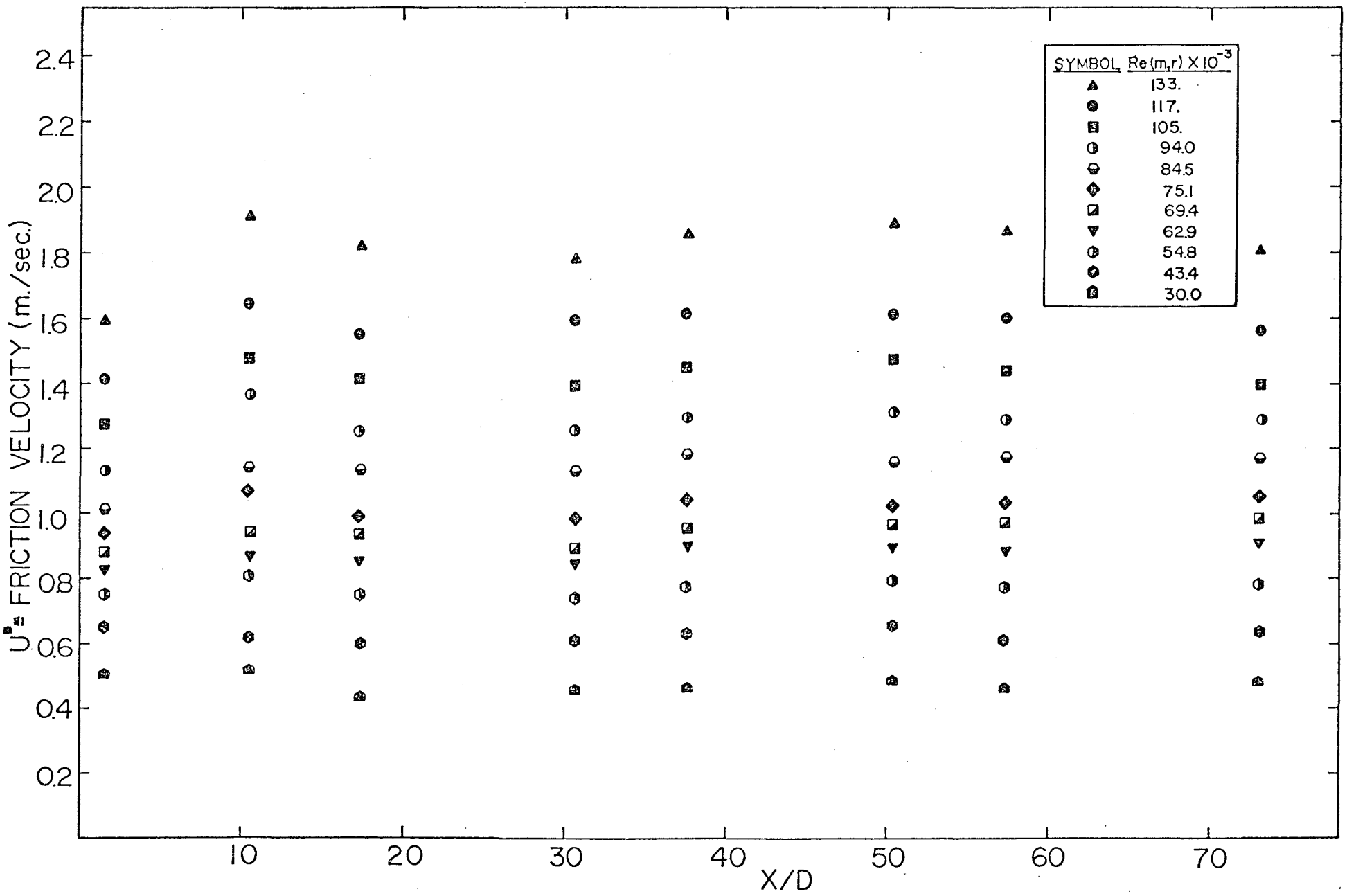

16. Hot film friction velocity results

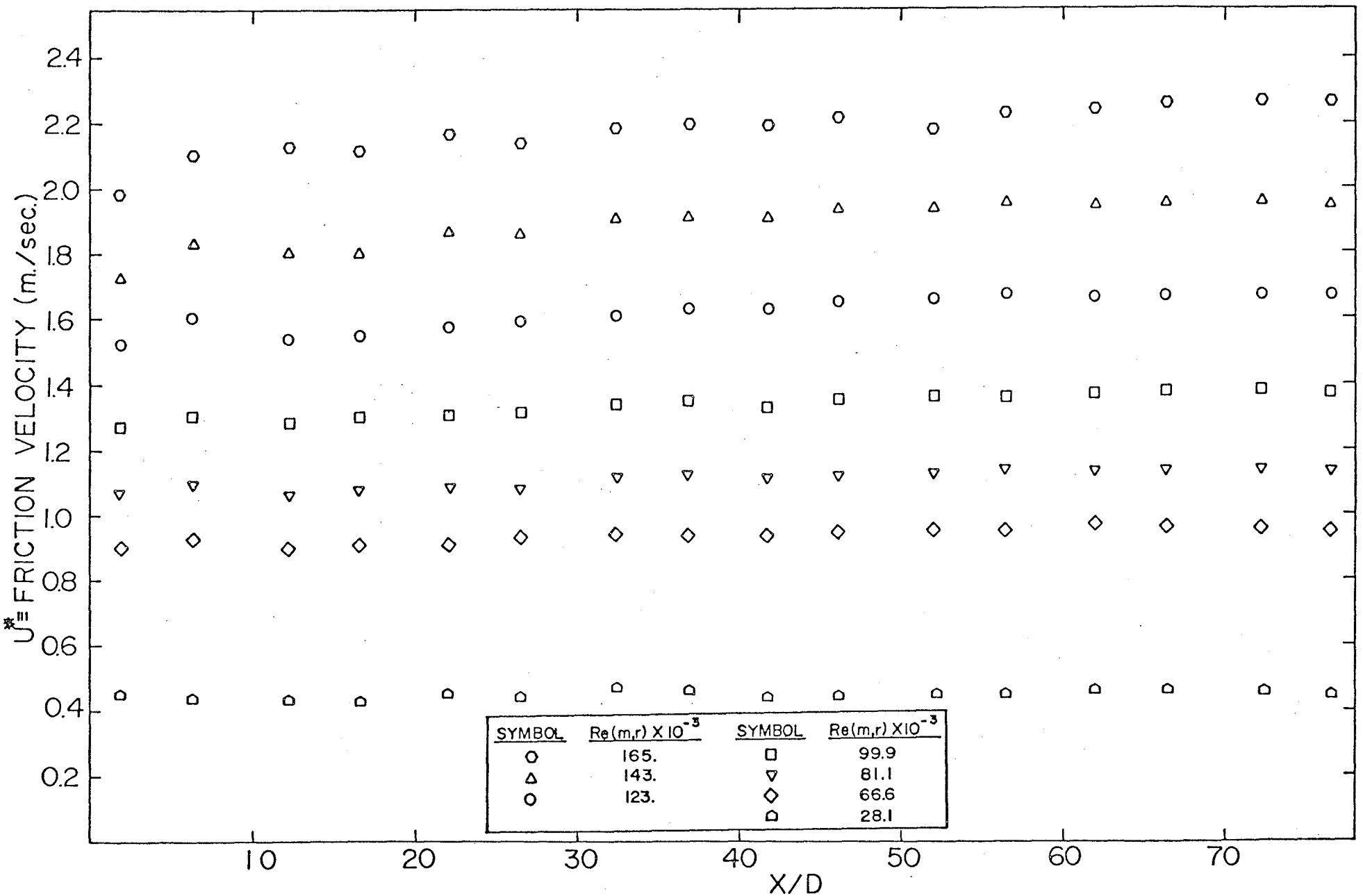

17. Preston tube friction velocity results

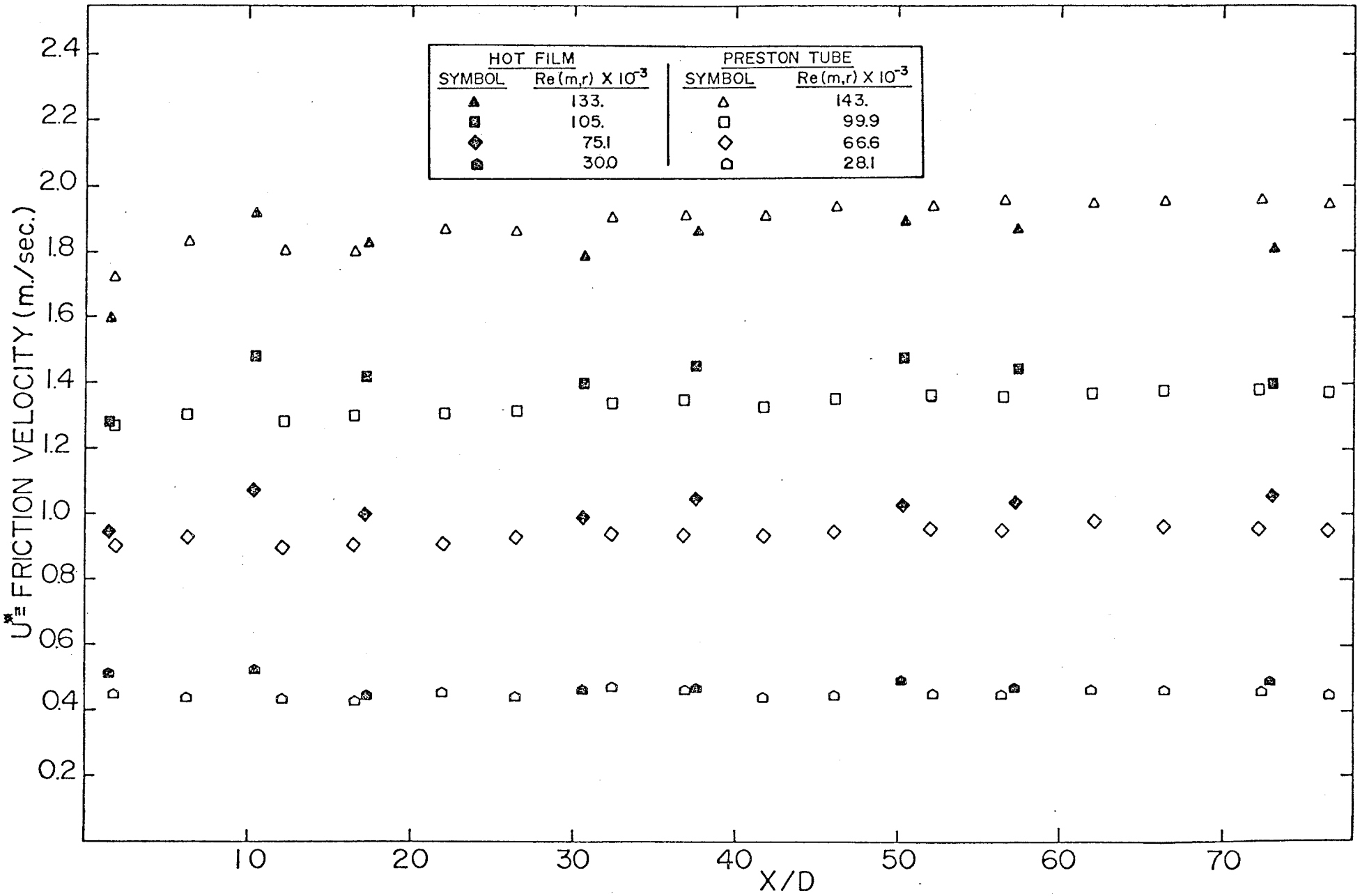

18. Comparison of hot film and Preston tube friction velocity results

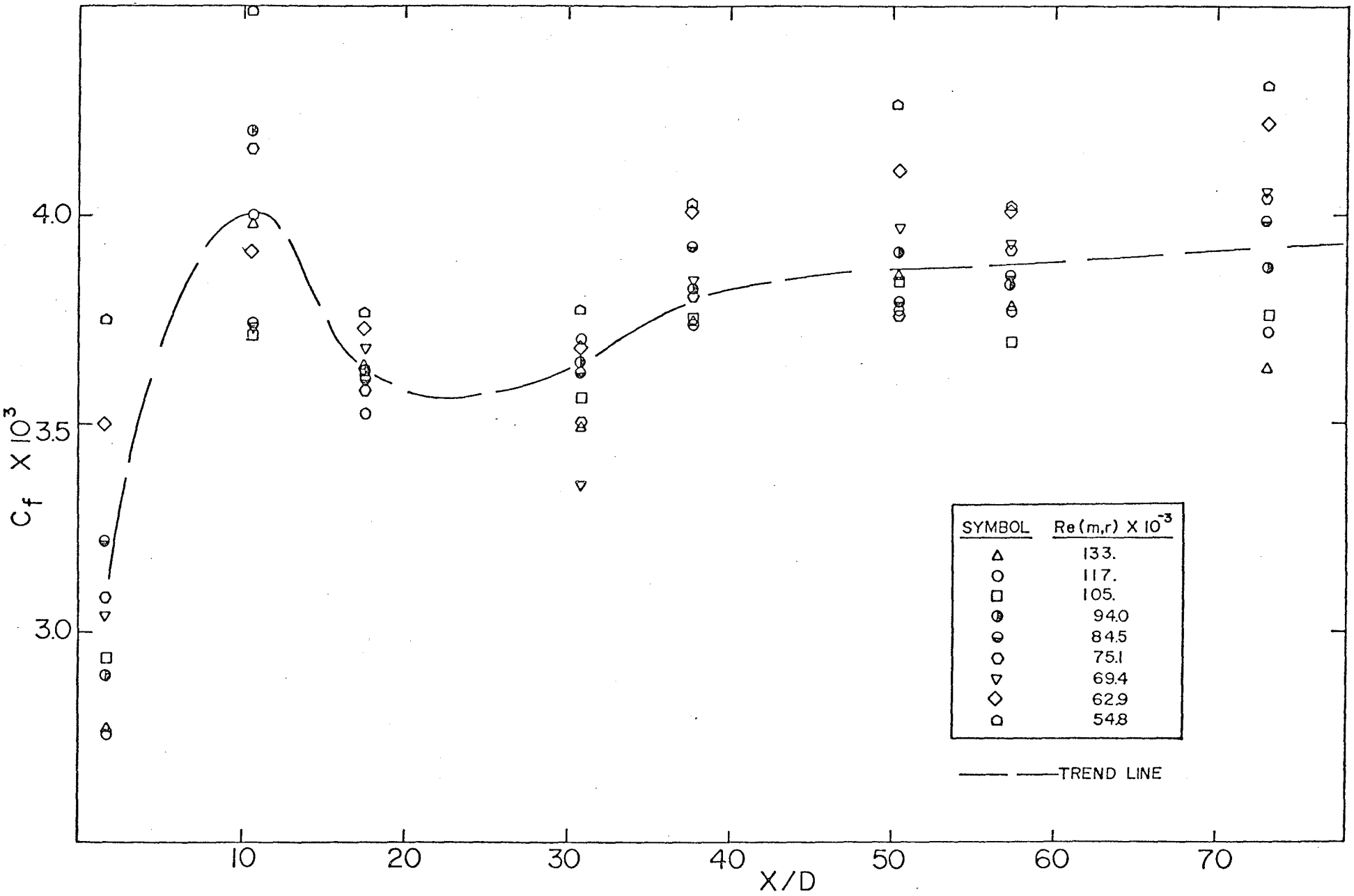

19. Hot film skin friction coefficient results

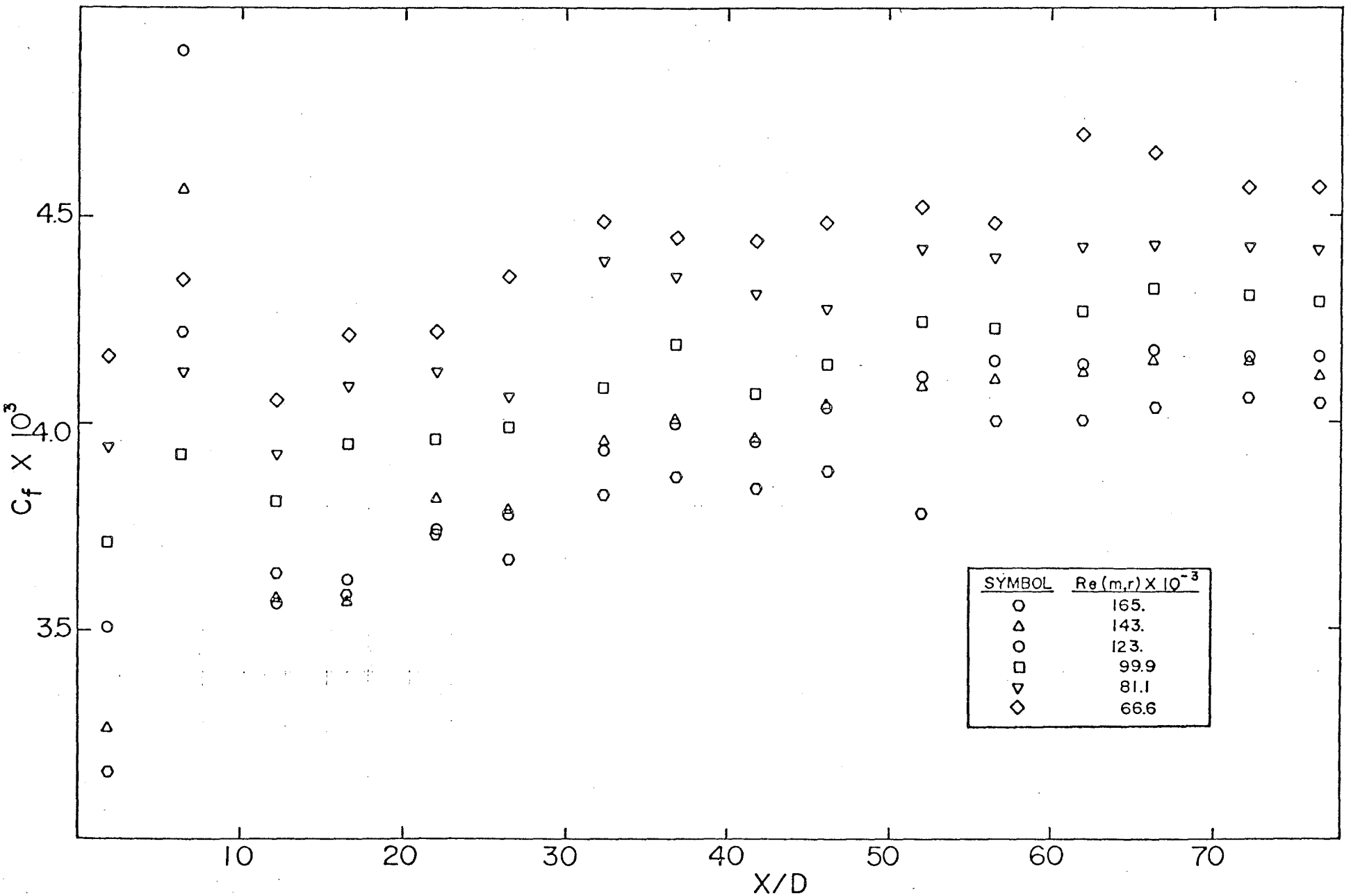

20. Preston tube skin friction coefficient results

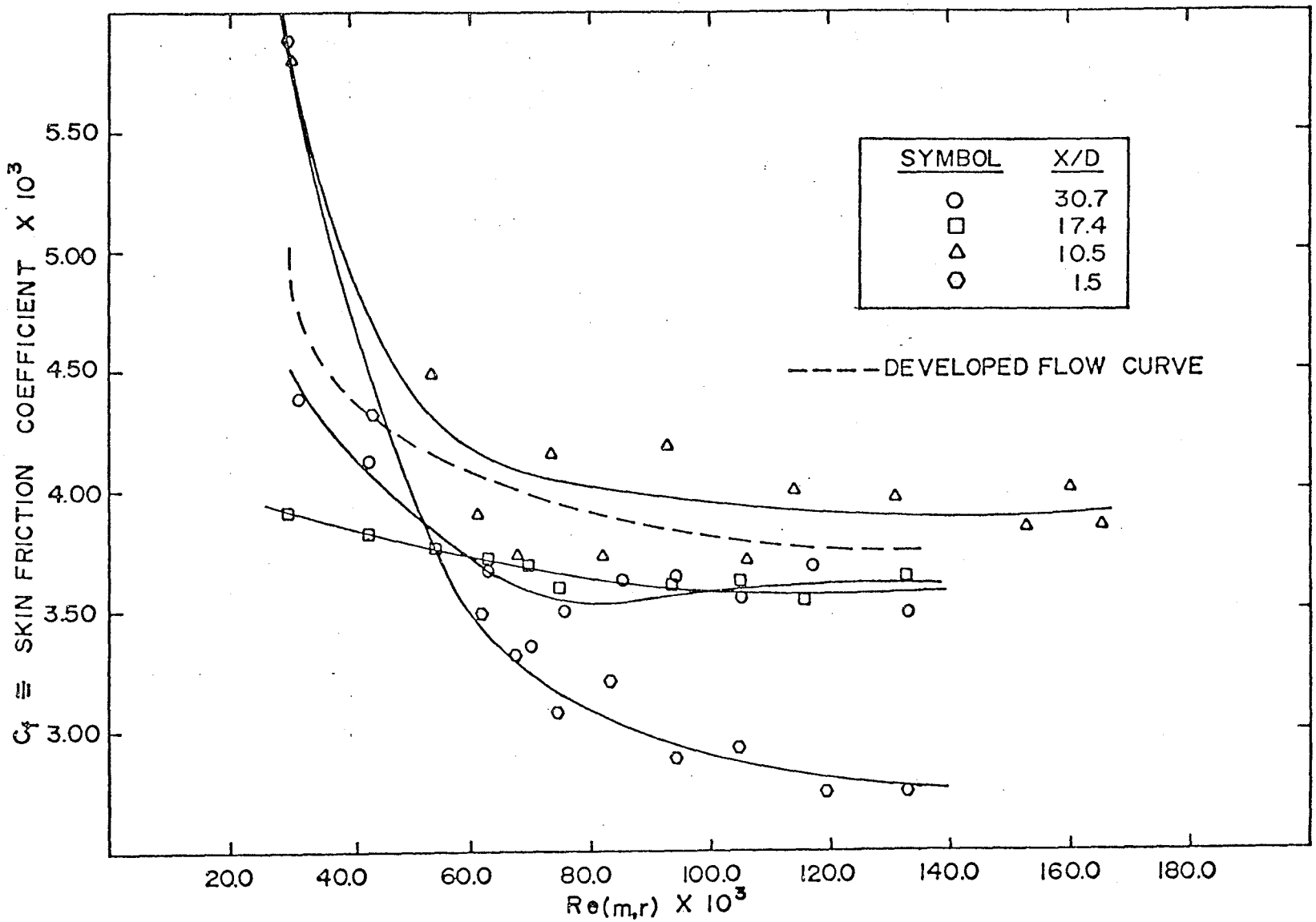

21. Reynolds number behavior of hot film skin friction coefficient results in developing flow

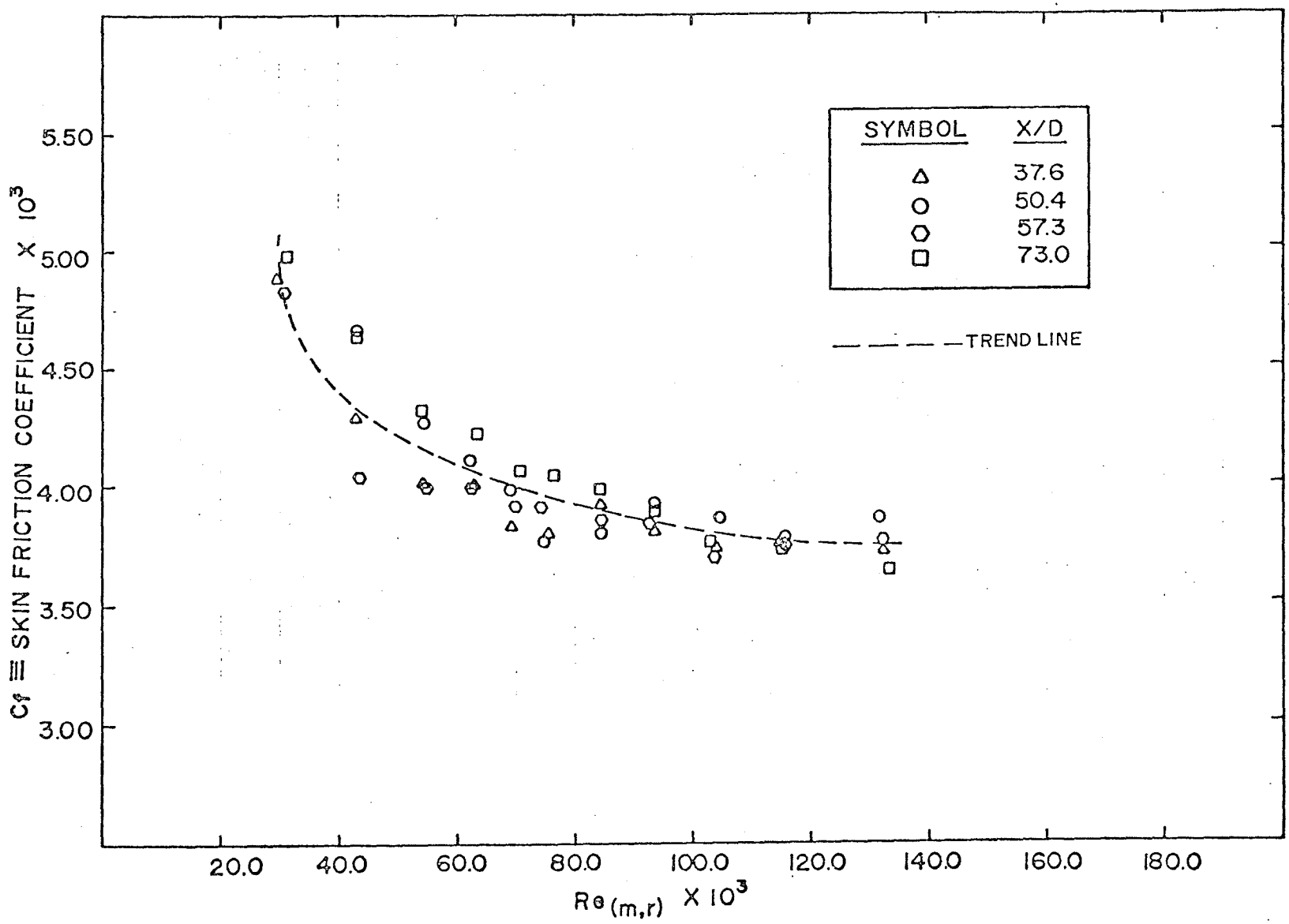

22. Reynolds number behavior of hot film skin friction coefficient results in developed flow

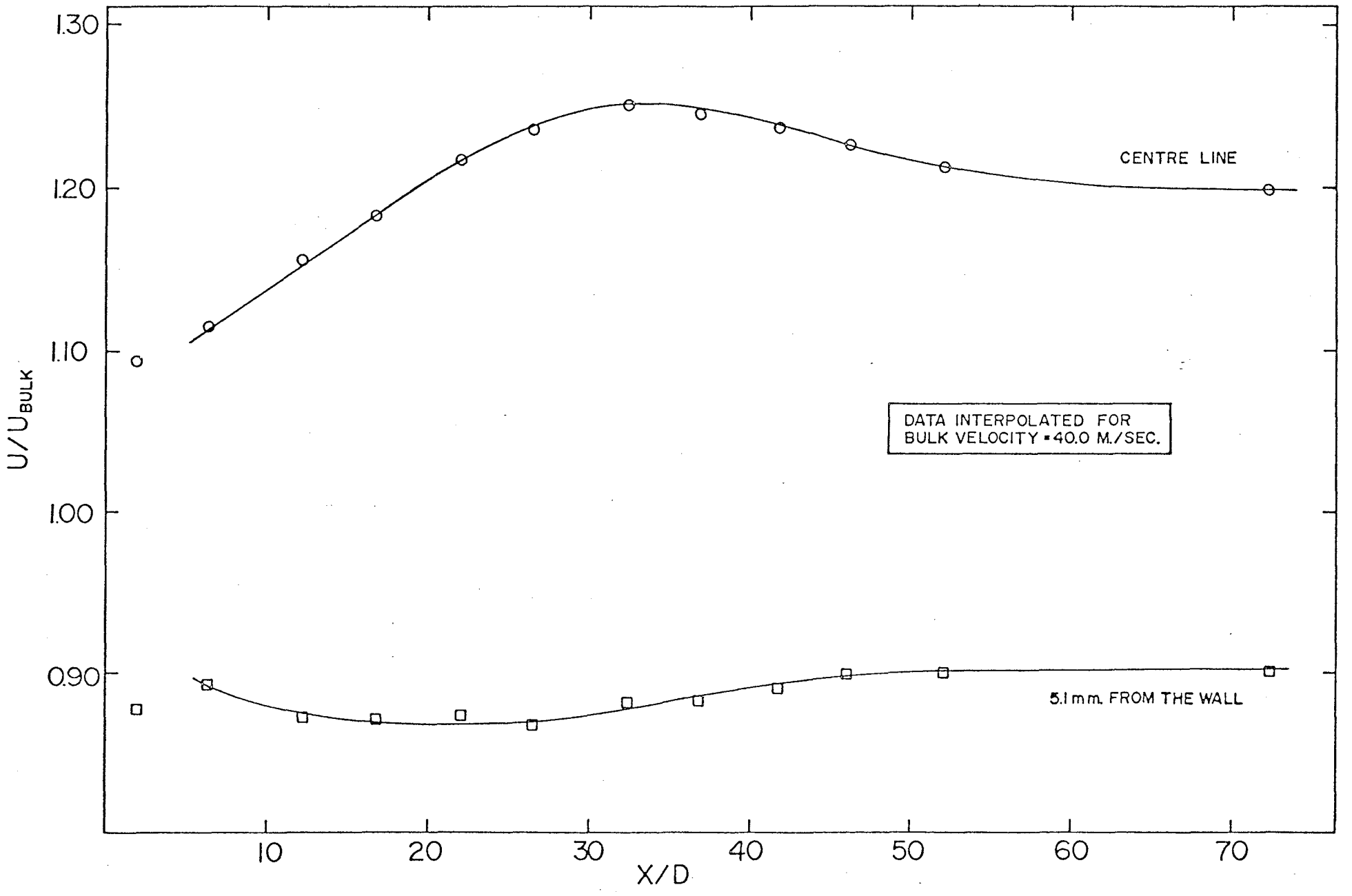

23. Longitudinal behavior of centerline and wall region velocity

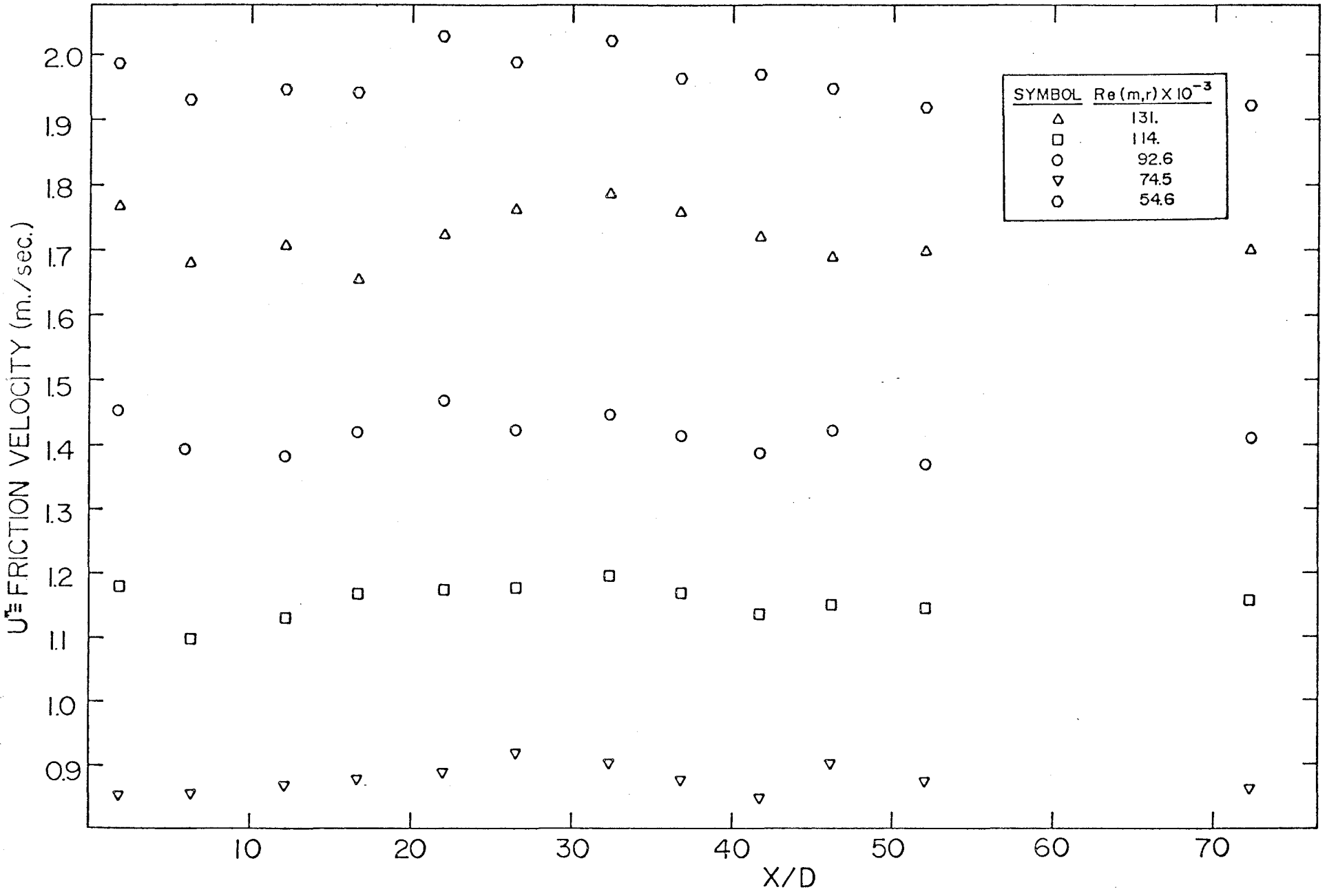

24. Cross plot of log technique friction velocity results

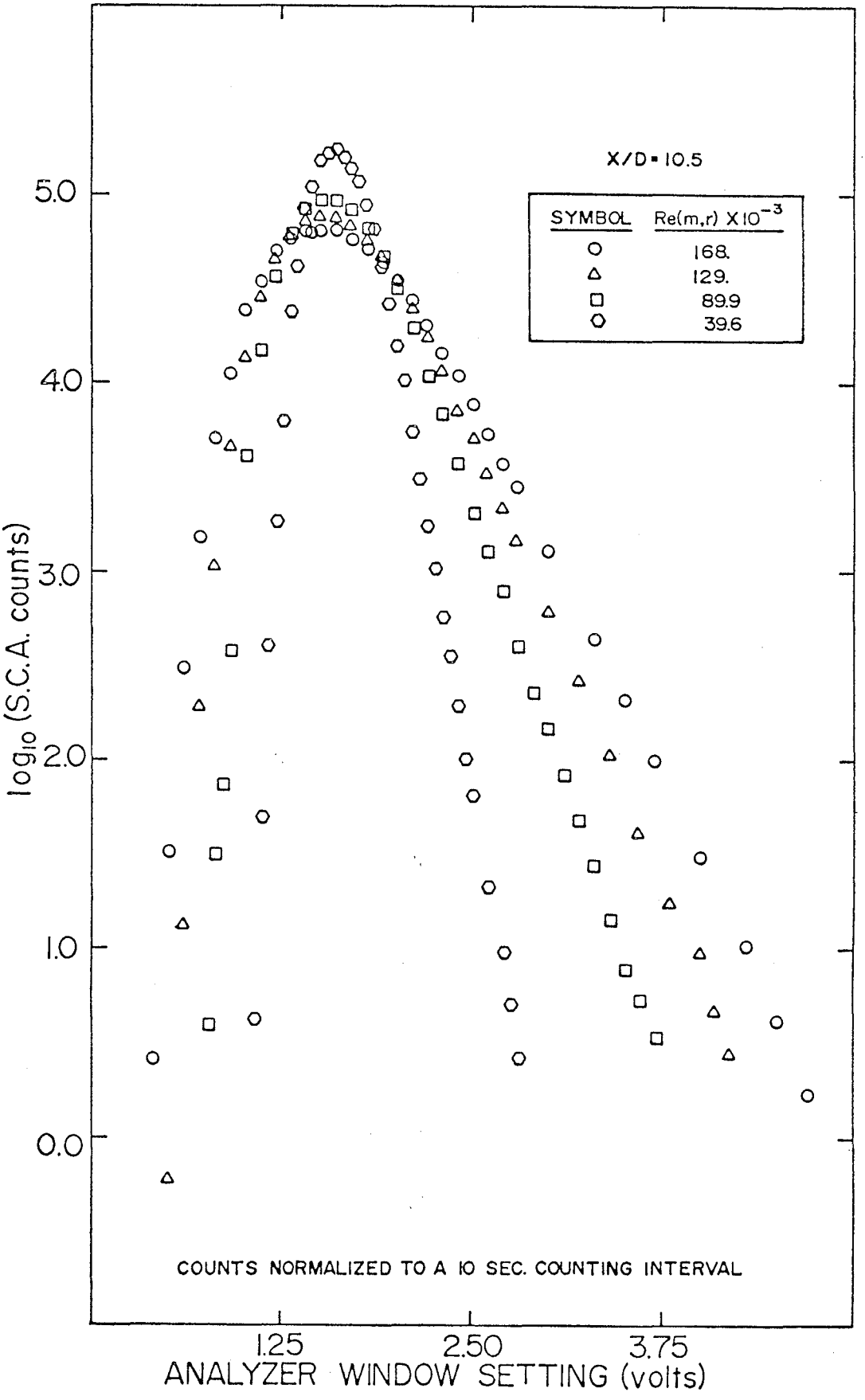

25. a) Probability distribution functions for the hot film probe output voltage at 10.5 diameters

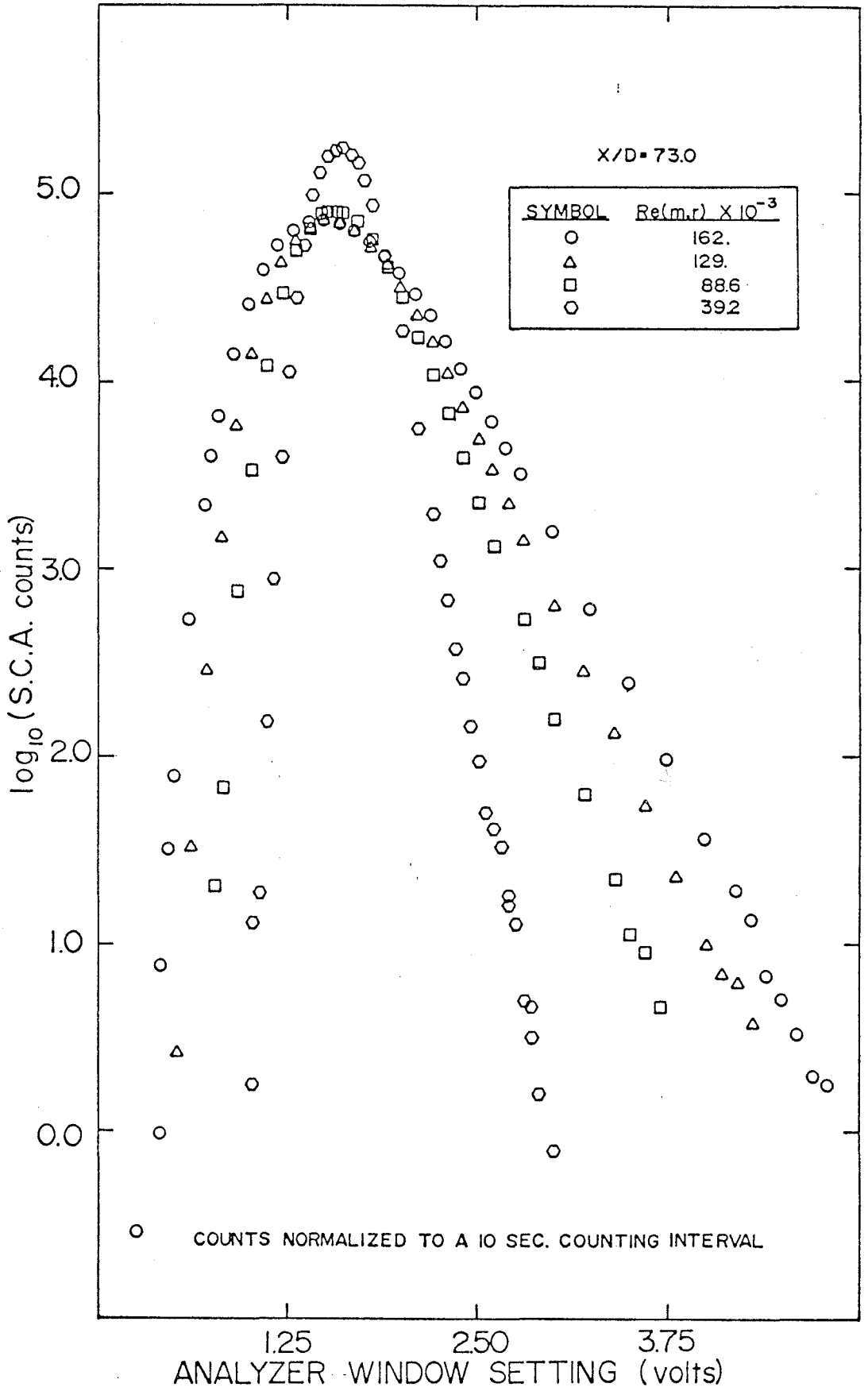

25. b) Probability distribution functions for the hot film probe output voltage at 73.0 diameters

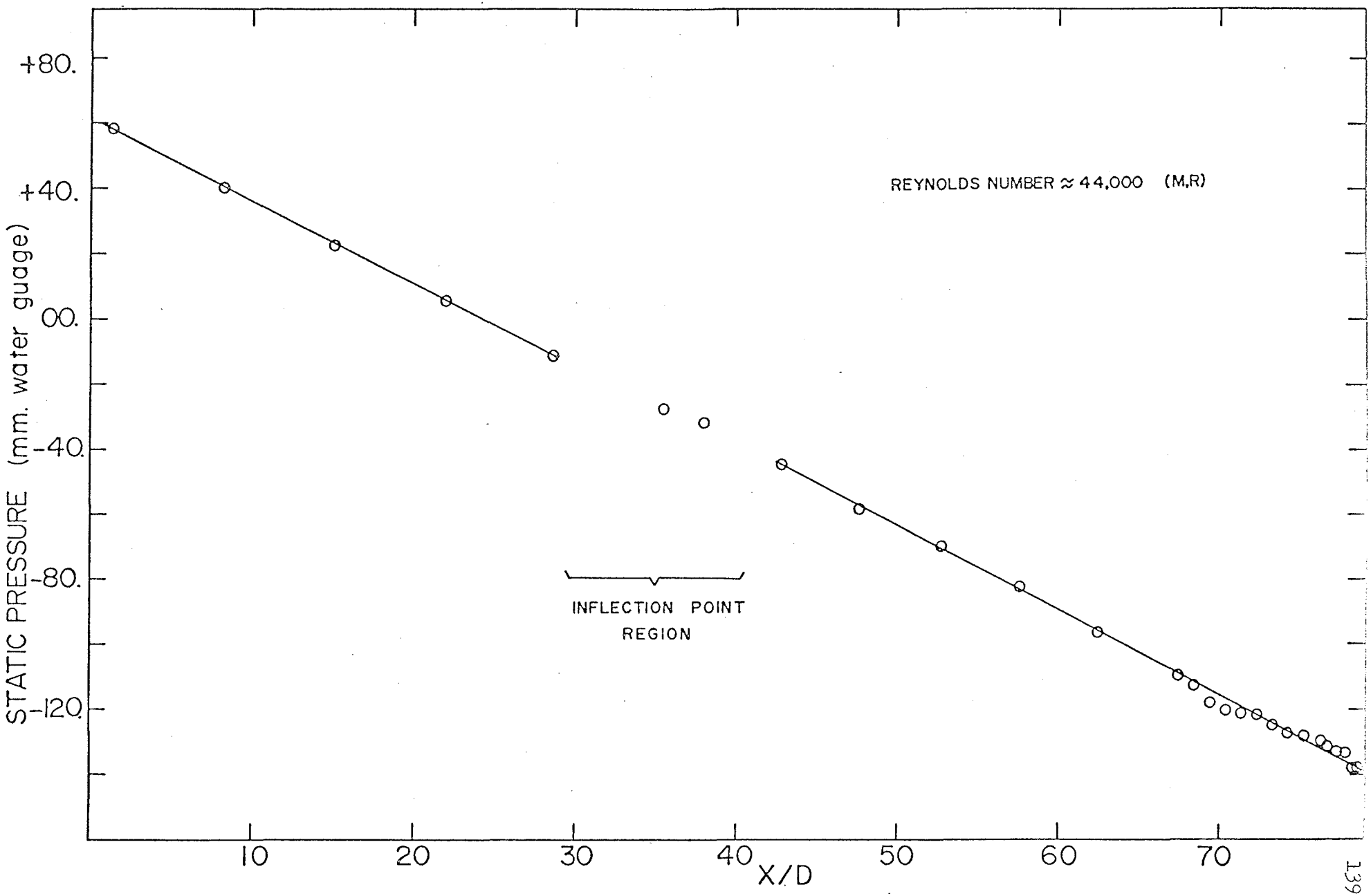

26. Longitudinal static pressure measurements

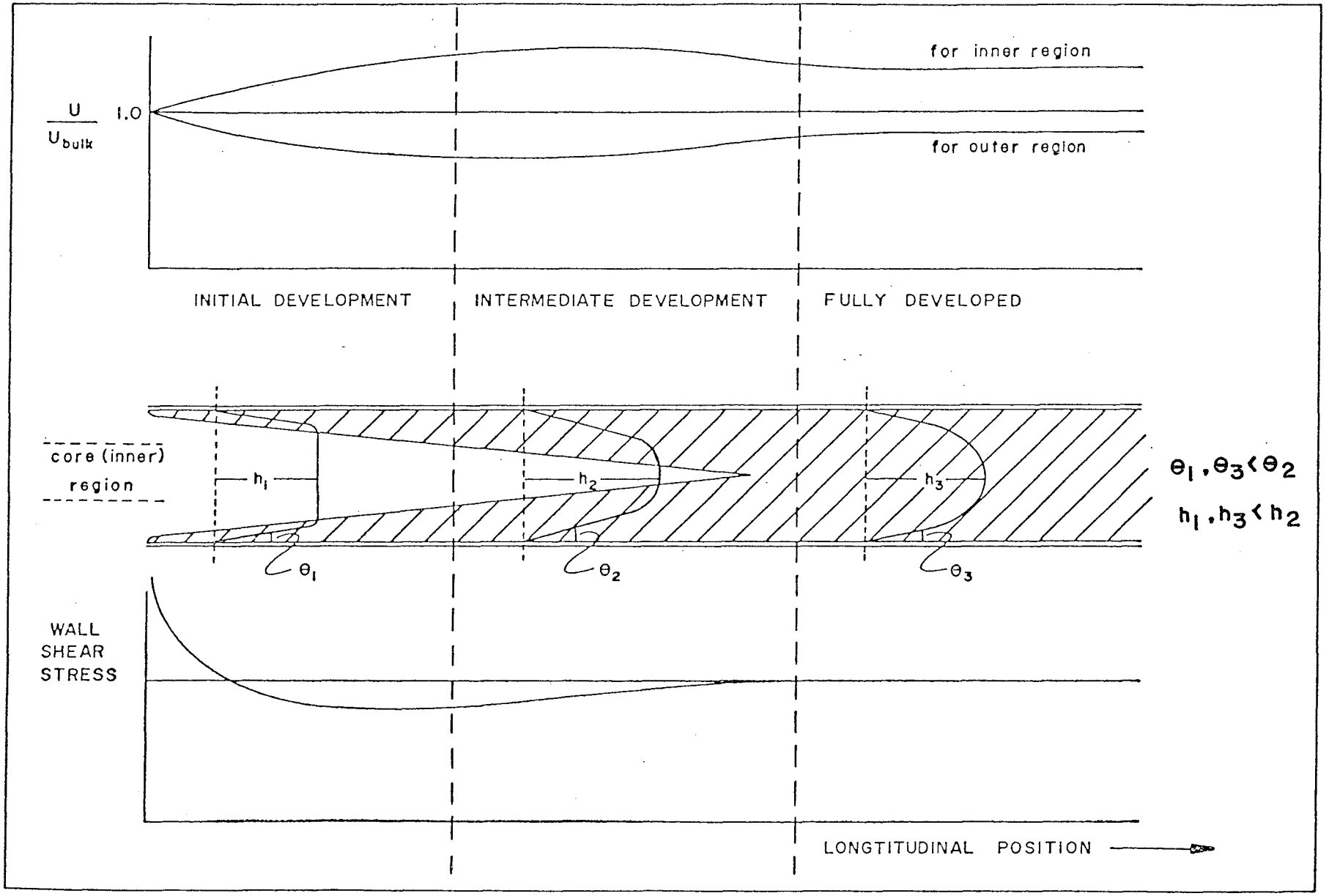

27. Proposed flow model schematic

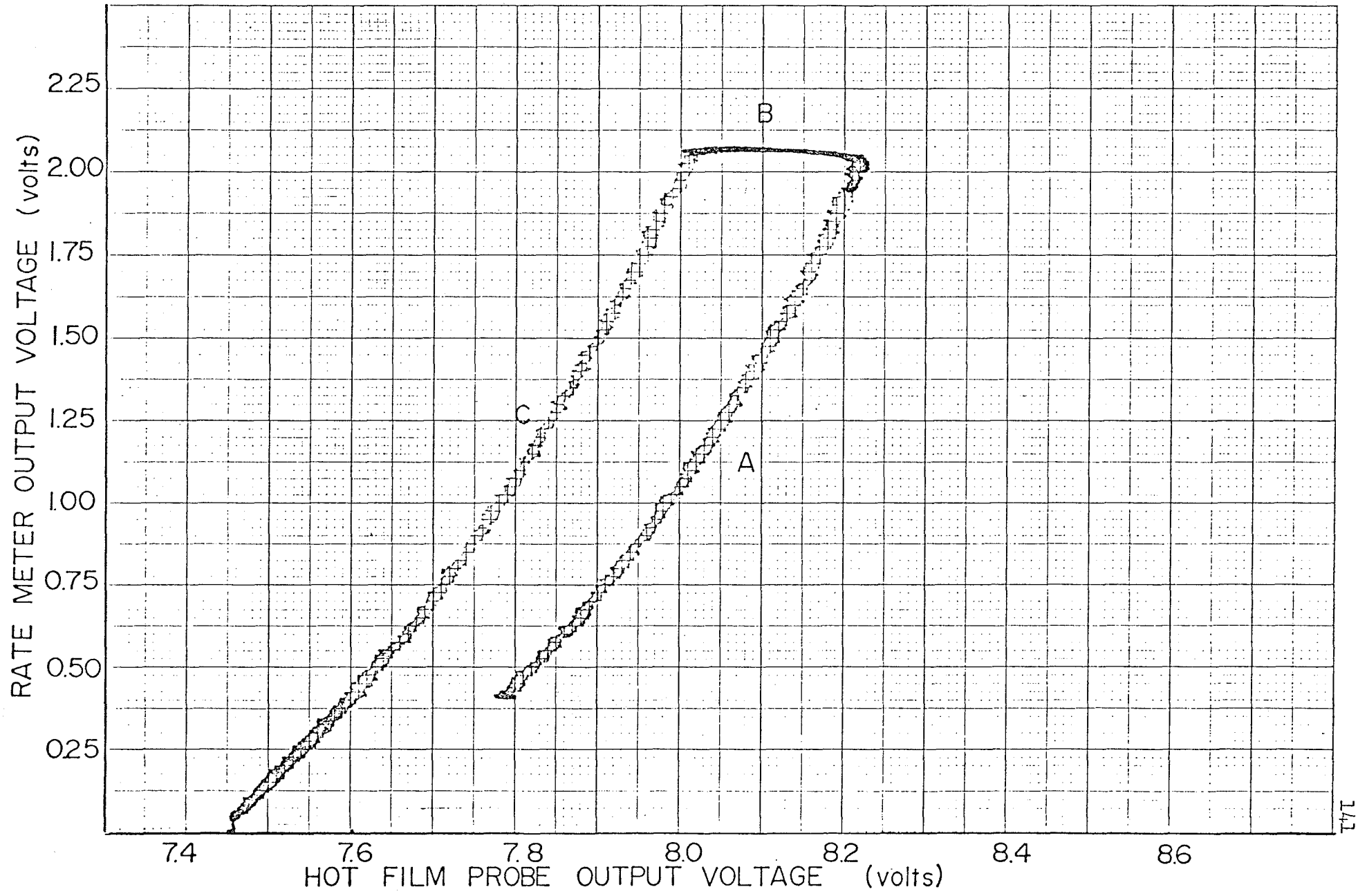

28. a) Continuous records of hot film output: equilibration at high speed

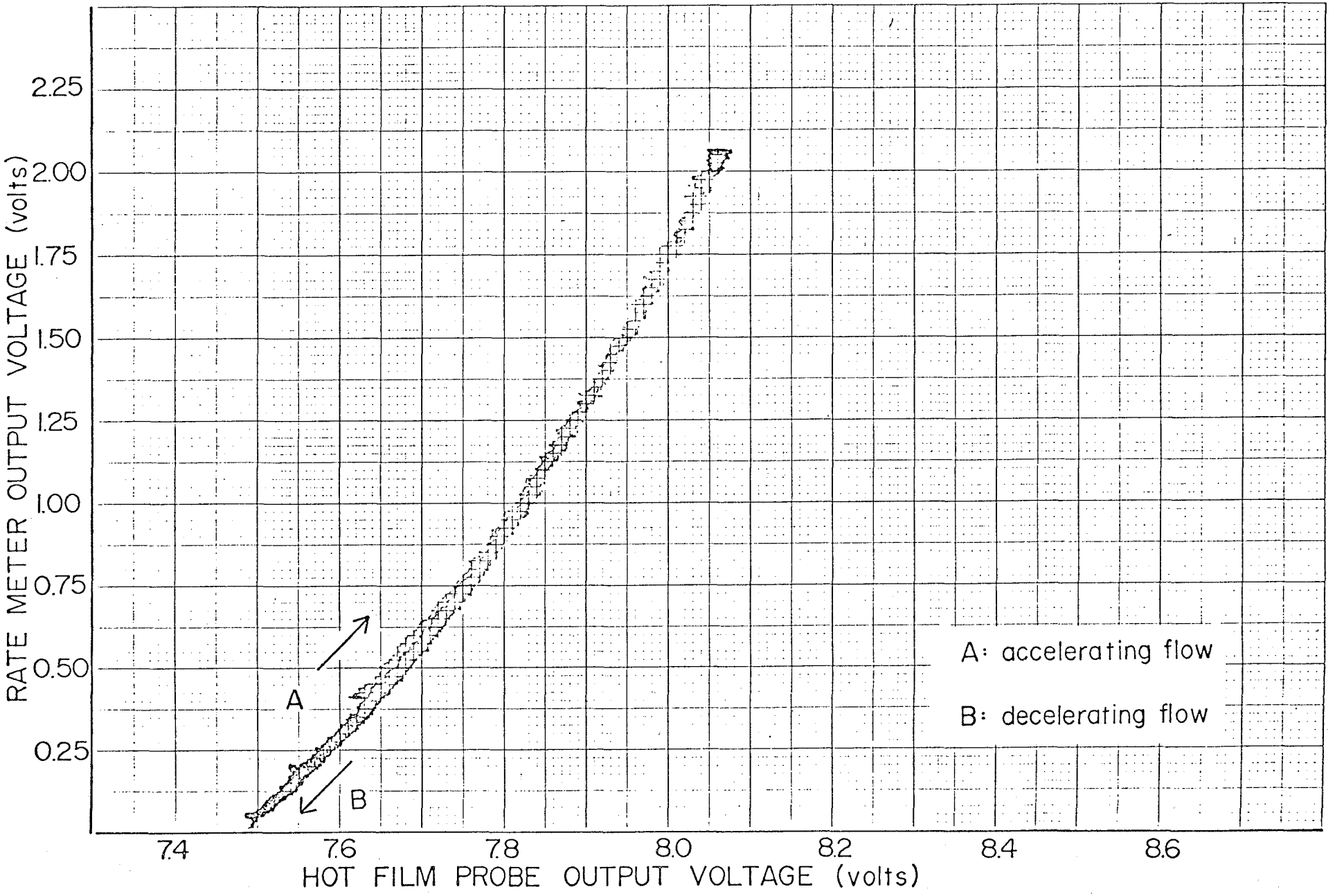

28 b) Continuous records of hot film output:no equilibration at high speed